博士論文

Fundamental research with respect to thermal phenomena of micro EDM

(微細放電加工の熱現象に関する基礎研究)

モハマド　ザヒルディン

Fundamental research with respect to thermal phenomena of micro EDM

(微細放電加工の熱現象に関する基礎研究)

指導教員　国枝　正典　教授

モハマド　ザヒルディン

Fundamental research with respect to thermal phenomena of micro EDM

(微細放電加工の熱現象に関する基礎研究)

Mohd Zahiruddin

Material removal in electrical discharge machining, EDM is by thermal erosion. Therefore, information on thermal phenomena of the process is required for further analyses of the process. Currently, demands on micro components increase the applications of EDM for micro machining significantly. This leads to the development of EDM with comparatively lower discharge energy than that of conventional EDM. In this work, for convenience the conventional and newly developed EDM is called macro and micro EDM, respectively. Although there is no difference in principle and mechanism of material removal between both processes, the micro EDM is capable of producing micro components with higher accuracy beyond the capability of macro EDM. However, unlike macro EDM, researches on the micro EDM thermal phenomena are limited due to the small spatiotemporal scale of the process, which makes both observation and analysis of the gap phenomena significantly difficult. Therefore, in this work thermal phenomena of micro EDM were obtained including energy distribution ratios, plasma diameter, power density and removal mechanism. These parameters were compared with those of macro EDM, and their influence on micro and macro EDM efficiencies were discussed. In this work, the efficiencies are represented by ratio of removal with respect to molten area volume or removal efficiency, R_e and ratio of energy consumed for material removal with respect to energy distributed into workpiece or energy efficiency, E_e. Both R_e and E_e of micro EDM were greater than those of macro EDM because the power density at micro EDM workpiece was found significantly higher than that of macro EDM. These results also explain differences in their performances such as the formation of white layer and residual stress. At the end of this work, to show the importance of the obtained results, an example application that describes deformation of micro fin machined by micro EDM due to thermal stress was discussed.

Table of contents

List of figures

List of tables

List of abbreviations and symbols

§: Section
1 – g: Ratio of removal by melting
a ($\equiv k/\rho c$):Temperature diffusion rate
AD594A: Thermocouple amplifier model
ANSYS: Finite element analysis software
C: Capacitor
c: Specific heat
Cd: Cutting depth
Cu: Copper
d: Plasma diameter
d_c: Simulated crater diameter
DC: Direct current
d_m: Diameter of crater
d_{max}: Plasma diameter at the end of discharge duration
E_{debm}: Energy carried away by debris due to melting
E_{debv}: Energy carried away by debris due to vaporization
EDM: Electrical discharge machining
E_e: Energy efficiency
ft: Fin thickness
fw: Fin width
g: Ratio of removal by vaporization
HAZ: Heat affected zone
i_e: Discharge current
INISTATE: Initial state command
k: Thermal conductivity
l, m, n: Spatial grid location or a point within the workpiece
L_m: Heat of fusion
L_v: Evaporation heat
NC: Numerical control
Ø: Diameter
p: Time step at a particular grid
P_e: Power density at the workpiece

PHOENICS: Numerical method software
PLANE183: 2-dimensional 8 nodes solid element
PLANE223: 2-dimensional 8 nodes coupled-field solid element
q: Discharge energy per single pulse
q'': Heat flux from discharge column
R: Resistor
RC: Relaxation circuit
R_e: Removal efficiency
SEM: Scanning electron microscope
T: Workpiece temperature
t: Time
$T_c(t)$: Calculated temperature rise
t_e: Discharge duration
Th: Workpiece plate thickness
T_m: Melting point
$T_m(t)$: Measured temperature rise
t_o: Pulse interval
T_s: Average temperature of electrode surface in steady state during machining
T_v: Boiling point
u_e: Discharge voltage
u_i: Open circuit voltage
V: Removal volume per pulse
V: Total removal volume per pulse
V_m: Volume of removal by melting
V_s: Volume of molten area
V_v: Volume of removal by vaporization
V_{vap}: Simulated vaporization volume
WEDG: Wire electrical discharge grinding
X: Energy distribution ratio into electrode
X_{con}: Ratio of energy loss due to heat conduction
X_{deb}: Ratio of energy carried away by debris
λ: Displacement at the tip of the fin or deflection
ρ: Density
$\sigma_r(z)$: Residual stress in the radial direction
$\sigma_x(z)$: Residual stress in the longitudinal direction

Chapter 1 Introduction

Electrical discharge machining (EDM) is a material removal process which is capable of producing components with intricate shapes on any electrically conductive materials regardless of hardness. Material removal occurs by means of thermal erosion which utilizes electrical discharge energy as the main source. This means, knowledge on thermal phenomena of the process is important for further analyses of the process.

The capabilities of EDM in producing intricate shapes on hard materials make the process widely used in tool and die making. However, material removal rate of EDM is significantly lower than that of conventional machining such as lathe and milling machines. In addition, high speed machining has been developed and it is capable of producing the tool and die significantly faster than EDM. This makes the EDM processes become less popular in the tool and die making industry.

On the other hand, consumer demands for customization and miniaturization of products serve to increase the applications of EDM for micro machining. This leads to the improvement of conventional EDM to become an EDM machine with comparatively lower discharge energy and higher precision equipment which capable of producing micro components with higher accuracy. In this work, for convenience the conventional EDM processes with normal EDM conditions is called as macro EDM. To distinguish from the conventional EDM, the EDM processes which ignite comparatively lower discharge energy compared to the macro EDM and more suitable in producing micro components beyond the capability of macro EDM is called micro EDM.

In principle, micro and macro EDM are the same, and there is no difference in the mechanism of material removal between both processes. However, micro EDM is capable of removing material from a workpiece surface with significantly small unit removal (at least 100 times smaller than that of macro EDM), and using higher precision machine tools compared to the macro EDM.

Currently, thermal phenomena of macro EDM have been reported by many researchers. The results of the thermal phenomena have been used for further understanding and improvement of macro EDM. However, researches on micro EDM are still limited, and one of the main reasons is no comprehensive report on thermal phenomena of the process. The significantly shorter discharge durations and narrower discharge gap make the observation and theoretical analyses of the micro EDM gap extremely difficult.

Most of the methods which have been used to analyze the thermal phenomena in the case of macro EDM cannot be used for micro EDM. Therefore, improvised or newly developed methods should be used for the researches on the micro EDM. In this work, the main purpose is to understand the fundamentals of micro EDM with respect to the thermal phenomena so that further improvement on the process can be made to fulfill current and future requirements of the micro machining.

1.1 Electrical discharge machining

EDM is widely used in various types of industries including electronic, automotive, and aerospace. It is one of the non-conventional machining processes which require no physical contact between tool and workpiece during machining. This makes the process capable in fabricating intricate features on a workpiece including thin walls, complex grooves and high aspect ratio holes which are unable to be produced by conventional machining processes such as drilling, turning and milling which apply a significantly high shear stress onto a workpiece surface during machining.

1.1.1 Types of EDM

EDM can be classified into several types. Sinking and wire EDM are two of the main EDM types which are commonly used. Schematic diagram of both processes are shown in **Figure 1.1** and **Figure 1.2**, respectively. In general, EDM is consisting of the combination of tool electrode and workpiece; a servo feed control to control the gap between the tool electrode and the workpiece; a power supply to generate the discharge pulse which is also known as pulse generator; dielectric such as mineral oil or deionized water to allow the formation of plasma channel for discharging, to cool the machining area and to flush the debris, which is important for an efficient machining; and numerical control, NC that controls the relative movement between tool electrode and workpiece.

In sinking EDM, at the end of the process the workpiece becomes the inverse shape of the pre-determined tool electrode with an offset. On the other hand, in wire EDM the vertically travelling wire tool electrode is fed horizontally in various X-Y plane directions into a workpiece which is capable of producing 2-dimensionally complex parts such as gears. Furthermore, by regulating the relative position of the top

and bottom wire guides, inclined cross section surface can also be produced using wire EDM. The typical diameters of wire electrode which are commonly used in the wire EDM are between 50 and 330 μm [1-3].

Basically, for micro and macro EDM, although they share the same machining principle, different machine tools are used. This is because micro EDM uses micro dimensions electrodes, and to reduce the unit removal in micro EDM, comparatively short discharge durations compared to the macro EDM must be ignited. Furthermore, since the working surface area is small, the probability of occurrence of discharge under the same gap width is lower than that in macro EDM. Hence, the gap width is significantly shorter than macro EDM, resulting in smaller diameter of arc plasma [4, 5]. In addition, the resolution of *X*-, *Y*- and *Z*-axes movement in micro EDM should be higher for better machining accuracy compared to macro EDM [2]. Further differences between micro and macro EDM will be discussed in **§ 1.2.1**.

Some examples products of micro EDM are fuel injection nozzles, spinneret holes for synthetic fibers, electronics devices, and other micro-mechanical parts. Similar to macro EDM, according to the parts or features to be produced, geometries of tool electrode and relative movements between tool electrode and workpiece, micro EDM processes also can be classified into several types [6-9]. Following are the types of micro EDM:

i. Sinking micro EDM; a tool electrode with micro features is used to produce cavity (inverse shape of the tool electrode) on workpiece.
ii. Micro wire EDM; similar to WEDM but the wire electrode diameter between 20 and 50 μm [2], about 5 to 10 times smaller than the case of macro EDM.
iii. Micro EDM drilling; micro electrodes with diameters 5 to 100 μm are used to produce micro holes in the workpiece, about 10 to 20 times smaller than the typical minimum size could be produced using macro EDM.
iv. Micro EDM milling; micro electrodes with diameters 5 to 100 μm are used to produce 3-dimensional cavities.
v. Wire electro discharge grinding (WEDG); a process which is capable to reduce diameter of a micro rod down to less than 5 μm. This type of micro EDM was developed by Masuzawa et al. [9].

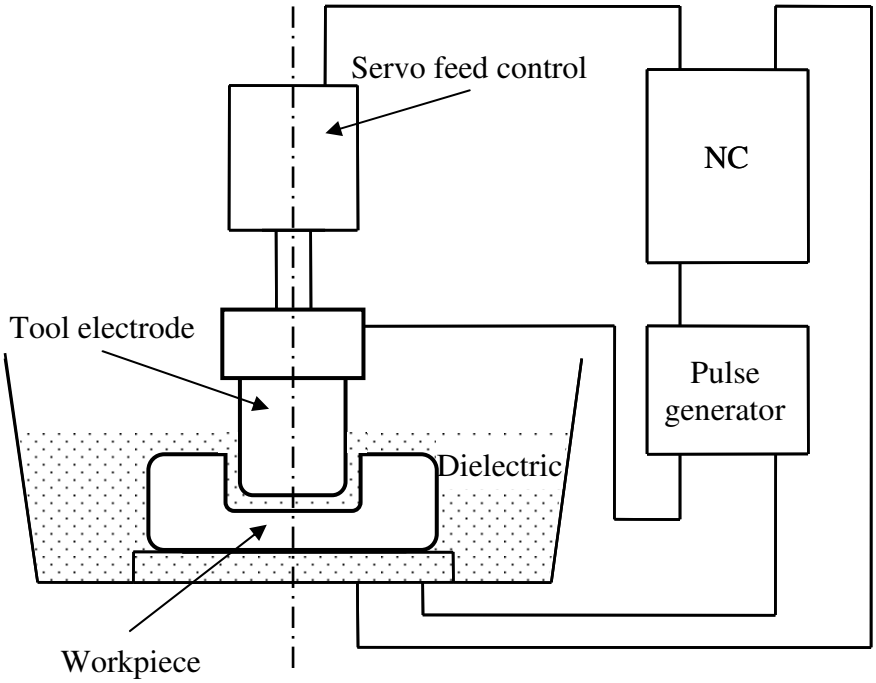

Figure 1.1: Schematic diagram of sinking EDM

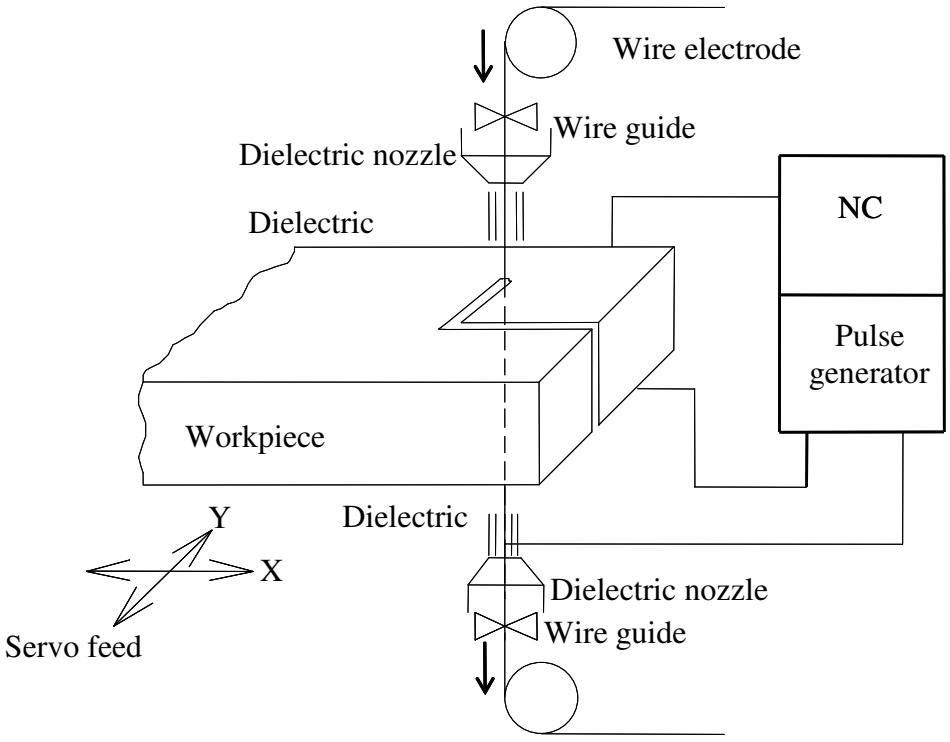

Figure 1.2: Schematic diagram of wire EDM

In this work, micro EDM machine which is equipped with WEDG as shown in **Figure 1.3** a. was used. WEDG is commonly used to machine a micro rod before it is used as a tool electrode to produce micro features on a workpiece. The principle of WEDG is shown in **Figure 1.3** b. As shown in the figure, wire electrode is used to cut a micro rod which is rotated during machining similar to turning operation, except that the wire electrode is continuously travelling along the groove of the wire guide.

The typical travelling speed of the wire electrode is between 1 and 3 mm/s. Since the rotation of micro rod is below 3000 rpm [9, 10], the peripheral speed of micro rod is 15 mm/s. On the other hand, the discharge duration is 100 ns or less, during which the relative displacement between the wire electrode and the micro rod is 1.5 μm or less. This means the wire travelling or the wire electrode rotation will not influence the discharge column significantly.

Furthermore, although the wire electrode seems to form a curvature near the machining area, the confronting surfaces in the gap between wire electrode and micro rod are almost parallel, which is similar to macro EDM process with electrodes that have flat surfaces facing each other. This allows WEDG to machine side surface of a micro rod into a flat surface. The method to produce the flat surface of a micro rod is explained in **§ 5.1.2**.

Normally, micro rod is connected to positive polarity of a power supply during the rod machining. Then, the rod polarity is changed to negative to act as tool electrode without removing it from the rod holder or mandrel. This is to keep the same rotational axis of the rod so that it will not be wobbling while machining a workpiece which is fixed on the xy table within the same machine.

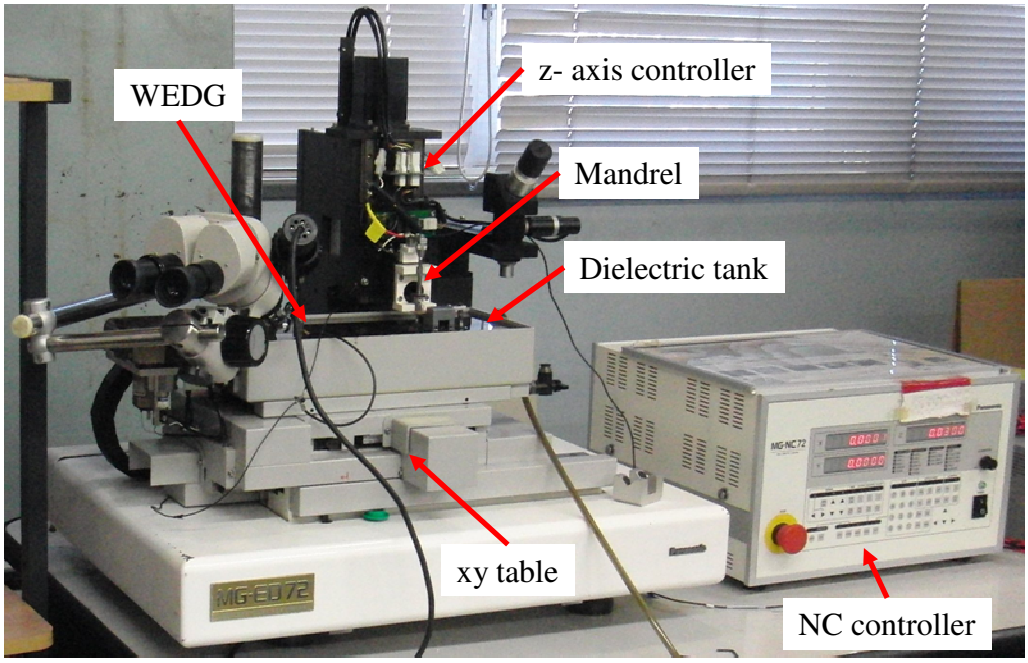

a. Overview of micro EDM machine

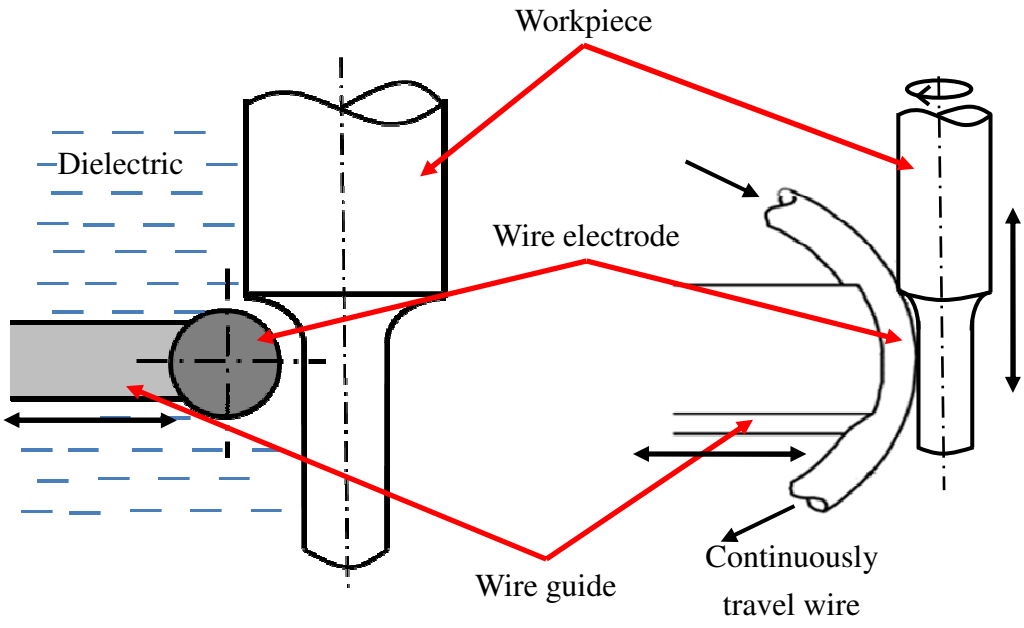

b. Principle of WEDG

Figure 1.3: Micro EDM machine which is equipped with WEDG

1.1.2 EDM principle

In EDM, the removal process is accomplished by generating high frequency pulse discharges within a narrow gap between electrodes consisting of tool electrode and workpiece that are held at different polarities of a pulse generator. During the process, when the gap between the tool electrode and workpiece which is filled with dielectric becomes closer, the intensity of the electrical field within the gap becomes greater. At a sufficiently narrow gap, electrical discharge is formed at the area where the strength of the electrical insulation of the dielectric breaks and current flows between the electrodes through the gap.

Under each discharge pulse, a fraction of the discharge energy is used to generate a plasma channel within the gap, and the other fraction of the discharge energy is distributed into the tool electrode and the workpiece. The energy that is distributed into the electrodes heats their surface and removes a limited portion of the heated area by vaporization and by melting to form a crater on those electrodes. The progress of material removal in EDM is basically the accumulation of the craters formation which is caused by the repetition of pulse discharge between the tool electrode and workpiece.

Normally, direct current is supplied between the electrodes by pulse generator. If the discharge concentrates only on a single location, the machining will not progress because no discharge can be produced at other locations on the surface of the electrodes. In order to prevent this occurrence, recurring discharge current is generated to stop the present discharge, and then after the plasma channel disappears, pulse voltage is applied again to allow discharge to occur at a different location. **Figure 1.4** illustrates the formation of craters under each discharge.

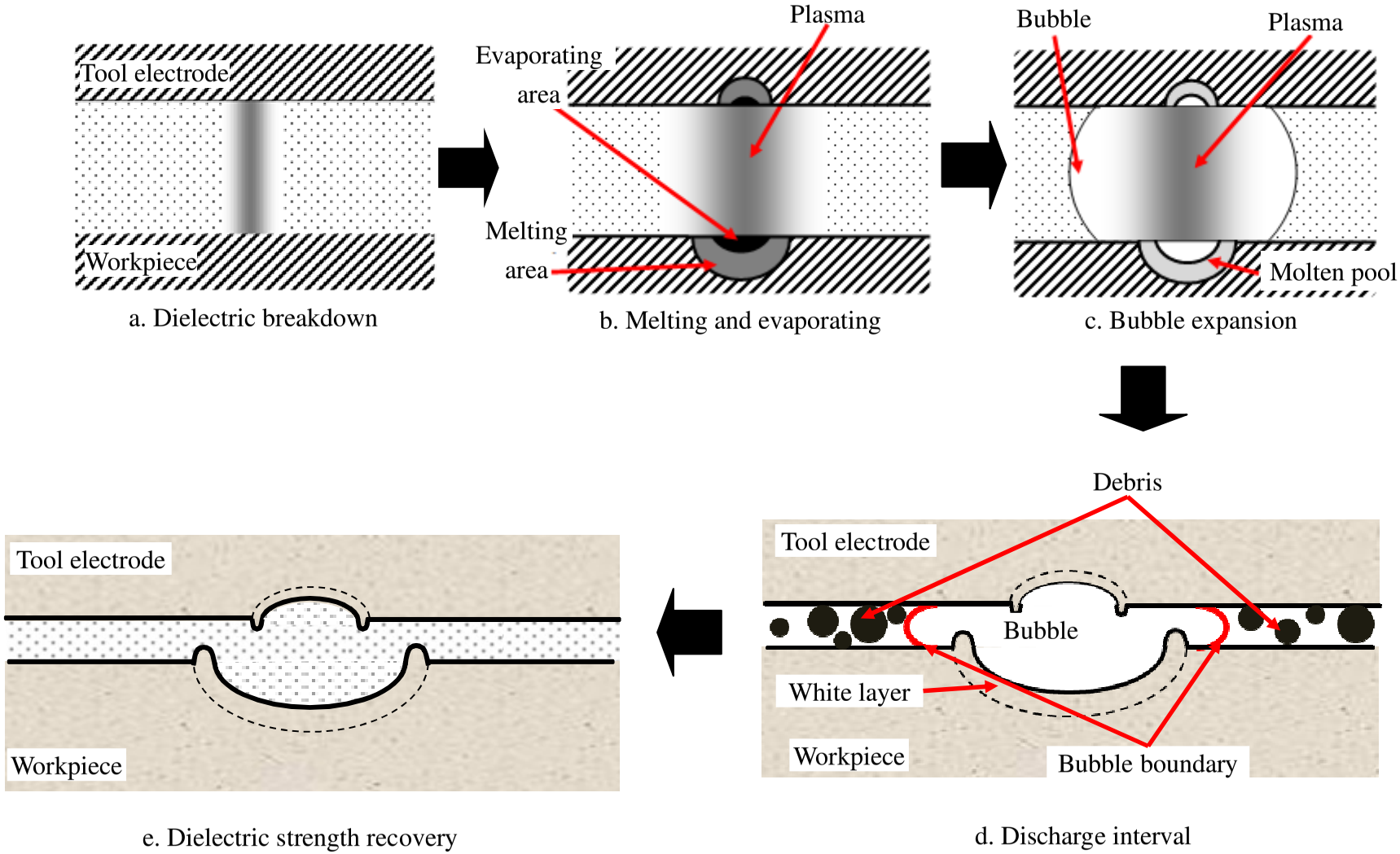

Figure 1.4: Principle of material removal in EDM

a. Dielectric breakdown

When the voltage of the pulse generator is set in the order of tens to hundreds volt and applied between EDM tool electrode and workpiece which are separated by several tens μm gap and immersed in dielectric, a small number of electrons that exist within the gap are accelerated by the generated electrical field. The accelerated electrons with sufficiently large kinetic energy collide with neutral particles causing the bonded electrons around the neutral particles to be released. This is known as impact ionization which causes the formation of ions and more free electrons. The free electrons are then accelerated by the electrical field and impact ionization process is repeated until electrons avalanche occurs [11].

The positive ions collide with negatively charged EDM electrode so-called cathode and the secondary electrons are released. Besides, the temperature of the cathode surface increases and thermal electrons are released. Furthermore, the electrical field on the cathode surface also releases the electrons. Those electrons are accelerated by electric field towards positively charged EDM electrode so-called anode, and impact ionization is again repeated.

At sufficiently high temperature on the electrodes surface, ionization based on collisions between neutral particles also occurs. As a result, during discharging high level ionization of plasma within the gap between electrodes is developed allowing the formation of arc discharge with high density current at discharge voltage of approximately 20 V [1].

Arc discharge is formed within the gap at a location where insulation breakdown is most likely to occur. Once the insulation breakdown occurs, more atoms, ions and electrons exist within the plasma channel which causes the current to flow more easily. Therefore, at the same time mostly there is no discharging at other locations. However, the occurrence of several discharges under one pulse is not impossible but at a low probability. In this work, it is assumed that only a single discharge occurs under each pulse.

b. Melting and evaporating

Power density at electrodes is so high that capable to melt and vaporize the tool electrode and workpiece surface. During discharging, electrons and positive ions are accelerated towards anode and cathode, respectively. The collisions of electrons and ions at electrodes surface immediately increase the temperature of electrodes' surface. As a result, power density higher than 10^8 W/m^2 at electrodes is formed, and the plasma channel temperature was reported to reach higher than 6000 K [12 - 15]. A fraction of the heated area on electrodes exceeds boiling point and vaporizes. However, during discharging total removal volume per pulse was only 1 to 10% of the area whose temperature exceeds melting point in the case of sinking EDM with macro discharge energy [16].

c. Bubble expansion

Along with plasma expansion, surrounding dielectric and electrodes material vaporize, dissociate, ionize and form a bubble. Consequently, the gap between tool electrode and workpiece is mostly occupied with gasses that are generated due to dielectric dissociation [17-21].

d. Discharge interval

This bubble continues to expand although the discharge ends due to the inertia of surrounding dielectric. The inner pressure of the bubble becomes negative and its diameter reaches maximum value. Then, the bubble starts to shrink. After that, the expansion and shrinkage process is repeated several times performing damped oscillation movement. The fluctuation of the pressure distribution caused by sudden expansion of the bubble is believed to remove portion of molten area on the surface of the electrodes [22-24]. Due to the surface tension of the molten material, the removed part is solidified in small spherical particles so-called debris. The diameter of debris particles is in the same order as the gap width. The debris particles are then mixed with dielectric and flushed away [22-24].

e. Dielectric strength recovery

When power supply between tool electrode and workpiece is stopped at the end of discharge duration, energy input into the plasma is also stopped. Consequently the plasma temperature is dropped, and then the positive ions and electrons recombined. Here, the electrical conductivity of the plasma becomes lower and finally the insulation of dielectric within the electrodes gap is recovered. It has been reported that the plasma temperature of 5000 K is considered as the threshold of deionization [14]. Normally, to assure a stable machining in consecutive discharges, the bubbles and debris particles are flushed away from the gap in order to prevent the localization and concentration of discharge locations [25].

The remaining molten area solidifies and forms a white layer on the electrodes' surface. The diameter of the white layer observed from the top surface of the electrodes determines the crater diameter. The adjacent area of the white layer on the electrodes which is not melting during discharge but experiences sufficiently high temperature and becomes thermally modified is known as heat affected zone, HAZ. **Figure 1.5** describes an image of cross section of the crater.

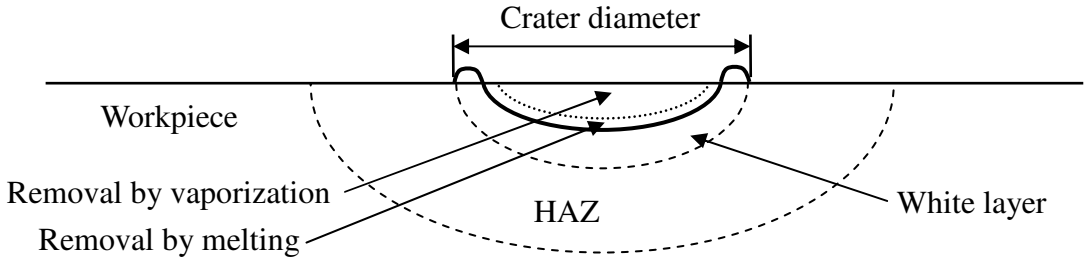

Figure 1.5: Cross section of a crater due to EDM discharge

1.2 Research background and objective

In this work, the main purpose is to understand the thermal phenomena of micro EDM, which is expected to be more difficult compared to the case of macro EDM. Even in macro EDM, the fundamental knowledge of the process including the thermal phenomena is still not fully understood and need to be explored further. This is ongoing by the recent developments of computer technology, metrology, and other analysis tools and instruments that contribute to the new findings which sometimes contradict to what have been accepted as fundamental knowledge regarding EDM so far.

The work began by obtaining several important fundamental parameters of micro EDM with respect to the thermal phenomena through extensive experimental works and iterative calculations. Then, based on the obtained results and from references, both micro and macro EDM processes will be evaluated and compared so that the differences in their performances can be understood thoroughly. Specifically, the heat source parameters of micro and macro EDM including plasma diameter, energy distribution ratio into workpiece and power density will be compared, and then the influence of these parameters on the efficiencies of both processes which are represented by the removal efficiency, R_e and energy efficiency, E_e will be discussed.

R_e is the ratio of total removal volume per pulse with respect to the volume of the area that exceeds melting point of workpiece material during discharging. This is based on the fact that under each discharge, not the whole area on workpiece that exceeds melting point is removed from the workpiece's surface because a part of the molten area remains to form a white layer [16, 26-31]. On the other hand, E_e is the ratio of energy consumed for material removal and carried away by debris with respect to the energy distributed into the workpiece. During discharging not all energy distributed into the workpiece is consumed for the material removal, and in the case of macro EDM a large fraction of discharge energy is lost due to heat conduction within the workpiece [16, 26-31].

By knowing R_e and E_e, differences between both micro and macro EDM performances including the degree of white layer formations due to each discharge can be explained. Besides, the results of thermal phenomena also can be applied for other analyses for better understanding and improvement of the process.

Another particularity of thermal phenomena in micro EDM compared to macro EDM is the influence of the residual stress generated by EDM on the deformation of machined micro parts. Hence, at the end of this report, thermal stress analysis followed by structural analysis of micro EDM workpiece deformation will be discussed. For the

application example, copper (Cu) workpiece which is low in toughness was machined using a micro EDM. This analysis also shows the importance of the obtained heat source parameters; plasma diameter and energy distribution ratio into workpiece.

Figure 1.6 shows an example picture of Cu workpiece which was machined in this work. As shown in the figure, the workpiece deformed although there was no physical contact between tool electrode and workpiece during the machining and reaction force acting on the workpiece was ignorable [20, 21]. There are two types of residual stress which may cause the deformation of the workpiece [32-35]. One of the types is from the fact that the material removal in EDM involves thermal erosion. Hence, deformation of the workpiece may be caused by the thermal stress due to discharges [32-35].

On the other hand, the deformation can also be caused by residual stress that exists within the workpiece prior to micro EDM process [34]. Residual stress that exists in a workpiece prior to machining is the result of plastic deformation processes such as plate rolling and wire drawing, and it can be released by annealing [34]. Therefore, in order to explain the deformation of micro EDM Cu workpiece as an example application of the thermal phenomena results, first the effect of pre existing residual stress prior to machining will be eliminated to assure the deformation is caused only by the thermal stress. Then both thermal and structural analyses will be conducted.

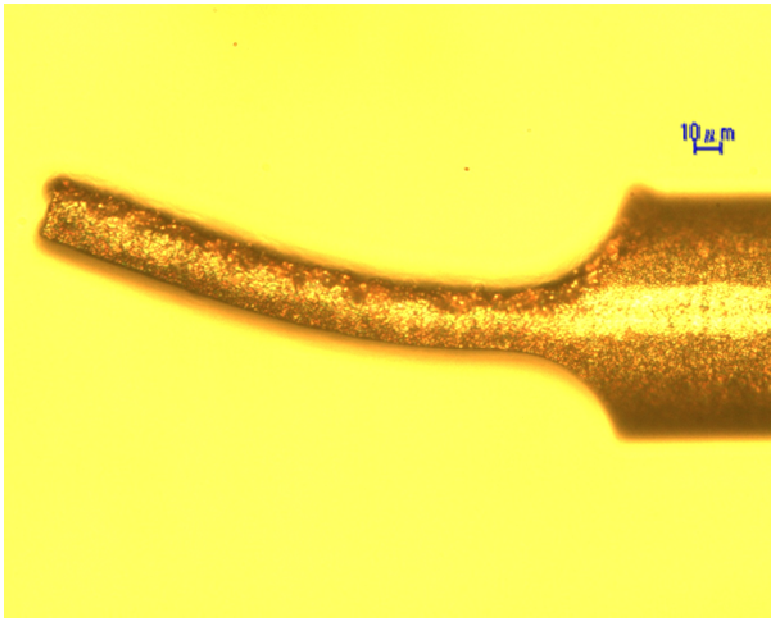

Figure 1.6: Deformation of Cu workpiece due to micro EDM

1.2.1 Micro and macro EDM

Researches on macro EDM have been conducted by many researchers covering many topics including electrodes removal and discharge energy distribution [26-31, 36-38], arc plasma [14, 15, 39-45] and thermal stress [32-35, 46-52]. In addition, consumer demands on micro components encourage researchers to study on the possibility of producing micro components using macro EDM machine [53-55].

In general, two main requirements to realize micro machining are reduction of unit removal and improvement of equipment precision [2]. Compared to conventional machining processes, currently available macro EDM machines have lower unit removal and better equipment precision [3]. Therefore, EDM machines have ability to produce micro components to certain extent. Typically, the minimum machinable sizes in macro EDM are in the range of 50 to 100 μm [54, 55].

However, continuous demands on further miniaturization of components are now beyond the capability of the conventional macro EDM machines. There are several factors that may limit the minimum machinable sizes in macro EDM including crater size, HAZ, residual stresses, tool wear, and equipment sensitivity [34, 53, 55].

Normally, transistor type pulse generator is used to generate discharges in macro EDM because of its high controllability of pulse voltage and current waveforms and stability of consecutive discharges. However, the lowest discharge energy which could be produced by the transistor type of pulse generator is significantly higher than that of the relaxation pulse generator which is used in micro EDM [1]. This may be one of the reasons that limit the minimum machinable sizes in macro EDM.

In addition, further improvement on equipment precision is required for further miniaturization [2, 54]. To reduce the discharge energy per pulse, the influence of the stray capacitance and inductance should be minimized [9, 34]. Hence, the electric feeders should be short, and the tool electrode holder and work table might as well be made of dielectric materials.

Therefore, micro EDM machine has been invented especially to reduce the minimum machinable sizes for micro machining. In contrast to macro EDM, micro EDM must ignite comparatively lower discharge energy so that lower unit removal can be obtained, which contributes to a higher accuracy that is required in producing micro components. The discharge energy is the product of discharge current (i_e), discharge voltage (u_e) and discharge duration (t_e) which are measurable at discharge gap during machining.

Table 1.1: Typical parameters and characteristics of micro and macro EDM

Parameters	micro	macro
Pulse generator type	Relaxation [1, 9]	Transistor [1]
Open circuit voltage [V]	40 to 110 [56]	50 to 380 [3]
Current setting [A]	0.001 to 0.01 [57]	0.1 to 500 [3]
Capacitor setting [pF]	10 to 3300 [56]	-
Discharge gap width [µm]	1.5 to 5 [58]	10 to 100 [1]
Discharge frequency [Hz]	Up to 10^7 [59]	10^3 to10^6 [1]
Typical workpiece polarity	Positive [1]	Negative [1]
Discharge durations	Below 200 ns	Above 2 µs [54]
Discharge energy per pulse [µJ]	Below 100 [58]	Above 1000 [60]
Unit removal [μm^3]	1 to 10	10^3 to 10^5 [3]
Material removal rate [mm^3/min]	Below 0.01 [61]	2 to 400 [3]
Plasma during discharge	Transient [42]	Nearly steady state [1]
Power density [W/m^2]	Up to 10^{12}	Up to 10^9 [1]
Tool wear / workpiece removal [%]	1.5 to 100 [57]	1 to 5 [3, 57]
Surface roughness [µm]	0.007 to 1 [57]	0.8 to 3.1 [57]
Producible rod diameter [µm]	Above 5 [56]	Above 50 [55]
Wire electrode diameter [µm]	20 to 50 [2]	200 to 330 [1, 2]

As explained in **§ 1.1.2**, u_e is approximately 20 V during discharging. Thus, to reduce the energy, micro EDM requires comparatively shorter t_e and lower i_e than those of macro EDM. Compared to the transistor type, relaxation type pulse generator is more capable of producing significantly short t_e with constant pulse energy, and thus the relaxation type is commonly used in micro EDM [1, 9]. Therefore, in this work the main focus is on the relaxation type pulse generator. Furthermore, it was reported that micro EDM can easily produce micro rods with diameter greater than 5 µm [56], which is at least 10 times smaller than the minimum machinable sizes in macro EDM.

Table 1.1 shows several parameters with their typical ranges, and characteristics of micro and macro EDM. Open circuit voltage and current setting are two adjustable parameters in most of EDM machines. For the relaxation type pulse generator, capacitor is also adjustable. Besides, discharge gap, discharge frequency and electrodes polarity are also adjustable parameters and properly controlled in some cases. These parameters determine the machining conditions of EDM process including i_e, u_e and t_e.

Under these parameters' ranges, discharge durations of micro EDM are less than 200 ns at longest which are about 100 times shorter than the average discharge durations that are used in macro EDM. Accordingly, as shown in **Table 1.1** the typical discharge energy in micro EDM is less than 100 µJ which is about 10 times smaller than the minimum discharge energy of macro EDM. Furthermore, the unit removal in micro EDM is at least 100 times smaller than that of macro EDM.

The characteristics of discharge craters at different levels of discharge energy have been observed [60]. **Figure 1.7** shows an example comparison of craters due to macro and micro EDM which describes the effect of the discharge energy [58]. The smaller crater which is indicated in the figure is less than 5 µm in diameter. This is the result of micro EDM single pulse which was ignited at discharge energy of 0.1 µJ. Han et al. [56] reported that, the diameter of craters due to micro EDM discharge on tungsten, cemented tungsten carbide and cemented tungsten carbide made of superfine particles were approximately 2 and 12 µm at finishing and roughing conditions, respectively.

Besides, the observation of total material removal rate (MRR) of anode and cathode shows that MRR was depending on discharge energy only at comparatively higher level of energy, and not at the energy below 100 µJ [62]. In addition, MRR of anode is always greater than that of cathode at discharge energy below 100 µJ, while at comparatively higher discharge energy, MRR of cathode is significantly greater than that of anode [29, 62]. However, the energy distribution into anode and cathode itself cannot explain this phenomenon. Better explanation on the relationship between MRR and polarity will be discussed in **§ 2.1**.

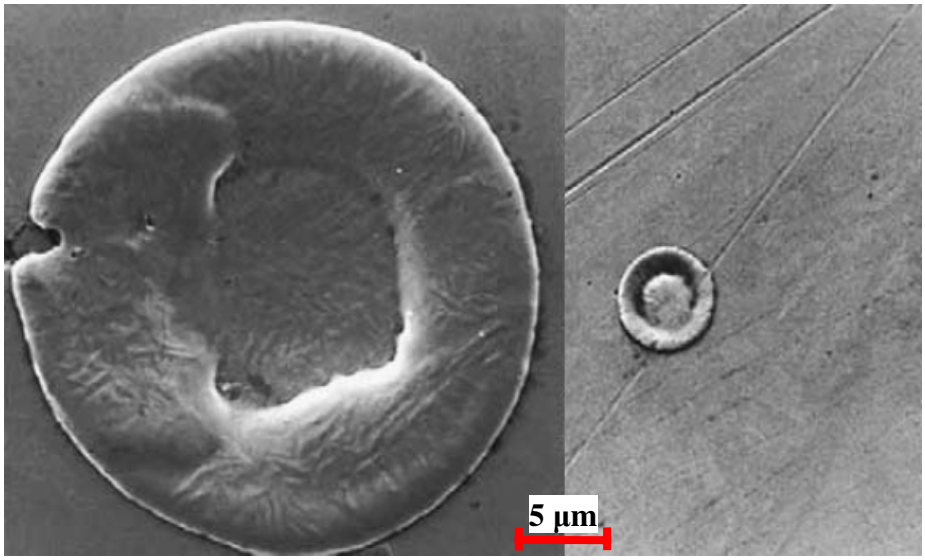

Figure 1.7: Comparison of craters due to macro and micro EDM single discharge [58]

Furthermore, it was found that energy required to remove a unit volume of material or specific energy at discharge energy below 50 μJ was much less than that at comparatively higher discharge energy, and thus thermal erosion efficiency at low discharge energy is considered higher than that at high discharge energy [60]. However, the discussion on erosion efficiency may not be accurate because the specific ratio of energy consumed for material removal with respect to the energy distributed into the workpiece itself was not considered in [60]. This will be discussed in **Chapter 3**.

In general, EDM is known as thermal process and the material removal rate is not influenced by material hardness, strength and toughness because no involvement of mechanical energy during machining [3]. However, in micro EDM the machining speed was influenced by the crystal orientation of mono-crystal tungsten, which indicates that micro EDM is not a pure thermal process but may be influenced by chemical reactions [34].

As explain in **§ 1.1.2**, generally damage layers including white layer and HAZ will be formed due to EDM. **Figure 1.8** a. shows a cross-sectional area of a Cu electrode which was machined by EDM. In the figure, three layers that result from three different levels of temperature rise during machining can be observed. In the white layer, besides the formation of high tensile residual stress, normally micro cracks are also formed [46], and they may reduce the reliability of the component in certain applications. The micro cracks also may influence the residual stress within the white layer. On the other hand, within HAZ workpiece micro structure is thermally modified and this is also not desirable.

Also in micro EDM, the damaged layer can be observed. **Figure 1.8** b. shows an example of tungsten micro rod machined by micro EDM at rough machining condition. The thickness of damaged layer was found to be 5 μm [56]. However, it was also found that, in some cases the damage layer was not visible. As shown in **Figure 1.8** c. no white layer can be observed using a normal scanning electron microscope (SEM) when a tungsten carbide micro rod was machined using the same condition that was used to machine the tungsten micro rod which is shown in **Figure 1.8** b. In the case of macro EDM, white layer can always be observed using SEM.

In micro EDM, the micro cracks may exist within white layer, but their present in the layer has never been reported. On the other hand, the presence of pores within the white layer has been reported [63]. This may influence the residual stress due to micro EDM. However, in this work for simplicity the influence of the pores or the micro cracks on the residual stress calculation is ignored.

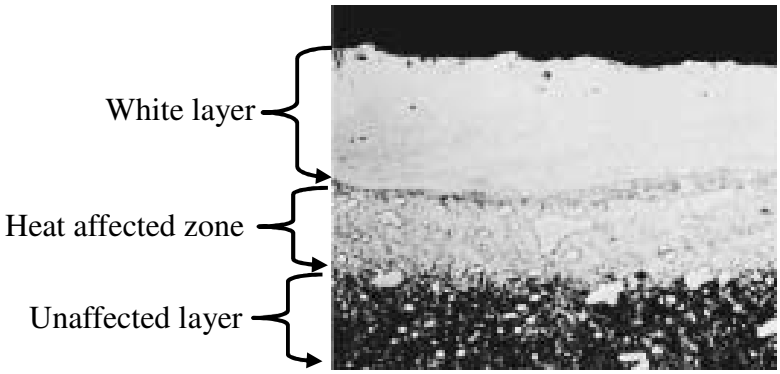

a. Cross-sectional area of EDM copper electrode after machining
machined at t_e = 200 µs
(Taken from UDDEHOLM: EDM of tool steel)

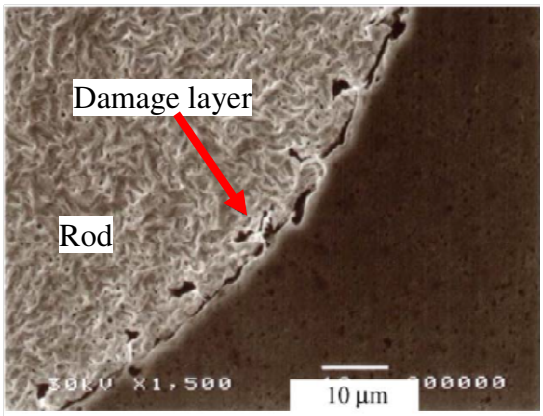

b. Tungsten micro rod
machined with roughing condition at t_e below 200 ns [56]

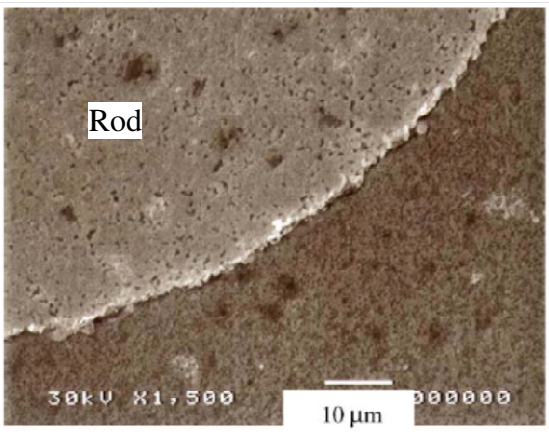

c. Tungsten carbide micro rod
machined with roughing condition at t_e below 200 ns [56]

Figure 1.8: Damaged layers due to macro and micro EDM

On the other hand, based on the observation of discharge gap using a high speed camera, at sufficiently long discharge durations of macro EDM, the discharge plasma expands to a maximum diameter within the first 2 μs, and then it remains at that size until the end of the discharge durations [43]. This means plasma in macro EDM is mostly in steady state, and at this state u_e is approximately 20 V [1].

However, discharge durations in the case of micro EDM are significantly shorter than 2 μs. Besides, Hayakawa et al. [31] also suggested that in the early stage of discharge duration, a large fraction of discharge energy is consumed for the generations and enthalpy increases of plasma. Therefore, it is reasonable to say that plasma is still growing during discharge durations of micro EDM. Thus, in this work the plasma diameter was assumed to be time dependent and linearly increase during discharging. Furthermore, because the plasma is in transient state and its diameter is still small, u_e should be higher than that of macro EDM.

The short discharge durations of micro EDM that limit plasma from expanding may also result in different power density at electrodes. This is believed to be another important reason that may cause the differences in machining characteristics between micro and macro EDM. This is because, in macro EDM processes, it was found that even under identical pulse energy conditions, differing performances can be observed between discharges with higher peak currents at shorter discharge durations and that of lower peak currents at longer discharge durations [1].

Since discharging area in micro EDM is significantly narrow, the gap width in micro EDM is shorter than that in macro EDM. This is based on the fact that the discharge probability is proportional to the surface area of electrodes [5]. The gap width in macro EDM is in the order of several tens of μm, whereas it is ten times smaller in micro EDM. It is known that smaller gap width results in smaller plasma diameter [43]. Hence, measurement of the plasma diameter in micro EDM is very important to investigate the thermal phenomena of micro EDM.

The variation in peak currents, discharge durations, and gap width will cause different level of power density distributed at electrodes, which significantly influences the EDM performances [1]. However, comparison of power density at micro and macro EDM electrodes has never been reported because exact heat source diameter in micro EDM has never been obtained. In this work, the heat source diameter is obtained and the influence of the power density on the micro EDM performances will be discussed.

1.2.2 Thermal phenomena in micro EDM

Figure 1.9 shows the relaxation type pulse generator which is commonly used in micro EDM. The circuit is composed of a direct current (DC) power supply, a resistor, R and a capacitor, C. Initially, voltage is applied across the capacitor and it is charged. Voltage across the capacitor increases to a maximum value which is regulated by the DC power supply. During this time, the voltage that is measured at the gap between tool electrode and workpiece is known as open circuit voltage, u_i. In this work, u_i was between 50 and 110 V. On the other hand, C was made variable between 10 pF (stray capacitance) and 3300 pF, which cover from minimum to the maximum values of typical capacitor setting in micro EDM.

Then, the tool electrode is brought towards the workpiece, and at a sufficiently small gap width, the dielectric insulation breaks and the discharge begins. The gap voltage immediately falls during the discharge duration, t_e. For example, at u_i = 100 V and C = 1000 pF, t_e was about 70 ns and the discharge voltage, u_e and discharge current, i_e was approximately 24 V and 1.14 A, respectively.

At the end of discharge, capacitor is recharged. Time to recharge the capacitor before the following discharge begins is known as pulse interval, t_o. Then the recharge and discharge operations continue until the gap width becomes too wide for the discharge to occur, or the power supply is switched off. In this work, t_o was about 12 times longer than the discharge duration with the tool electrode feed speed used in the experiment. The discharge energy per single pulse, q can be expressed as follows:

$$q = i_e \cdot u_e \cdot t_e \tag{1.1}$$

From Equation 1.1, the discharge energy per pulse in this work can be calculated and it was found that in the case of micro EDM it was not more than 2 μJ. As shown in **Table 1.1**, in macro EDM the discharge energy per pulse is in the order of 1 mJ, which means more than 1000 times greater than the energy of micro EDM discharge used in this work. Consequently, differing performances of micro EDM in this work from those of macro EDM including crater size, MRR, unit removal and specific energy can be expected. However, for further understanding of differences between micro and macro EDM, as explained in **§ 1.2.1**, the power density at micro and macro EDM electrodes should be obtained. Two main parameters required in order to obtain the power density at electrodes are discharge energy distribution ratio and plasma diameter.

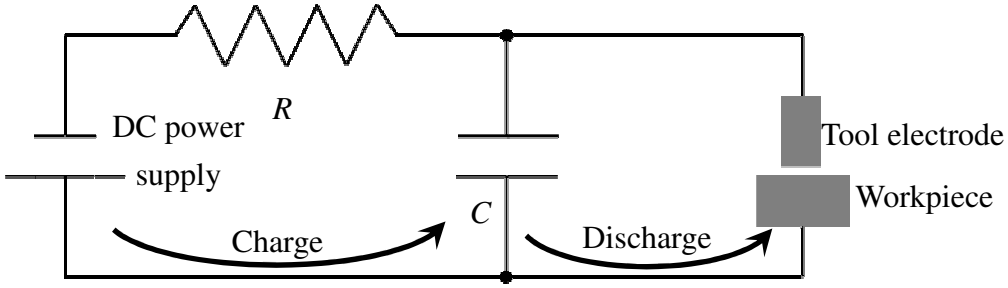

a. Relaxation circuit

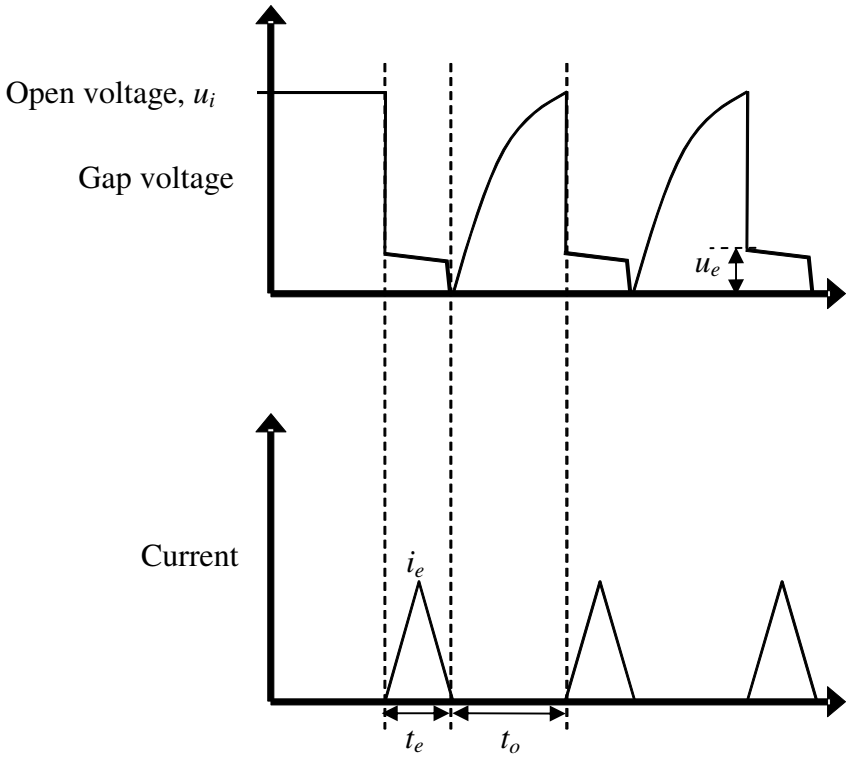

b. Discharge waveforms

Figure 1.9: Circuit and measured discharge waveforms of relaxation type pulse generator

Comprehensive studies regarding the discharge energy distribution ratio in macro EDM have been reported by Xia et al. [26-30]. **Figure 1.10** shows the energy distribution in the EDM process. As shown in **Figure 1.10** a. during discharging the total discharge energy is distributed into tool electrode, workpiece and the gap between them. As shown in the figure the energy distribution ratios into tool electrode and workpiece can be defined as the ratios of energy into tool electrode and energy into workpiece with respect to the discharge energy, respectively.

As shown in **Figure 1.10** b. energy distributed into workpiece is then lost due to heat conduction, consumed for material removal and lost due to heat convection and radiation. This means, the energy distribution ratio into workpiece is the sum of the ratios of energy loss due to heat conduction in workpiece, energy consumed for material removal and carried away by debris, and energy loss due to convection and radiation with respect to the total discharge energy.

All the above ratios have been obtained in the case of macro EDM [26-31]. Hayakawa et al. [31] calculated the heat flux due to convection and radiation at extraordinarily long discharge durations and found that it was negligibly small and most of the discharge energy was conducted into the electrodes. Furthermore, Xia et al. [29] determined the energy distribution into electrodes based on the summation of energy loss due to heat conduction and energy carried away by debris only; the heat due to convection and radiation was ignored.

Xia et al. [29] obtained the energy loss due to heat conduction by comparing the measured temperatures of the electrodes with the calculated results obtained under the assumed ratio of the energy loss due to heat conduction into the electrodes using the calculation model and experimental setup shown in **Figure 1.11**. And the ratio of energy carried away by debris was obtained by measuring the electrodes removal amount due to single discharge.

On the other hand, the diameter of plasma in the case of macro EDM has been obtained by observing the arc column using a high speed camera and by conducting the spectroscopic analysis [43]. Based on those findings, the power density at macro EDM electrodes has been calculated.

However, the ratios of energy distribution and plasma size in micro EDM which are required to calculate the power density have never been reported. It is believed that the power density in micro EDM may be different compared to the case of macro EDM based on the above fact that the discharge in micro EDM occurs in a significantly narrow gap space and is ceased before the steady arc is established.

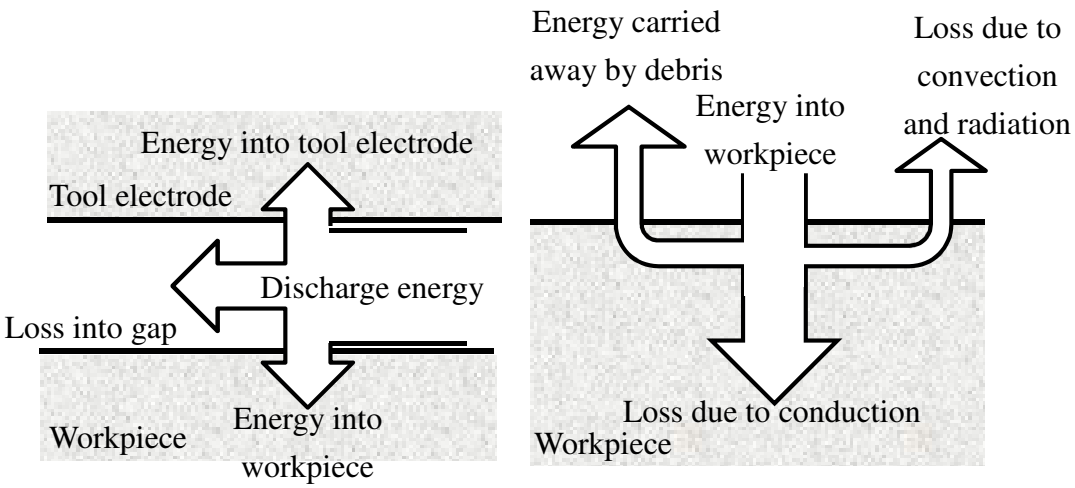

a. Distribution of discharge energy b. Energy distribution in workpiece

Figure 1.10: Distribution of discharge energy during EDM process

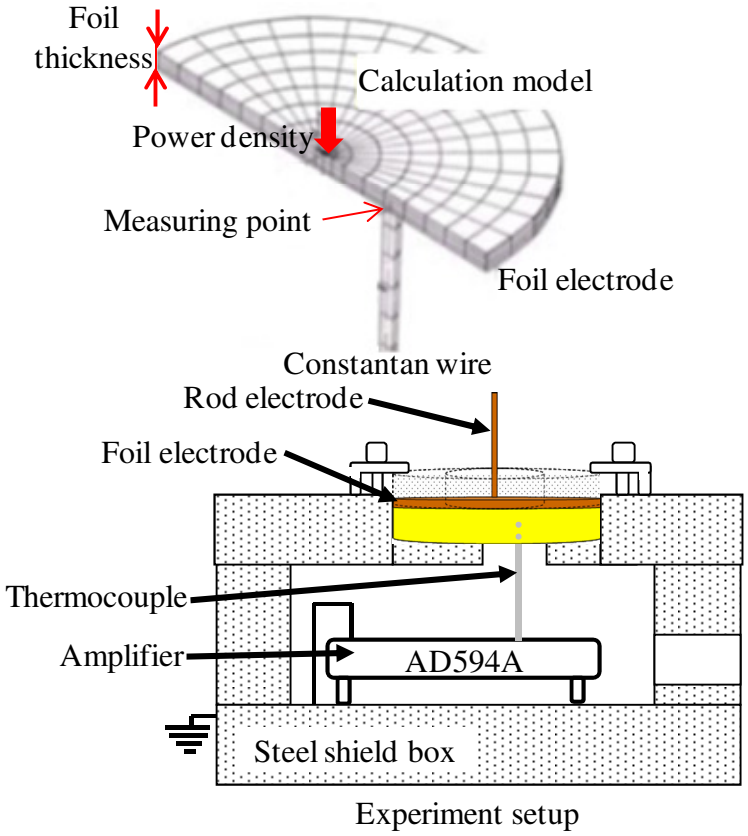

Experiment setup

Figure 1.11: Method to obtain energy distributed into electrode in single pulse discharge [29]

Table 1.2: Summary of micro EDM parameters in this work

Parameters	Value / type
Pulse generator type	Relaxation
Open circuit voltage [V]	50 to 110
Capacitor setting [pF]	10 to 3300
Workpiece polarity	Positive
Discharge durations [ns]	Below 200
Discharge energy per pulse [μJ]	Below 5
Plasma during discharge	Transient
Power density [W/m^2]	Up to 10^{12}
Unit removal [μm^3]	Below 2

Table 1.2 summarizes parameters of the micro EDM which were used in this work. As shown in the table with discharge durations below 200 ns and discharge energy below 5 μJ, it is impossible to observe the expansion of arc column within this short period using the high speed camera as reported by Kojima et al. [43]. Additionally, the intensity of light emitted from those electrodes is so weak, and therefore the application of the spectroscopic analysis is difficult to determine the plasma size in the case of micro EDM.

Furthermore, the temperature rises on electrodes due to single pulse discharge is also not measurable as in macro EDM [29] because the interference of electromagnetic noise due to discharge is larger than the temperature signal. Therefore, improvised method or totally different approaches with respect to the case of macro EDM are required in order to study the thermal phenomena in the case of micro EDM.

1.2.3 Application example; thermal stress and structure analyses

Thermal deformation analysis is one of the applications of the main results obtained in this work. To discuss this example, a Cu wire was cut into a micro fin. More than a million discharges were ignited to complete the machining of Cu workpiece to form the fin that was previously shown in **Figure 1.6**. It was impossible to simulate more than a million discharges on the micro fin model in order to understand the deformation. Thus, residual stress due to single discharge was first obtained. Then the result of the residual stress due to single discharge was imposed within the physical model of the fin for the structural analysis.

Before that, it is important to understand the formation of thermal stress that causes the deformation. Theoretically, it is known that a solid body expands on heating and contracts on cooling. If the body is restrained from expanding or contracting when its temperature is changed, the stress within the body is formed. In a solid body with uniform properties, when the temperature rise is not uniform, each element within the body tends to expand differently. However, as a continuous body, each part is allowed only to expand in proportion to the temperature rises. Therefore, elements within the body are restrained each other at any point in the body.

The stress equivalent to the restraining action is known as the thermal stress. In other words, when temperature is distributed non-uniformly within a body, the thermal stress exists to keep the continuity of the displacement of its elements. Or we can say that the thermal stress is a stress which is produced by the restraining action among elements within a body to prevent from expanding and contracting freely when its temperature is changed. This means, restraining actions will cause compressive stress on the heated surface and tensile stress on the cooling surface.

Figure 1.12 describes qualitative explanation of the deformation of fins fabricated using micro EDM. The positive marks (+) indicate the area where tensile stress is formed. As explained earlier, only a fraction of the area above the melting point due to discharge is removed. The remainder is solidified to form a white layer.

While the white layer is still in liquid state, no stress is formed due to free movement of the molten elements. After solidified, the non-uniform cooling process of the white layer begins. This is the reason of the formation of the tensile stress at the adjacent of EDM machining area [32-35, 46-52].

As shown in **Figure 1.12** a. tensile stress is formed and remains at both sides of the 1st slot after the first cutting. During the 2nd slot cutting, the stress on fin surface at the adjacent area of the 1st slot is released. At the same time, in the region on the fin surface at the adjacent area of the 2nd slot, tensile stress is formed. When the fin width, *fw* is sufficiently small, the tensile stress at the adjacent area of 2nd slot will cause the fin to be bent toward this slot as shown in **Figure 1.12** c.

To obtain quantitatively the fin bending due to EDM, it is necessary to conduct the structural analysis to calculate the workpiece deformation caused by the thermal stress. Hence, specific formation of residual stress due to single discharge should be known. Here, for simplicity several assumptions are required including:

i) All the pulse discharges are assumed to be ignited uniformly on the workpiece at identical power density. Then, the calculation result of thermal stress distributed in the depth direction at the center of the crater due to single discharge will be imposed within the beam model uniformly to represent the residual stress due to the consecutive discharges.

ii) There is no interaction of residual stress distribution involved, which means the residual stress distribution generated in the depth direction of the workpiece by the previous single discharge is not affected by the following discharge.

iii) Two-dimensional model is sufficient in order to represent the actual three-dimensional process.

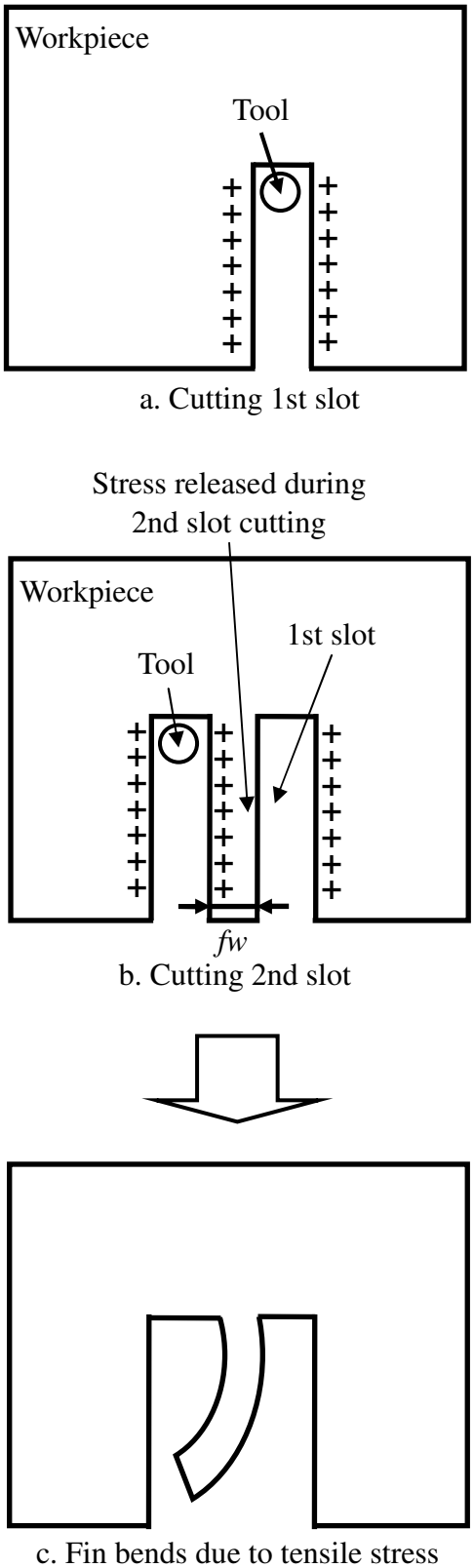

Figure 1.12: Theory of the formation of residual stresses and fin deformation

1.2.4 Objective

This research involves experimental works and iterative calculations based on physical models which are developed using numerical methods software to study the fundamentals of micro EDM with respect to thermal phenomena. Then, the results of the thermal phenomena will be used to calculate removal and energy efficiencies to be compared between the micro and macro EDM. Finally, for the application example, the thermal stress and structural analyses to understand the deformation of the Cu workpiece will be discussed. The objectives of this work can be summarized as follows:

i. To obtain the energy distribution ratios and plasma diameter in micro EDM.
ii. To obtain power density at micro EDM workpiece.
iii. To understand the removal mechanism in micro EDM process.
iv. To compare micro and macro EDM efficiencies based on the results of thermal phenomena to understand differences between those processes.
v. To understand deformation of micro EDM workpiece using thermal and structural analyses as an example application of the results of thermal phenomena.

In this dissertation, several results of the thermal phenomena in micro EDM were reported. In **Chapter 2**, the energy distribution ratios during discharging will be discussed. In **Chapter 3**, the discharge plasma diameter, power density at micro EDM workpiece, and material removal mechanism of the workpiece will be explained. Furthermore, for comparison between both micro and macro EDM, two indexes will be introduced namely ratio of removal with respect to molten area volume or removal efficiency, R_e and ratio of energy consumed for material removal with respect to energy distributed into workpiece or energy efficiency, E_e. The way how the power density at micro and macro EDM workpiece influences these efficiencies will be discussed. In **Chapter 4**, a physical model of micro EDM single discharge on a workpiece will be developed using a software which is based on the finite element method in the thermal stress analysis, and then the residual stress due to the single discharge will be calculated. In **Chapter 5**, the result of thermal stress analysis which is obtained in **Chapter 4** will be used in the structural analysis to understand the deformation of micro fin due to micro EDM.

Chapter 2 Distribution of discharge energy in micro EDM

As explained in **Chapter 1**, the source of heat during the discharging is represented by power density and plasma diameter. For example, some researchers calculated the thermal stress caused by EDM single pulse discharge, but the power density and plasma diameter were assumed in their calculation, because these parameters were difficult to obtain. Hayakawa et al. [31] and Kojima et al. [43] measured the power density and plasma diameter in macro EDM, respectively. However, they are not known in micro EDM. One of the main parameters that are required to calculate the power density is energy distribution ratio into micro EDM workpiece. Hence, in this chapter, the method to obtain the energy distribution ratio into workpiece and factors that may influence the calculation model will be discussed.

2.1 Overview of energy distribution ratio

The formation of several layers on workpiece surface due to EDM discharges indicates that the temperature distribution within the electrode during EDM is not uniform. This nature of EDM should be studied for further analyses of the process. For instance, the non-uniform temperature distribution might be the main reason that causes the formation of the thermal stress. This means, the understanding of temperature distribution within the EDM electrodes is required in order to develop a model for the thermal stress analysis. Therefore, thorough discussion on the thermal phenomena including energy input and removal mechanism during EDM process is important for the modeling and simulation of the temperature distribution in the EDM process.

During EDM process, machining conditions to calculate the discharge energy including i_e, u_e, and t_e can be measured directly near the discharge gap by using an oscilloscope. However, the main difficulty here is that the discharge energy is distributed not only into the workpiece, but also into tool electrode and the gap between them as shown in **Figure 2.1** a.

The ratios of energy distributed into tool electrode, workpiece and the gap between those electrodes with respect to the discharge energy so-called the energy distribution ratios are different from each other. Xia et al. [28] determined the ratios in the case of macro EDM with discharge current and duration equal to 16 A and 100 μs, respectively.

The percentages of the ratios obtained by Xia et al. [28] are indicated in **Figure 2.1** a. However, the ratios have never been reported in the case of micro EDM. Therefore, the energy distribution ratios into the micro EDM electrodes need to be obtained in order to understand the thermal phenomena in the process.

In addition, based on the fact that the energy that is distributed into electrodes heats, and then erodes a fraction of the heated area of both the tool electrode and workpiece surface, it is found that the distribution of energy into electrodes directly influences the tool wear and workpiece removal. The wear and removal of electrodes are also the main parameters that determine the accuracy and the efficiency of the EDM process. Thus, the energy distribution ratios into electrodes are also important factors to explain the performances of EDM process.

Xia et al. [29] and Hayakawa et al. [31] estimated the energy distribution ratios into electrodes by comparing experimentally measured and calculated temperature rise on Cu electrodes due to single pulse discharge under normal EDM conditions and extraordinarily long discharge durations which are normally not used in EDM, respectively. These reports show that in total, 65% of the discharge energy was distributed into tool electrode and workpiece under the macro EDM conditions, and most of the discharge energy in the case of extraordinarily long discharge durations was distributed into the electrodes.

Furthermore, at sufficiently long discharge durations, elements of carbon which were generated due to the dissociation of dielectric are attracted to the electrode which was held at positive polarity of the pulse generator or anode [29, 64-68]. These carbon elements form a layer with a high sublimation temperature that protects the anode surface from wear.

However, at discharge durations shorter than a few μs, the formation of the carbon layer did not occur. Hence the material removal rate was solely dependent on the energy distributed into electrodes where the greater removal rate was obtained in the case of anode compared to that of electrode which was held at negative polarity of the pulse generator or cathode although both electrodes were made of the same material [29].

The report by Xia et al. [29] explains the reason of higher removal rate with respect to the anode compared to that of cathode at short discharge durations in macro EDM. In this work, the longest discharge duration of micro EDM process to be used is significantly shorter than the discharge duration that was used in the macro EDM as in [29]. Based on this reason, the material removal rate might be significantly low when the workpiece of micro EDM is held at negative polarity of the pulse generator.

Thus, for practical use of micro EDM, the workpiece is held at positive polarity. It might be difficult to observe the cathode workpiece deformation because it may require significantly longer machining time compared to that of anode workpiece to be machined to a certain size and geometry where the workpiece begins to deform. Therefore, in this work the workpiece is mostly held at positive polarity of the pulse generator to understand the thermal phenomena of micro EDM.

Method to obtain the energy distribution ratios into electrodes in the case of macro EDM has been reported in [26-30]. As shown in **Figure 2.1** b. the energy into workpiece is then lost due to heat conduction, carried away by debris, and lost due to convection and radiation. At the same time, energy into tool electrode is distributed similarly, but at different amount.

In order to determine the ratio of energy loss due to heat conduction, in the first step a single discharge is ignited between the tool electrode and workpiece. The temperature rise within the workpiece is measured at one location. Then, the temperature rise is calculated at the same location by a numerical method, with an assumed ratio of energy loss due to heat conduction within the workpiece, X_{con}. The calculation is repeated for different values of X_{con} until the result coincides with the measured temperature, which means X_{con} is now equal to the ratio of energy loss due to heat conduction within the workpiece.

Xia et al. [26] found that under the same assumption of energy distribution ratio, calculated temperatures at several locations with different distances from discharge point coincide well with the corresponding measured results. Based on this finding, they suggested that it is reasonable to neglect the energy loss due to convection and radiation from the electrode surfaces.

On the other hand, the energy carried away by debris during macro EDM was calculated based on the measured removal volume from the workpiece comprising both volumes of removal by vaporization and by melting [26]. However, the specific volumes of removal by vaporization and by melting have never been obtained separately. Based on the fact that more energy is consumed to vaporize the material compared to melt it, Xia et al. [26-29] calculated the maximum energy carried away by debris by assuming all the debris material is removed by vaporization.

The ratio of energy carried away by debris, X_{deb} is then determined by dividing the calculated energy carried away by debris with the discharge energy. Xia et al. [26-29] found that the energy carried away by debris is negligibly small compared to the energy loss due to conduction even when the debris is assumed to be completely removed by vaporization. **Figure 2.1** b. indicates the percentages of energy lost due to heat

conduction, carried away by debris, and lost due to convection and radiation with respect to the discharge energy in the case of macro EDM [28].

The energy distribution ratios into micro EDM electrodes have never been reported yet. In this work, the similar principle as in [26-31] is used to determine the energy distribution ratios. However, several difficulties are expected in the case of micro EDM compared to the work done in [26-31] due to extremely short discharge durations, low discharge energy and no comprehensive information on plasma size.

As discussed in **Chapter 1**, based on the report by Hayakawa et al. [31] and Kojima et al. [43], the ratio of energy distributed into the micro EDM gap can be expected to be comparatively larger than that into the electrodes. Thus, energy distribution ratios into micro EDM electrodes are expected to be lower than those of macro EDM. On the other hand, there is a possibility that energy carried away by debris cannot be ignored compared with the energy loss due to heat conduction within micro EDM workpiece. Hence, the energy distribution ratio into workpiece should be determined based on the summation of the energy distribution ratios due to heat conduction into electrode and the heat carried away by debris.

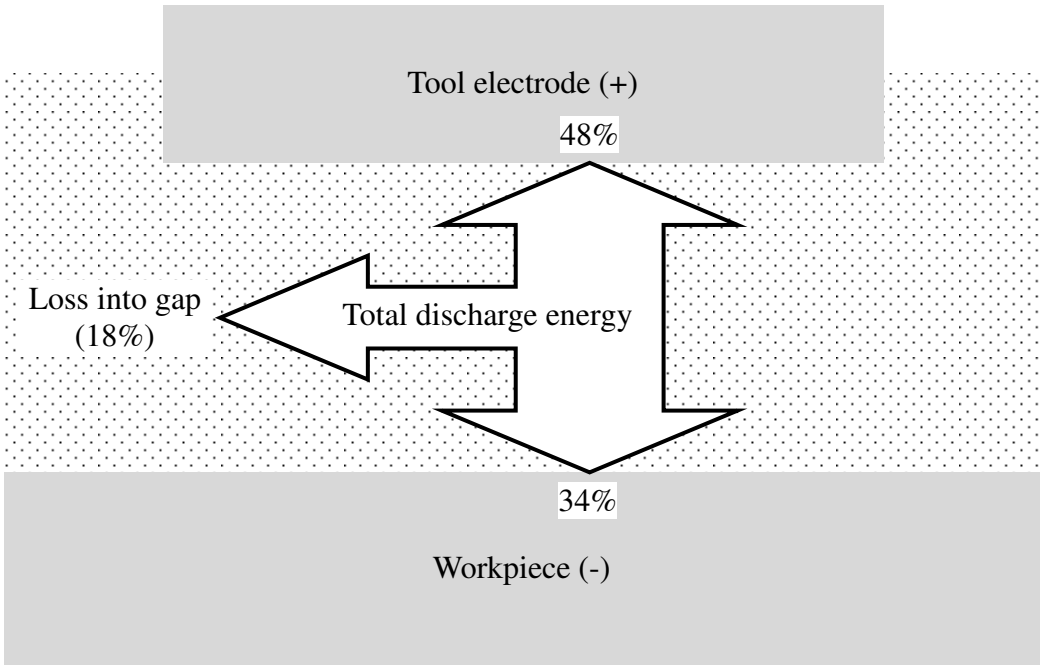

a. Total discharge energy distribution

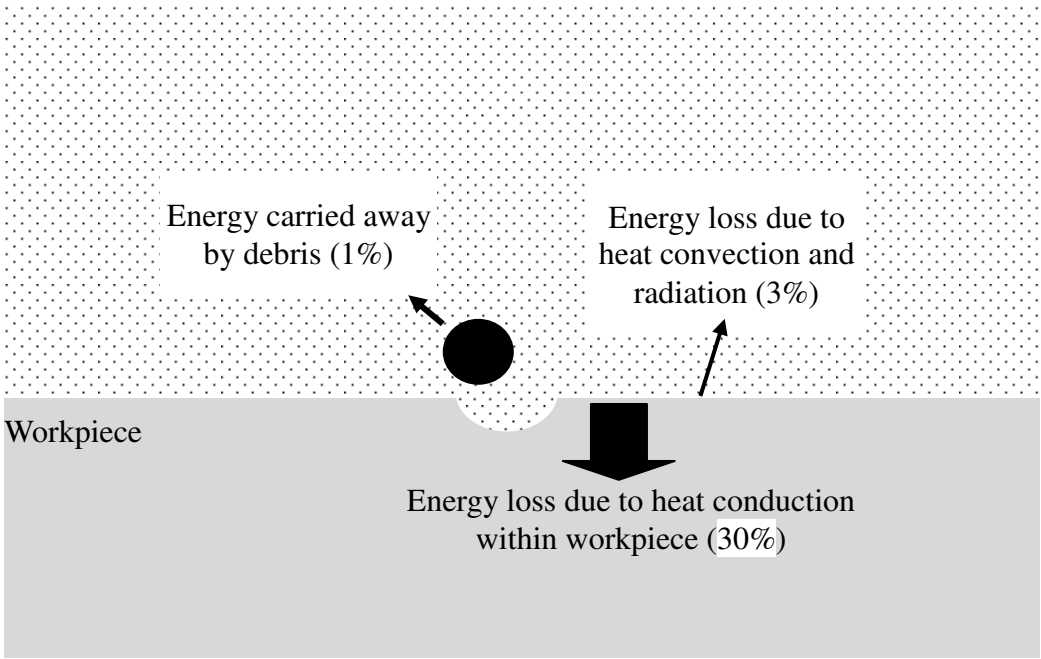

b. Energy distribution into workpiece

Figure 2.1: Distribution of discharge energy during macro EDM process

2.2 Principle of measurement of energy distribution ratio

In this work the energy distribution ratio into electrodes is determined based on the summation of the ratio of energy loss due to heat conduction and the ratio of energy carried away by debris. This is because the energy loss due to heat convection and radiation is negligibly small [31, 41, 42]. To support this assumption, comparison of measured and calculated temperature rises at several locations will be made to assure no heat convection and radiation between these points.

The energy loss due to heat conduction within electrode is determined by comparing measured and calculated temperature rise on the workpiece. The measured result is obtained using a thermocouple made of constantan wire and the workpiece's material. Then the temperature rise on the workpiece is calculated using finite difference method through a physical model which is built using a numerical analysis software i.e. PHOENICS.

As mentioned in **§ 2.1**, short discharge durations and low discharge energy result in several difficulties to determine the energy distribution ratio in the case of micro EDM compared to the case of macro EDM. Especially, the discharge energy in the case of micro EDM that results from a single pulse discharge normally is in the order of 1 μJ which is so small, while it is in the order of 10^3 μJ in the case of normal macro EDM.

Consequently, the signal of the temperature rise is so weak and might not be correctly detectable if the distance of the discharge location relative to the thermocouple junction is too long. However, the distance between the measurement junction and discharge location also could not be made too short due to two reasons.

First, the thermocouple amplifier is affected by electromagnetic noise due to the electrical discharge. Xia et al. [29] determined energy distribution into macro EDM electrodes by measuring temperature rise at a location more than 1 mm distanced from the discharge location. The result shows that the temperature measurement device only worked well 2 ms after the occurrence of the single discharge due to the electromagnetic noise. If the distance was not sufficiently long the temperature rise may reach its peak within the region which is affected by the electromagnetic noise. Consequently, the temperature peak cannot be measured correctly and unable to be compared with the calculated result which leads to a low reliability of the obtained result.

Secondly, plasma diameter in the case of micro EDM process is unknown and it cannot be observed and measured using the high speed camera (1 million frames per second at the maximum) and spectroscopic analysis which were used in the case of macro EDM [43], due to extremely short discharge durations and low discharge energy.

Therefore, the distance between measurement point and discharge location must be made sufficiently long so that the simulation result is not affected by the assumed plasma diameter. In this work however, discharge durations are shorter than 200 ns. Thus, the temperature signal of micro EDM is expected to be so weak and may not be detectable if only single pulse discharge is ignited at a location that is sufficiently far from the thermocouple junction. As a solution, instead of single pulse, multiple pulses discharges must be ignited at a sufficiently long distance from thermocouple junction so that higher discharge energy can be delivered, and then adequate temperature rise signal and its peak could be measured in the region that is not affected by the electromagnetic noise due to discharges.

Figure 2.2 shows a flowchart which indicates the method to determine energy distribution ratio into electrode. Initially, multiple pulses discharges are ignited between micro EDM electrodes, and then the temperature rise on the electrode is measured using an oscilloscope. Other results of experiment i.e. i_e and u_e are also measured simultaneously using the same oscilloscope.

Based on the discharge current measurement results, the discharges timing, discharge duration and discharge interval can be determined. Then, by using a microscope the distance between discharges location and temperature measurement junction are measured. These parameters are then used to develop the physical model to calculate the temperature rise on the electrode.

To determine the ratio of energy loss due to heat conduction within electrode, an assumption of energy distribution ratio, X_{con} = energy loss due to heat conduction within electrode / discharge energy, is required. Calculation of the temperature rise on electrode will be repeated by varying the assumed value of X_{con} until the calculated temperature rise, $T_c(t)$ coincides with the measured temperature rise, $T_m(t)$ which means X_{con} is now equal to the ratio of energy that is lost due to heat conduction within electrode.

The ratio of energy carried away by debris, X_{deb} = energy carried away by debris / discharge energy, is calculated based on the measured electrode removal volume. Side surface of a rotating Cu electrode is machined by igniting more than a million discharges using WEDG. The volume of the electrode before and after machining is measured using an optical microscope to obtain the removal volume. The removal volume per pulse, V is then used to calculate the energy carried away by debris. Thus, X_{deb} can be obtained by dividing the energy carried away by debris by the discharge energy. Then, the energy distribution ratio into electrode, X is determined from the summation of X_{con} and X_{deb}.

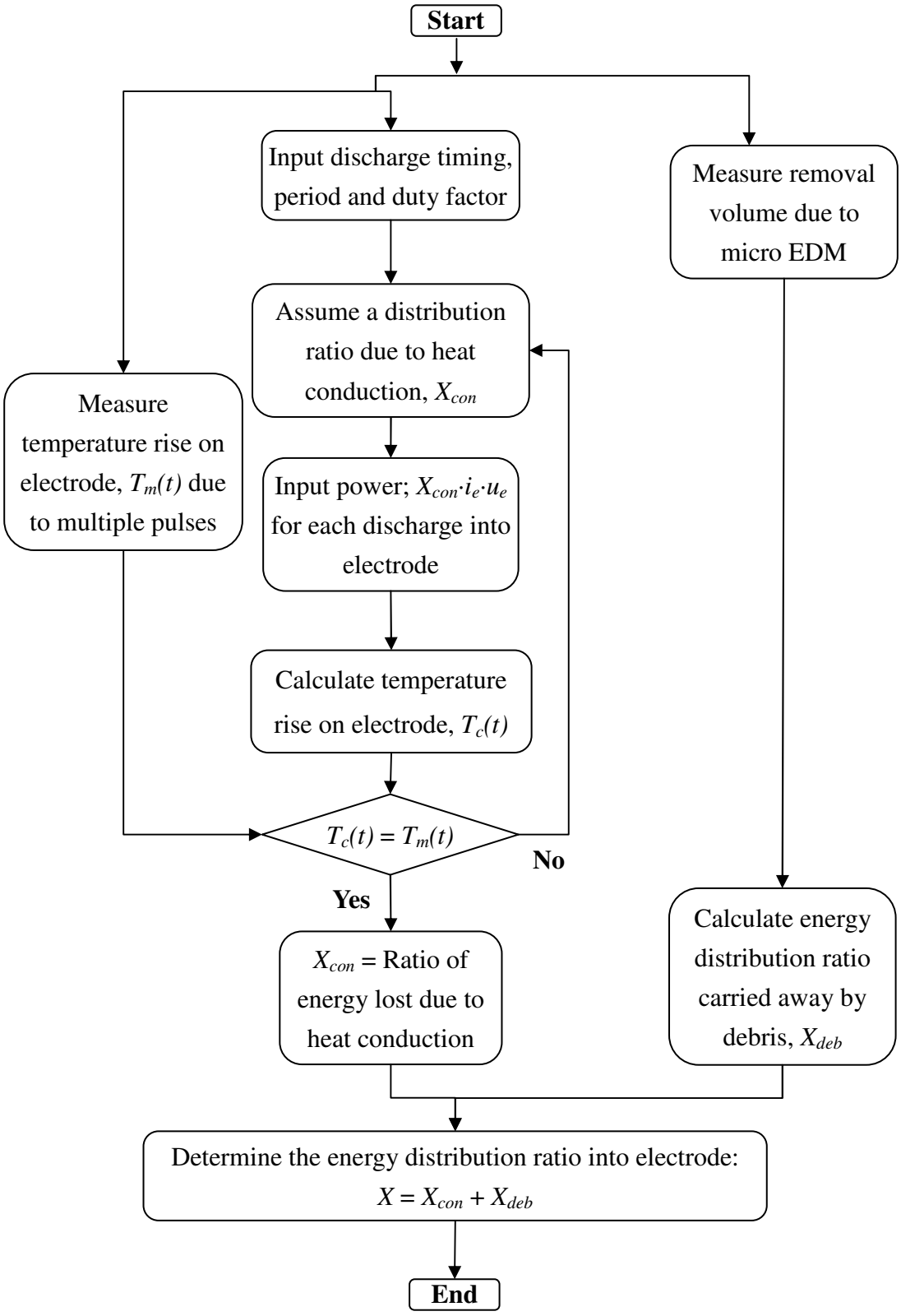

Figure 2.2: Overview of method to determine energy distribution ratio into electrode

2.3 Ratio of energy loss due to heat conduction

In this work, only combination of tool electrode and workpiece made of copper was considered. Hayakawa et al. [69] found that higher heat conductivity of electrode results in higher energy distribution into the electrode. This indicates that, different combinations of electrodes' material result in different energy distribution ratios. Qualitatively however, the dependence of the energy distribution ratio on the conductivity will not affect the results of comparison between micro and macro EDM.

The main idea in this work is to determine main parameters of micro EDM thermal phenomena and then they are compared with the case of macro EDM, and not to compare the parameters at different machining conditions within the range of micro EDM setting. This is because Xia [70] and Hayakawa [31] found that there is no different in the parameters including the energy distribution ratios into electrodes with respect to machining conditions within the range of normal EDM and EDM with extraordinarily long discharge durations, respectively. At the end of this chapter the correlation of results obtained in this work with those of normal EDM conditions and EDM with extraordinarily long discharge durations will be discussed.

In this work, although in most cases the machining conditions were fixed at one setting, the machining conditions at different settings were also tested by changing the capacitor setting while determining the ratio of energy lost due to heat conduction within electrodes which was one of the most important parameters in this work.

In this experiment an apparatus that produces discharges with conditions similar to those of micro EDM machines available in market comprised of relaxation type pulse generator and precision xyz table to control tool electrodes movement has been used. Measurements of temperature rise due to discharges which are produced by the apparatus were repeated in a great numbers until consistent results were obtained, and then compared with iterative calculations based on simulations.

2.3.1 Temperature rise measurement

An adequate amount of discharges must be ignited on the workpiece at a sufficiently long distance from the thermocouple junction. This is because the peak of the temperature rise must be measured correctly in order to increase the reliability of the obtained results. On the other hand, it is desirable to use the setup with Cu foil as done by Xia et al. in [29] because it represents common process of micro EDM where micro tools are used to drill micro holes with high aspect ratio on a significantly larger workpieces compared with the tool electrodes.

However, the number of pulses which can be ignited on the Cu foil workpiece are limited otherwise the foil could be penetrated. This means amount of discharge energy which can be distributed at Cu workpiece surface is limited. If, on the other hand, the foil thickness is large, the temperature rise on the reverse side of the foil is low because the heat is conducted not only in depth but also in the radial direction in the foil. Hence, Cu wire was also used in this work in order to determine the ratio of energy loss due to heat conduction within the workpiece. Since the heat conduction is one dimensional, the temperature rise can be high even if the thermocouple junction is located far from the end of the wire where multiple discharges are ignited.

Figure 2.3 shows experimental setup for temperature rise measurement on Cu foil workpiece. This setup was similar to that was used by Xia et al. in [29]. The setup was mainly consisting of a copper needle electrode with Ø0.3 mm in diameter, and 0.05 mm thickness Cu foil workpiece with Ø20 mm in diameter. These electrodes were connected to a pulse generator consisting of a DC power supply, a 1 kΩ resistor and a capacitor where the capacitances were varied from 68 pF to 6800 pF.

Temperature rises on the Cu foil workpiece were measured at a junction between a constantan wire and the workpiece material which forms a type-T thermocouple (thermocouple that is built based on the combination of constantan and copper materials). The signal of the temperature rise which was captured by this thermocouple junction was amplified by the thermocouple amplifier model AD594A, and then sent to an oscilloscope. In order to reduce the effect of electromagnetic noise from surrounding, the thermocouple amplifier, AD594A was installed inside a steel shieldbox. A picture of AD594A which was installed in the steel shieldbox is shown in **Figure 2.4**.

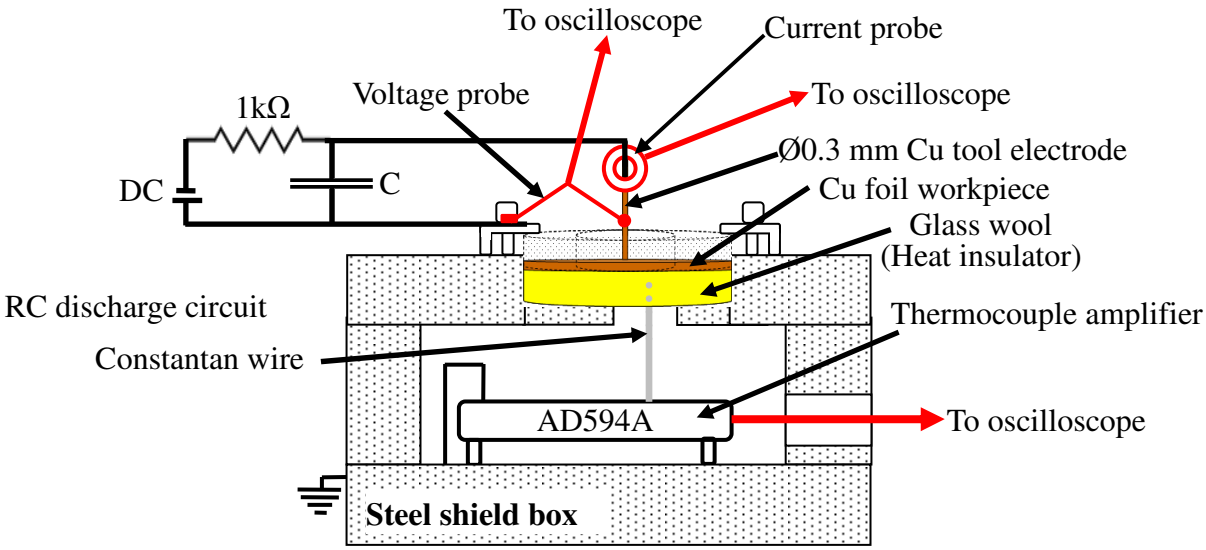

a. Overview of the experimental setup for Cu foil workpiece

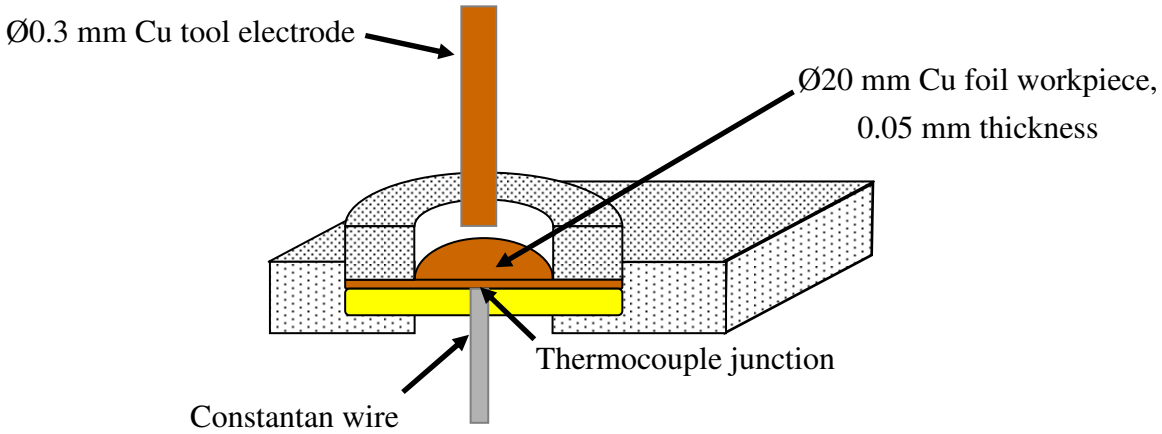

b. Magnification of electrodes' cross-sectional area

Figure 2.3: Experimental setup for temperature measurements on Cu foil workpiece

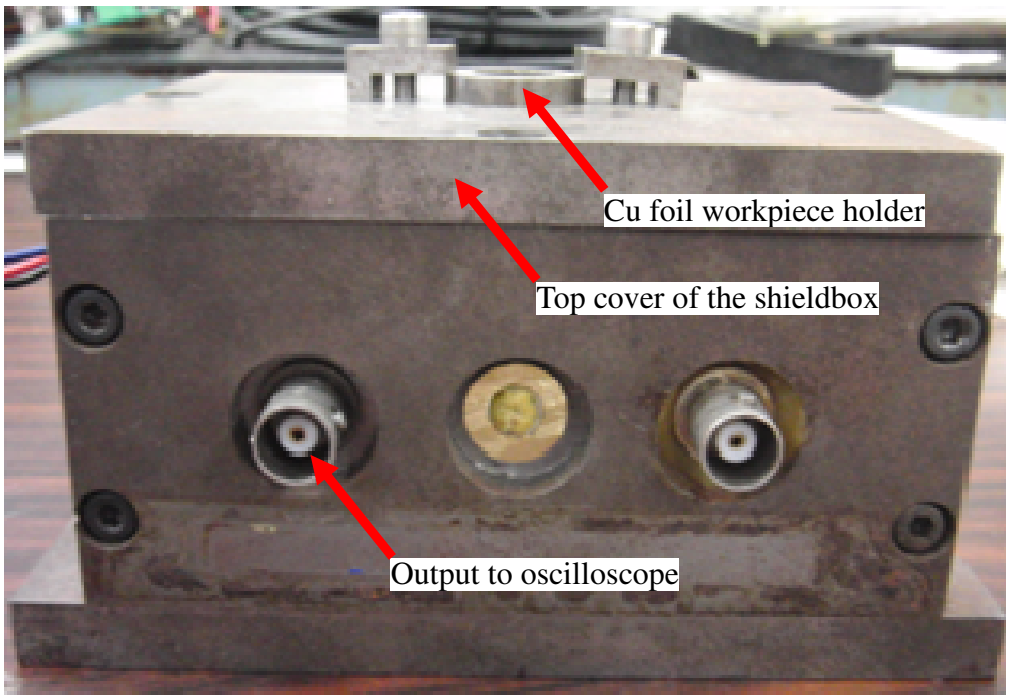

a. Side view of the steel shieldbox from outside

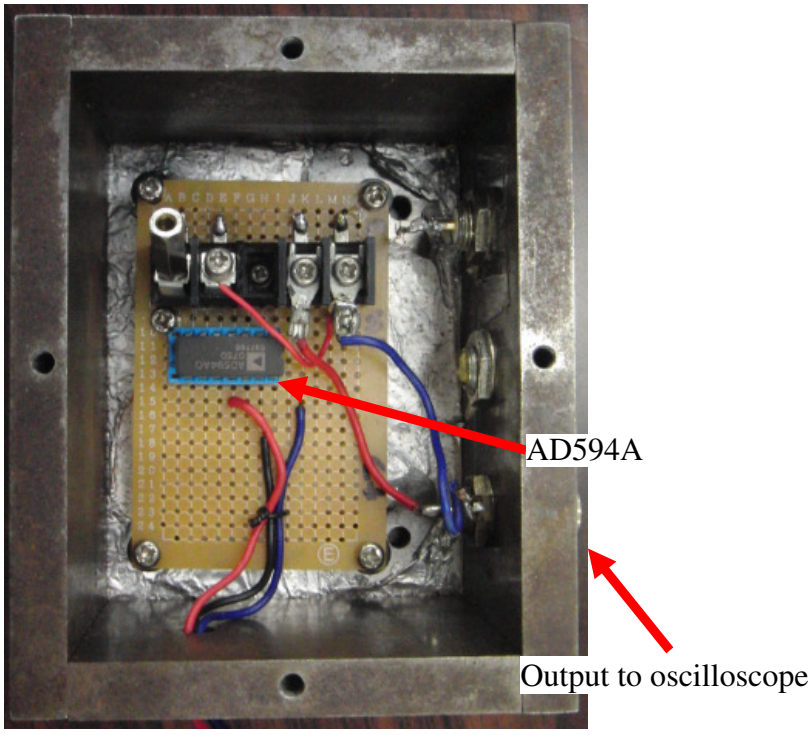

b. Top view of the steel shieldbox and the thermocouple amplifier AD594A inside the steel shieldbox

Figure 2.4: Steel shieldbox to reduce the effect of electromagnetic noise due to discharge

Although it was possible to measure the temperature rise from both tool electrode and workpiece simultaneously, to simplify the experimental setup only temperature rise on workpiece was measured. The workpiece polarity was changed accordingly so that energy distribution ratios into both anode and cathode workpiece could be determined.

First, the Cu foil workpiece and tool electrode were held at positive and negative polarity of the pulse generator, respectively to determine the temperature rise on anode workpiece. The tool electrode was manually moved downwards approaching the top surface of the Cu foil workpiece at the centre point of the foil. The electric field between the tool electrode and workpiece became stronger at narrower gap, and finally the electrical insulation within the gap between the electrodes broke and multiple pulses discharges were ignited.

During discharging, besides measured temperature, $T_m(t)$ the discharges conditions; discharge voltage, u_e and discharge current, i_e were also measured using the same oscilloscope. The oscilloscope readings of the $T_m(t)$, u_e and i_e are shown in **Figure 2.5** a. The data of the measured temperature were then used to create the temperature curve as shown in **Figure 2.5** b. This curve was compared with the calculated temperature rise, $T_c(t)$ in order to obtain the ratio of energy loss due to heat conduction, X_{con}. On the other hand, the measured discharge conditions were used to calculate the temperature rise on the workpiece.

In **Figure 2.5** the measured temperature rise, $T_m(t)$ seems to reach its peak after the overrange reading due to electromagnetic noise. However, there is a possibility that the temperature may reach its peak earlier; within the period where the temperature measurement was affected by the electromagnetic noise. This will be observed later in **§ 2.3.3** by comparing $T_m(t)$ with the calculated temperature rise, $T_c(t)$.

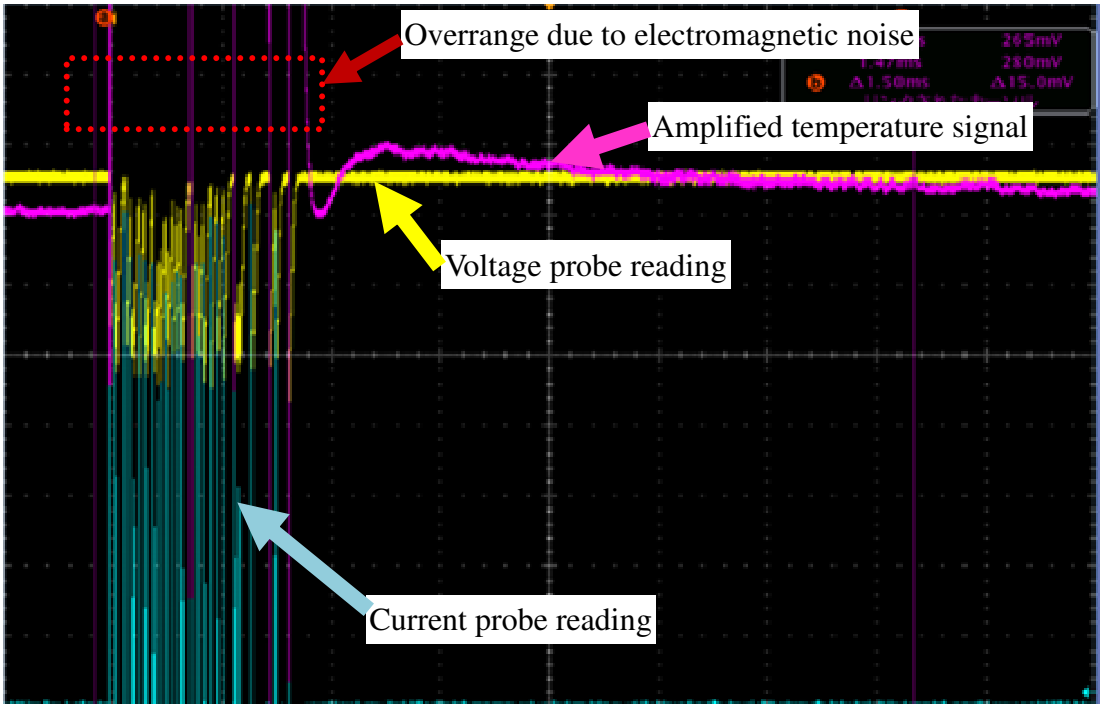

a. Oscilloscope reading

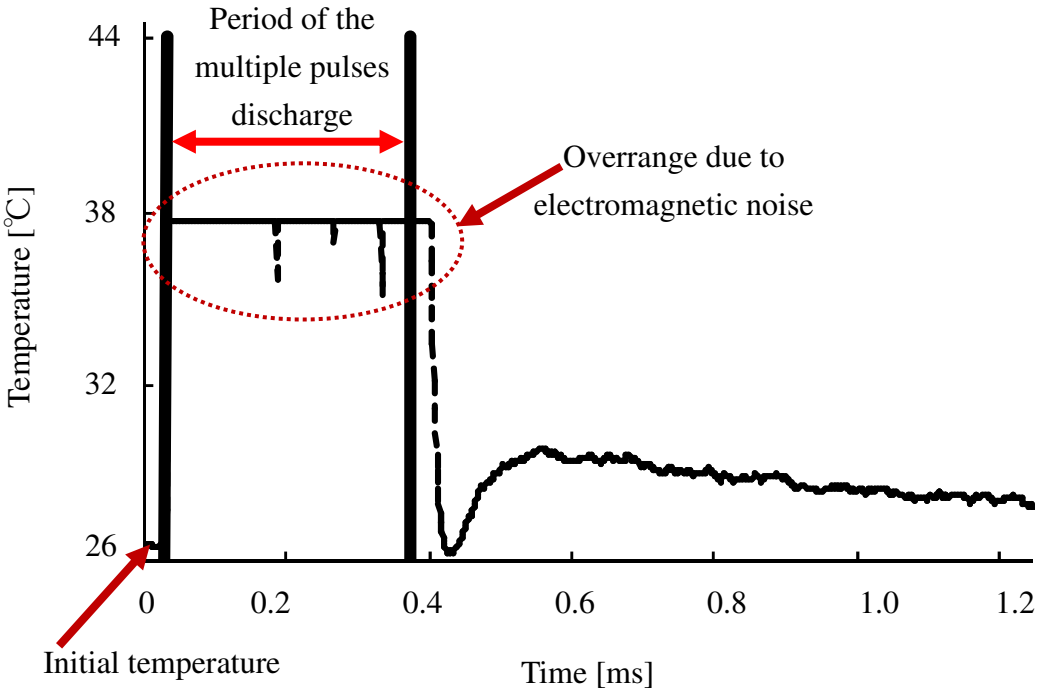

b. Temperature curve

Figure 2.5: Measurement of temperature rise and discharges conditions using an oscilloscope

Because the relative distances between discharges location and thermocouple junction should be made sufficiently long so that the peak of the temperature rise could be detected correctly, more discharges must be ignited so that sufficient temperature rise could be detected. Furthermore, the ratio of the Cu foil diameter with respect to the foil thickness is high, which means, more heat was dissipated in the radial direction rather than in the thickness direction of the Cu foil. Therefore, it might be difficult to obtain a sufficiently high temperature rise at the thermocouple junction using this setup.

Consequently, peak of the temperature rise may not be captured from the Cu foil workpiece setup and this leads to a low reliability of the obtained result. On the other hand, instead of Cu foil, Cu wire was also used as a workpiece so that more energy from discharges location could reach the thermocouple junction because the ratio of diameter to length of the wire is significantly smaller than the ratio of diameter to thickness of the foil, which means most of the energy will flow in the length direction in the case of Cu wire workpiece.

In addition, better quality of thermocouple junction could be prepared in the case of Cu wire workpiece because instead of welding the constantan wire on the workpiece as in the case of Cu foil which may thermally alter the micro structure of the materials at the joint area, heat insulation material (Teflon tape) can be used to tight up the constantan wire with the Cu wire workpiece which keeps the original condition of the materials at the thermocouple junction.

Figure 2.6 shows experimental setup for temperature rise measurement on the Cu wire workpiece. Compared to the set up that was shown in **Figure 2.3**, only the Cu tool electrode and the workpiece geometries and sizes were different. Here, Ø1.0 mm Cu tool was moved towards Ø0.3 mm Cu workpiece until multiple pulses discharges were ignited between those electrodes. In this setup, the precision xyz table as shown in **Figure 2.6** c. was used to control the tool movement.

Compared to the setup with Cu foil workpiece, more discharges can be ignited in the case of Cu wire workpiece. In the case of Cu foil workpiece, about 50 to 100 pulses discharges were ignited. On the other hand, in the case of Cu wire workpiece, more than 1000 pulses discharges were ignited. Furthermore, the relative distance between discharges location and thermocouple junction in the case of Cu wire workpiece was about 10 to 20 times longer than that of Cu foil workpiece.

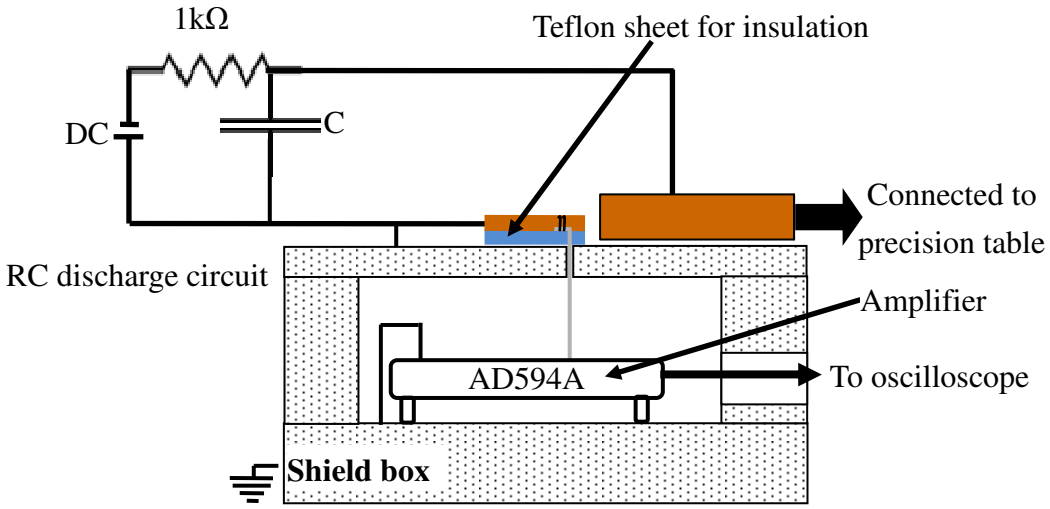

a. Overview of the experimental setup for Cu wire workpiece

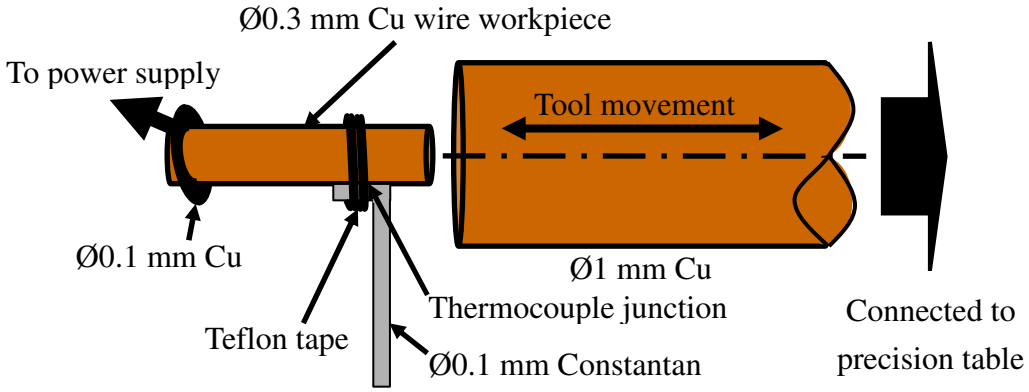

b. Magnification of electrodes area

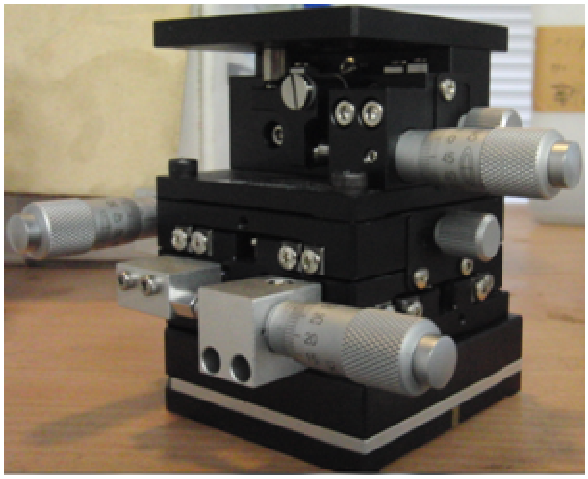

c. Precision xyz table used to control tool movement

Figure 2.6: Temperature measurements on Cu wire workpiece

The measured results in the case of Cu wire workpiece are shown in **Figure 2.7**. The oscilloscope reading of $T_m(t)$, u_e and i_e are shown in **Figure 2.7** a. **Figure 2.7** b. and c. show the temperature curve and discharge current and voltage created from the measured results, respectively. The next step is to calculate the temperature rise, $T_c(t)$ based on the measured machining conditions, the measured distance between discharges location and thermocouple junction, and the assumed ratio of energy lost due to heat conduction, X_{con}. Then, X_{con} is varied until $T_c(t)$ coincides with $T_m(t)$ to obtain the ratio of energy loss due to heat conduction within the workpiece.

.

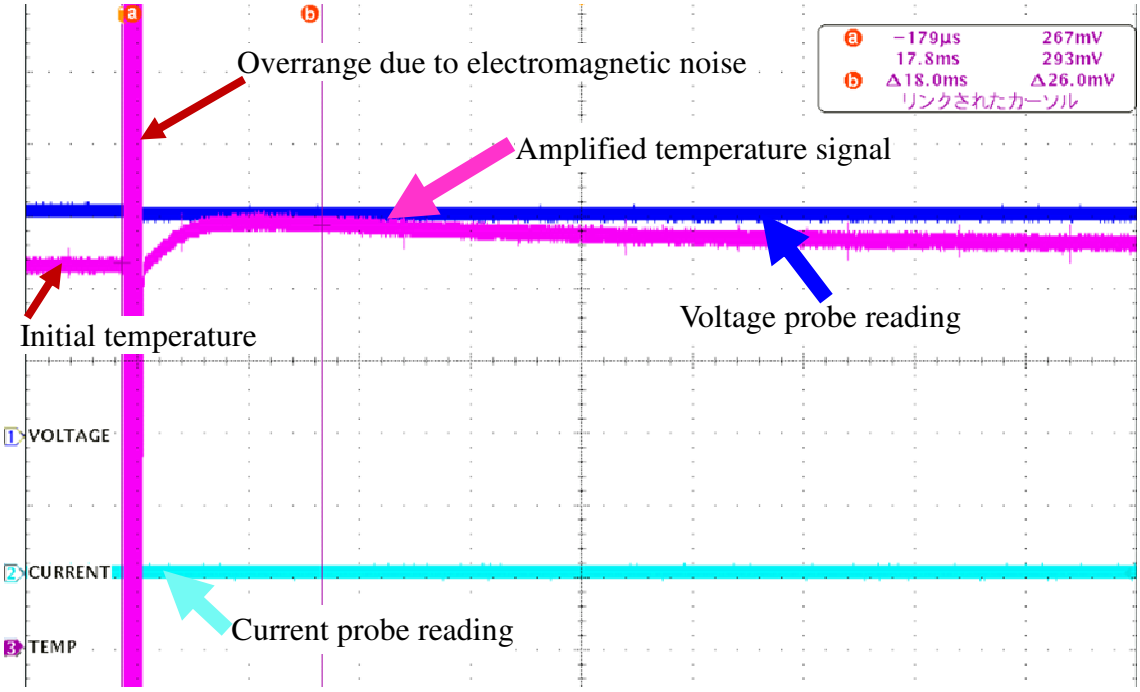

a. Oscilloscope reading

Figure 2.7: Measurement of temperature rise and discharges conditions for Cu wire workpiece

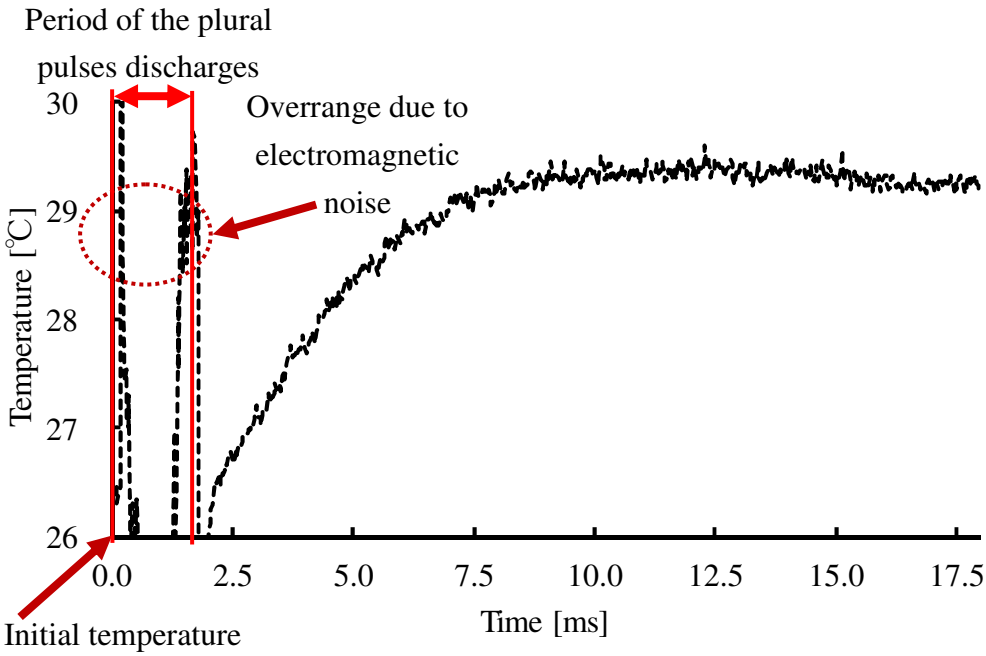

b. Measured temperature curve

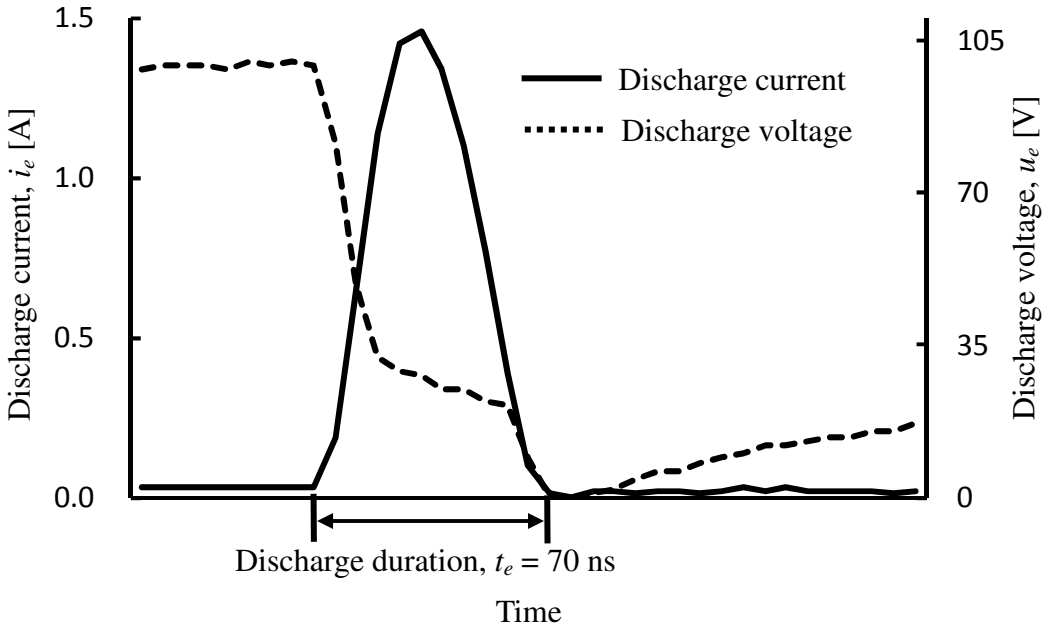

c. Discharge current and discharge voltage of one pulse

Figure 2.7: Measurement of temperature rise and discharges conditions for Cu wire workpiece

2.3.2 Temperature rise calculation

Figures 2.8 a. and b. show physical models which were developed using a numerical software namely PHOENICS in order to calculate the temperature rise within Cu foil and Cu wire workpiece, respectively. The Cu foil was modeled as a thin circular foil with Ø12 mm in diameter and 0.05 mm in thickness. Calculation area for the Cu foil was smaller than the actual size of Ø20 mm in diameter because temperature did not change during the measurement time in the outside region. Therefore, it was assumed that the circumferential boundary remains at room temperature. On the other hand, Cu wire workpiece was modeled similar to the actual size, where the diameter and length was Ø0.3 mm and 5.0 mm, respectively.

In fact, there was no significant difference between constantan wire diameter and workpieces size; Cu foil thickness and the Cu wire diameter. Hence, heat conduction within the constantan wire was expected to be significant. Thus, constantan wire was also included in the calculation model. A constantan wire with Ø0.10 mm in diameter and 0.75 mm in length was attached at the bottom-centre of Cu foil as shown in **Figure 2.8** a. Although the actual length of the constantan wire was longer than 50 mm, it was sufficient to set 0.75 mm within the model because calculation results showed no temperature change beyond this point. As shown in **Figure 2.8** b., the length of the constantan wire was set 1.7 mm within the model of the Cu wire workpiece which was less than the actual size due to the same reason as in the case of Cu foil workpiece. In the figure, the distance between discharges location and constantan wire, a and the length of the constantan wire that was in contact with the Cu wire, b was modeled according to the result of measurement using an optical microscope, where the range of a and b was 0.5 mm to 1.0 mm and 0.7 mm to 1.3 mm, respectively.

In this work, all the surfaces within the analysis domain were assumed adiabatic except at discharges location and the thermocouple junction. Part of the discharge energy of each pulse was lost due to heat conduction within the workpiece. Thus, the heat input due to each discharge at the discharges location was calculated based on the assumed ratio of energy loss due to heat conduction, X_{con} and the measured discharge conditions so-called heat flux; $q" = X_{con} \cdot i_e \cdot u_e / (\pi \cdot d^2/4)$, where d is plasma diameter. However, the actual size of plasma during discharging in micro EDM has never been reported. Therefore, the plasma diameter, d was assumed to be equal to or 10 times larger than the measured average size of the crater and constant during the discharge duration. Then the sensitivity of the calculation results with regard to d was investigated.

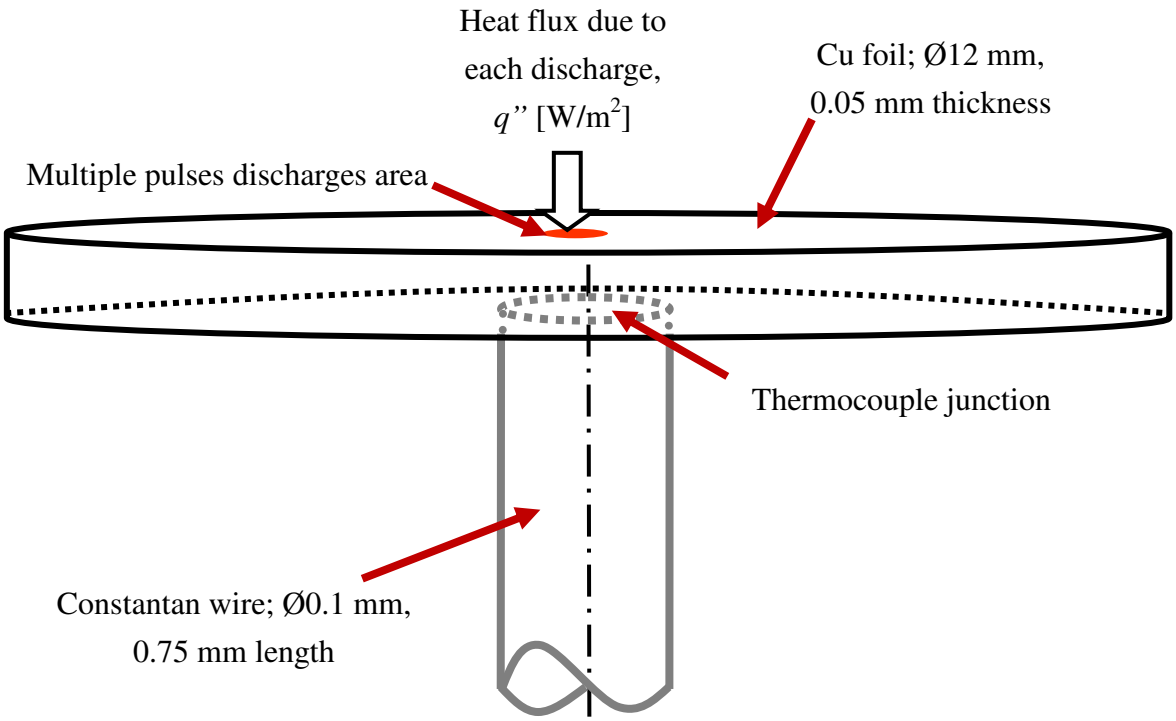

a. Calculation model for Cu foil

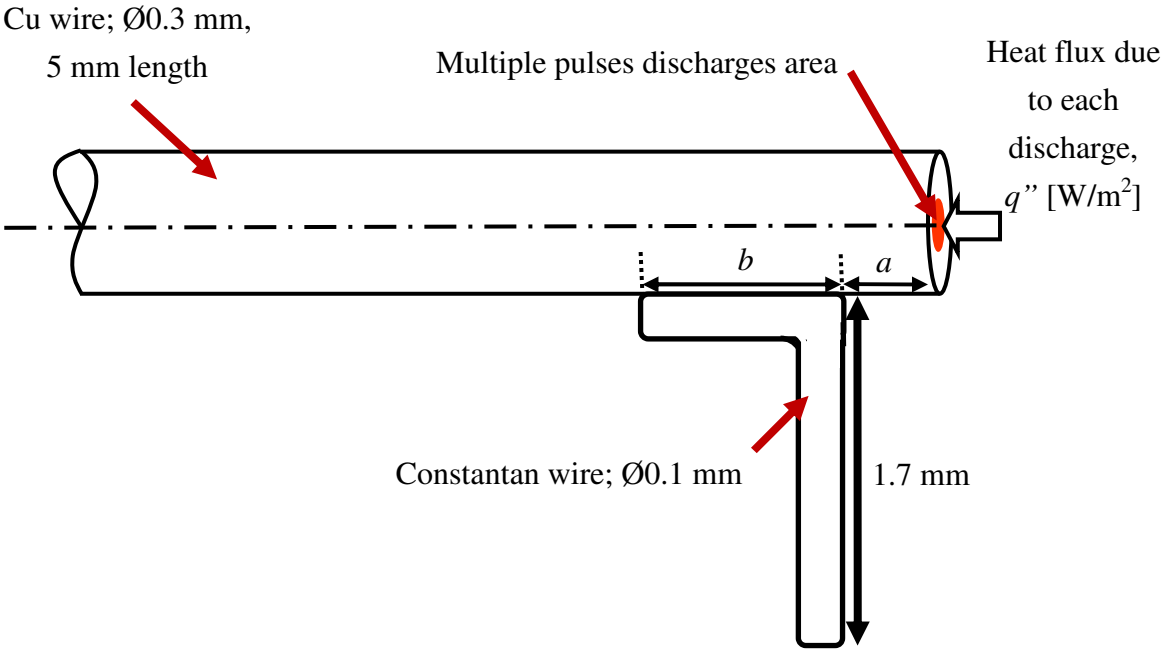

b. Calculation model for Cu wire

Figure 2.8: Temperature rise calculation on Cu workpiece

The measurement of the workpiece temperature is based on the output of the thermocouple which is determined by the temperature at the interface between the constantan wire and the Cu workpiece. However, the temperature is not uniform at the interface. Hence, the output of the thermocouple indicates the average temperature at the interface. Therefore, the measured temperature should be compared with the average of the temperature distribution calculated at the interface between constantan wire and workpiece within the model. In PHOENICS, workpiece temperature is calculated based on finite different method. The basic equations to calculate the workpiece temperature at the thermocouple junction are as follows:

Assuming the generation of heat in the workpiece is negligible, the temperature change within the workpiece can be calculated from the following equation for normal Cartesian coordinate with three-dimensional heat conduction:

$$\rho c\frac{\partial T}{\partial t} = \frac{\partial}{\partial x}\left(k\frac{\partial T}{\partial x}\right) + \frac{\partial}{\partial y}\left(k\frac{\partial T}{\partial y}\right) + \frac{\partial}{\partial z}\left(k\frac{\partial T}{\partial z}\right) \quad (2.1)$$

where, ρ is density, c is specific heat, k is thermal conductivity, T is workpiece temperature, and t is time.

If the thermal conductivity, k of the workpiece is assumed constant, above equation can be written as follows:

$$\frac{\partial T}{\partial t} = a\left(\frac{\partial^2 T}{\partial x^2} + \frac{\partial^2 T}{\partial y^2} + \frac{\partial^2 T}{\partial z^2}\right) \quad (2.2)$$

here, a ($\equiv k/\rho c$) is so-called temperature diffusion rate.

Within the workpiece, if temperature and heat flow do not change in time or in steady state, $\frac{\partial T}{\partial t}$ is equal to zero and Equation 2.2 becomes:

$$\frac{\partial^2 T}{\partial x^2} + \frac{\partial^2 T}{\partial y^2} + \frac{\partial^2 T}{\partial z^2} = 0 \quad (2.3)$$

However, transient heat conduction needs to be solved in this work, where the temperature and heat flow change in time. It is difficult to solve three-dimensional transient heat conduction analytically. Thus, numerical method was used.

Here, $\frac{\partial T}{\partial t}$ in Equation 2.2 is not equal to zero and its approximation to finite difference equation can be written as follows:

$$\frac{\partial T}{\partial t} \approx \frac{T_{l,m,n}^{p+1} - T_{l,m,n}^{p}}{\Delta t} \tag{2.4}$$

where, l, m, n indicate spatial grid location or a point within the workpiece, and p indicates time step at a particular grid.

On the other hand, the finite difference approximation of the term in the right side of Equation 2.2 can be written and rearranged as follows (explicit method):

$$T_{l,m,n}^{p+1} = \Delta ta \left\{ \begin{array}{c} \frac{T_{l+1,m,n}^{p} - 2T_{l,m,n}^{p} + T_{l-1,m,n}^{p}}{\Delta x^2} + \frac{T_{l,m+1,n}^{p} - 2T_{l,m,n}^{p} + T_{l,m-1,n}^{p}}{\Delta y^2} \\ + \frac{T_{l,m,n+1}^{p} - 2T_{l,m,n}^{p} + T_{l,m,n-1}^{p}}{\Delta z^2} \end{array} \right\} + T_{l,m,n}^{p} \tag{2.5}$$

In order to increase the accuracy of the calculation, temperature dependent thermophysical properties should be considered. However, the temperature measurement point within the workpiece is comparatively far from discharges location. Furthermore, as shown in **Figures 2.5** b. and **2.7** b., the temperature rises was less than 5 K at the measurement point. Therefore, for now the temperature dependent thermophysical properties are not important. However, the study of temperature distribution at vicinity of discharges location in **Chapter 3** may require the consideration of temperature dependent thermophysical properties within the model.

2.3.3 Comparison of measured and calculated temperature rise

The measured and calculated temperature rises on the Cu foil and the Cu wire workpiece that were caused by multiple pulses discharges are shown in **Figure 2.9** a. and b., respectively. In the case of Cu foil anode, as shown in **Figure 2.9** a., by assuming that the plasma diameter was equal to the measured crater size and constant during discharge duration, calculated result at X_{con} = 5% coincided well with the measured result approximately after 0.7 ms of the measurement time.

As shown in **Figure 2.9** a., from 0.03 ms to 0.7 ms, there was inconsistency between calculated and measured results. Discharges were ignited 41 times approximately from 0.03 ms to 0.36 ms, and during this discharging period the inconsistency between the results was caused by the electromagnetic noise, and the later inconsistency was due to the malfunction of the thermocouple amplifier which was unable to work well just immediately after the overrange load was removed.

In this work, it is most desirable that the peak of the temperature rise could be measured correctly and compared with the calculated result. However, as shown in **Figure 2.9** a. the calculated temperature rise reaches the maximum values in the region where the measured temperature rise was affected by the electromagnetic noise due to the multiple pulses discharge. The measured and calculated temperature gradient could be compared only at the time sufficiently long after the multiple pulses discharges, and this leads to low reliability of the results.

In order to increase the reliability of the results, more discharge arcs were ignited at longer distances relative to the thermocouple junction by using Cu wire as a workpiece. As shown in **Figure 2.9** b., calculated results at X_{con} approximately 6.02% and 3.25% coincided with the measured temperature rise on anode and cathode, respectively. As shown in the figure, the peaks of the measured and calculated temperature rise could be compared and this indicates the reliability of the result was better than that of Cu foil workpiece. In this work, the X_{con} was between 5 and 7%, and 2 and 4% in the case of anode and cathode workpiece, respectively. In this example 1000 pF capacitor was used. Other examples of comparison between measured and calculated temperature rise using different capacitors are shown in **Appendix A**.

In both Cu foil and Cu wire workpiece, the results of the ratio of energy loss due to heat conduction within electrodes were almost similar. The slight difference of the ratio may be caused by the effect of the plasma diameter assumption during temperature rise calculation and/or the effect of the distance between discharges location and thermocouple junction which will be discussed in **§ 2.3.4**.

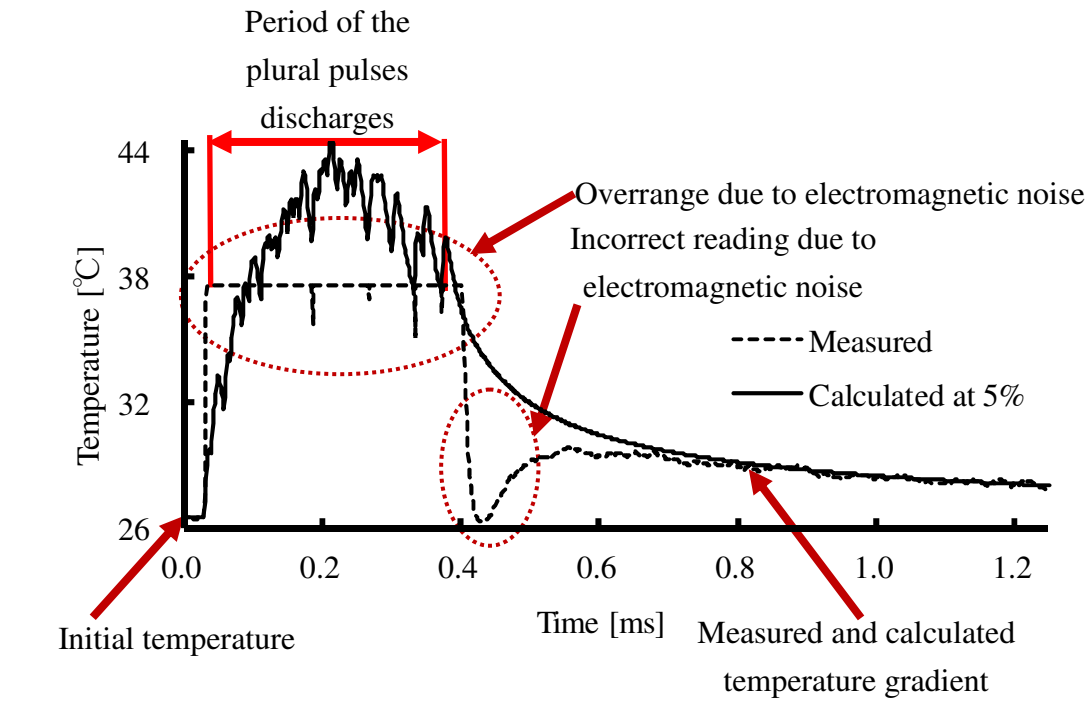

a. Cu foil workpiece (anode)

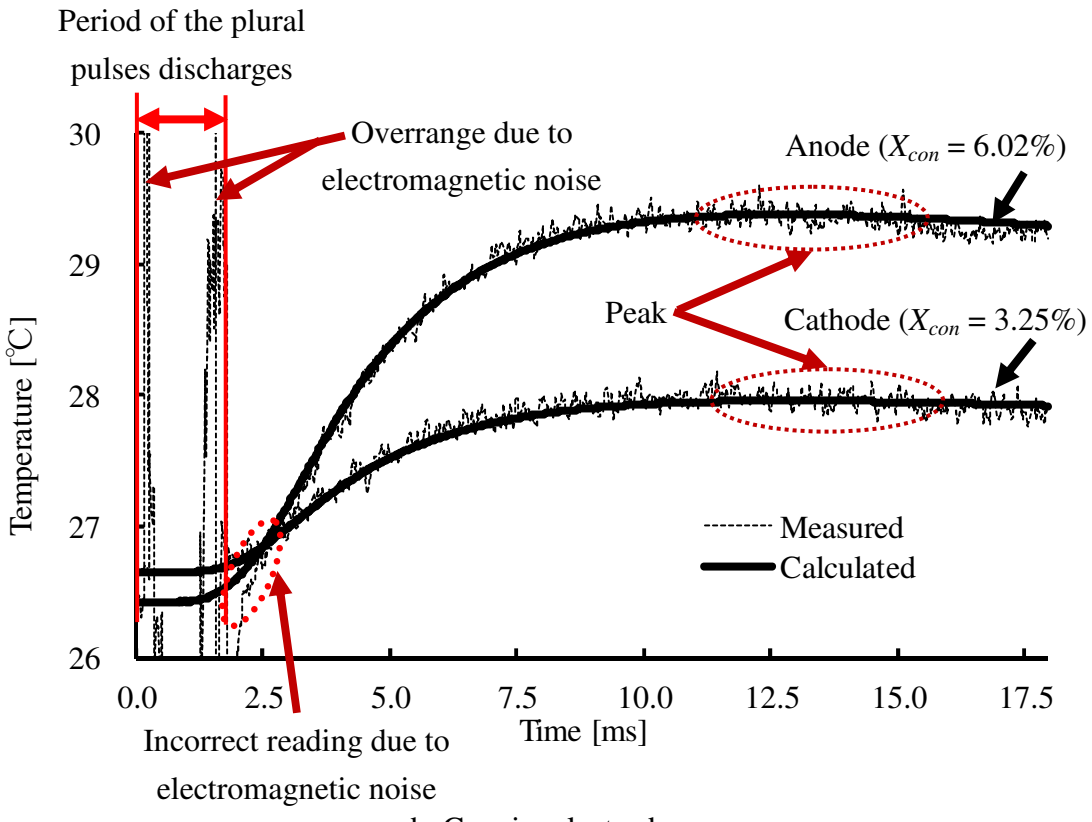

b. Cu wire electrodes

Figure 2.9: Comparison of measured and calculated temperature rise on workpiece

2.3.4 Factors influencing calculation

In order to increase the reliability of the obtained results, a couple of factors which were expected to influence the results were investigated. The first was the effect of the assumed plasma diameter on the temperature calculation. The second was the effect of the relative distance between discharges location and thermocouple junction on the ratio of the energy loss due to heat conduction. This is because some amount of heat may be lost over the electrode surface due to heat convection.

Figure 2.10 shows the effect of assumed plasma diameter on temperature rise calculation. In the case of Cu foil as shown in **Figure 2.10** a., when plasma diameter was assumed 100 μm which was 10 times larger than the measured crater diameter, the calculation result became higher than the result when the plasma diameter was assumed equal to 10 μm. The main reason was the distance between thermocouple junction and discharges location within the calculation model not sufficiently long.

On the other hand, in the case of Cu wire workpiece as shown in **Figure 2.10** b., the calculation result was not affected by the assumed plasma diameter at all. This results from sufficiently long distance between discharges location and thermocouple junction which was 10 to 20 times longer than the case of Cu foil workpiece.

Besides, the effect of distance between discharges location and thermocouple junction on the ratio of energy loss due to heat conduction at Cu wire workpiece was also investigated. First, the temperature rise was measured at two different locations on the Cu wire workpiece. Then, the temperature rise on Cu wire workpiece at both locations was calculated to be compared with the measured results.

Figure 2.11 shows the comparison of measured and calculated temperature rise at 1.59 mm and 0.88 mm distance between thermocouple junction and discharges location. As shown in the figure, the measured temperature rise coincides with the calculated one when the ratio of energy loss due to heat conduction, X_{con} was assumed approximately 3% in both cases. This means the energy lost due to heat convection or radiation within the distance between both locations is negligibly small, and thus the ratio of energy that is lost due to conduction within electrode is not sensitive to the relative distance between discharges location and thermocouple junction in the case of Cu wire.

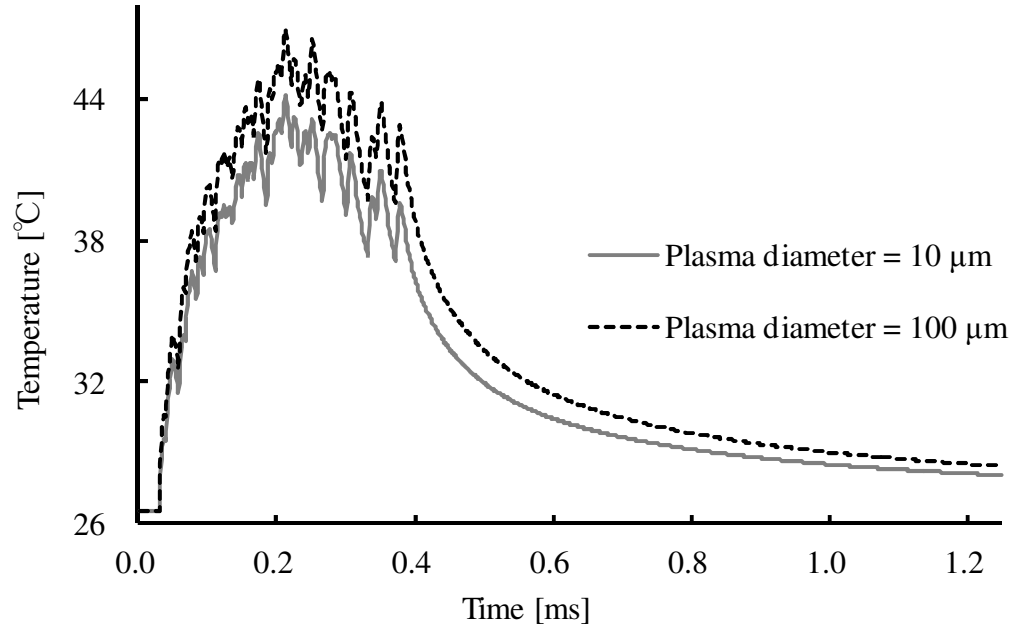

a. Cu foil workpiece

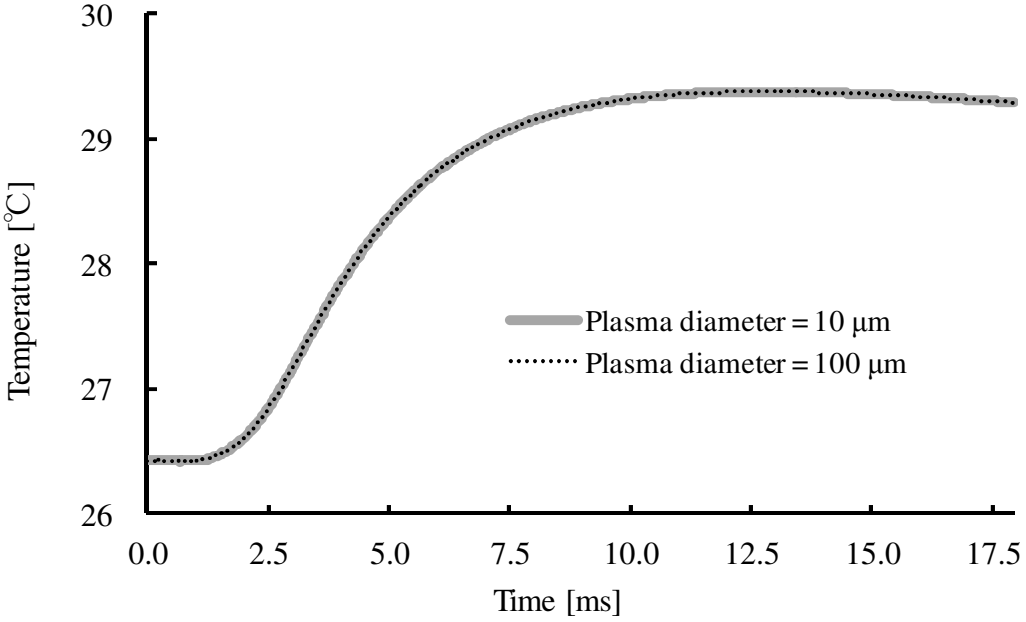

b. Cu wire workpiece

Figure 2.10: Effect of assumed plasma diameter on temperature rise calculation

In addition, the temperature rise due to single pulse discharge in micro EDM was also investigated. When igniting single pulse discharge on Cu foil workpiece the correct temperature signal was undetected. **Figure 2.12** shows the comparison of the measured and calculated temperature rise on the micro EDM Cu foil workpiece when a single pulse discharge was ignited. As shown by solid line in the figure, instead of temperature rise only the effects of electromagnetic noise were recorded by the oscilloscope within the measurement period.

The measured signal was compared with the calculated result by assuming the X_{con} was equal to 5%. In **Figure 2.12**, the calculated temperature reaches its peak before 0.1 ms of the measurement time (15 μs after discharge) and gradually dropped. Moreover, the calculated temperature increased by only one degree Celsius from initial state to the peak. Thus, comparison of measured and calculated temperature rise could not be done successfully by igniting only a single pulse discharge in micro EDM.

As a solution, multiple pulses discharges must be ignited on workpiece at sufficiently long distance from the thermocouple junction in order to determine the ratio of energy loss due to heat conduction within the micro EDM workpiece. Although the results show no significant difference between the case of Cu foil and Cu wire workpiece, the Cu wire workpiece is more suitable because the calculated temperature at workpiece was not sensitive to the assumed plasma diameter. Furthermore, the ratio of energy loss due to heat conduction was not affected by the distance between discharge location and thermocouple junction in the case of Cu wire.

As a result, it was found in this work that the ratio of energy loss due to heat conduction, X_{con} is between 5 and 7%, and 2 and 4% in the case of anode and cathode workpiece, respectively. In the following experiments, mostly capacitor of 1000 pF will be used. Therefore, the result as shown in **Figure 2.9** b. is used, where X_{con} is equal to 6.02% and 3.25% in the case of anode and cathode workpiece, respectively. Furthermore, since there was no significant difference in the results between the case of Cu foil and Cu wire workpiece, the result of Cu wire is reliable and can be used to represent the ratio of energy loss due to heat conduction within micro EDM electrodes.

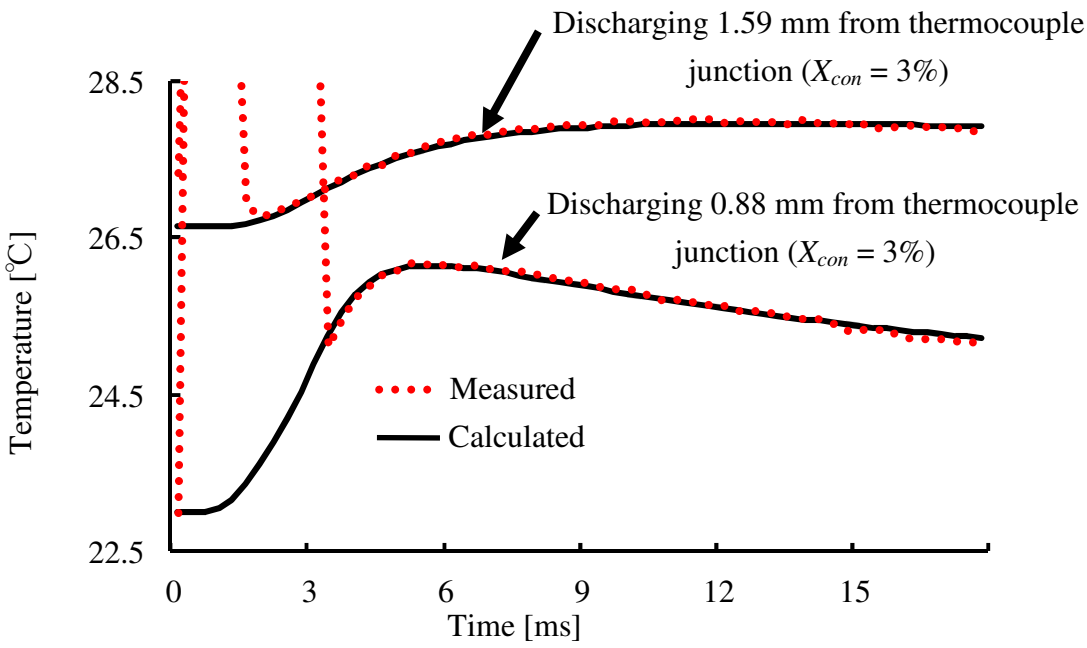

Figure 2.11: Effect of distance between thermocouple junction and discharges location

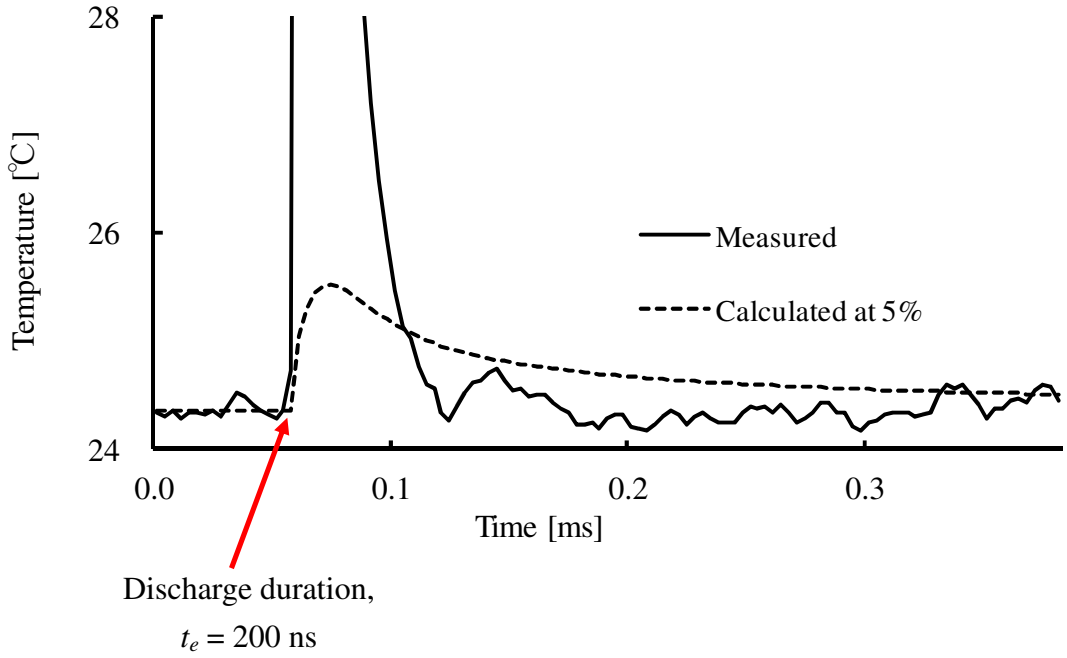

Figure 2.12: Measured and calculated temperature rise for single pulse in micro EDM

2.4 Ratio of energy carried away by debris

In macro EDM, the ratio of energy carried away by debris is significantly lower than that was lost due to heat conduction within electrodes [26]. However, in micro EDM, the plasma diameter is in the initial stage of development due to the short discharge duration leading to extremely high power density. Since high power density results in high removal efficiency, the energy carried away by debris is believed to be significant and cannot be ignored.

High density heat flux in the order of 10^8 W/m^2 or greater is formed at the electrodes' surface during discharging in macro EDM. The heat flux instantaneously increases the electrodes' surface temperature and part of the heated area reaches boiling point and vaporizes from the surface. At a deeper level within the electrodes, part of the heated area exceeds melting point. However, in EDM process only portion of the area above melting point or molten area is removed and the remainder forms a white layer. It was reported that the ratio of removal volume with respect to the molten area so-called removal efficiency was between 1 and 10% in the case of macro EDM [16].

In order to determine the ratio of energy carried away by debris, X_{deb} the amount of energy carried away by debris due to vaporization, E_{debv} and due to melting, E_{debm} is required. In this work, it was assumed that the area at electrodes' surface that reaches the boiling point is immediately vaporized from the surface. On the other hand only a portion of the molten area is removed towards the end of discharge.

However, the ratio of removal by vaporization and by melting with respect to the total removal volume per pulse during discharging is unknown especially in the case of micro EDM, and this ratio is required to calculate E_{debv} and E_{debm}. Thus, at this stage the unknown ratio of removal by vaporization is set as g ($\equiv V_v / V$), and based on the fact that total removal volume per pulse, V in EDM is the summation of volume of removal by vaporization, V_v and volume of removal by melting, V_m, the ratio of removal by melting is equal to $1 - g$ ($\equiv V_m / V$).

The unknown value of g is in between 0 and 1. If $g = 1$; material removal is 100% by vaporization which means the energy carried away by debris is maximum. This is based on the fact that more energy is consumed to vaporize the material than to melt it. On the contrary, if $g = 0$; material removal is only by melting action and the energy carried away by debris is minimum. Here, only V is measurable through an experiment, and g is varied from 0 to 1 to calculate V_v and V_m, and then E_{debv} and E_{debm} are determined to obtain the range of the ratio of energy carried away by debris, X_{deb} with respect to g.

2.4.1 Total removal volume per pulse

In order to determine the ratio of energy carried away by debris, X_{deb} first the total removal volume per pulse, V of micro EDM process is obtained. Discharge energy per pulse of micro EDM process is in the order of 1 μJ. Thus, the unit removal of micro EDM process is significantly small and cannot be measured successfully if only single pulse discharge is ignited.

Therefore, in this work approximately 1 million and 10 millions discharges were ignited to reduce approximately 20 μm of anode and cathode Cu rod diameter, respectively using wire electrical discharge grinding, WEDG with cutting length approximately 300 μm in the axial direction. The number of discharges or the pulses number during discharging was counted using a universal counter that detected and counted each discharge current.

Figure 2.13 shows the Cu rod which was machined by WEDG. The difference in volumes between before and after machining of the rod workpiece was obtained. Then, this removal volume was divided by the number of discharges which was counted using the universal counter to obtain V.

As shown in **Figure 2.13** b., the shaded region indicates the removed area or the difference between before and after Cu rod machining using micro EDM. In order to calculate the volume of the removed area, the overall volume before machining was calculated based on the diameter of the rod before machining and overall length of the machined area. Then the volume of Cu rod after machining was calculated from the summation of the tapered area volume and the cylindrical area volume as shown in **Figure 2.13** b.

The setting of WEDG power supply during Cu rod machining was 1000 pF in capacitance and 100 V in open circuit voltage, and the generated discharge conditions were 1.8 A in peak current and 70 ns in discharge duration. It was found that the total removal volume per pulse, V was between 1.8 and 2.0 μm^3 in the case of anode Cu rod. On the other hand, V in the case of cathode was about 1/10 of that of anode Cu rod. Several examples of machined Cu rod are shown in **APPENDIX B**.

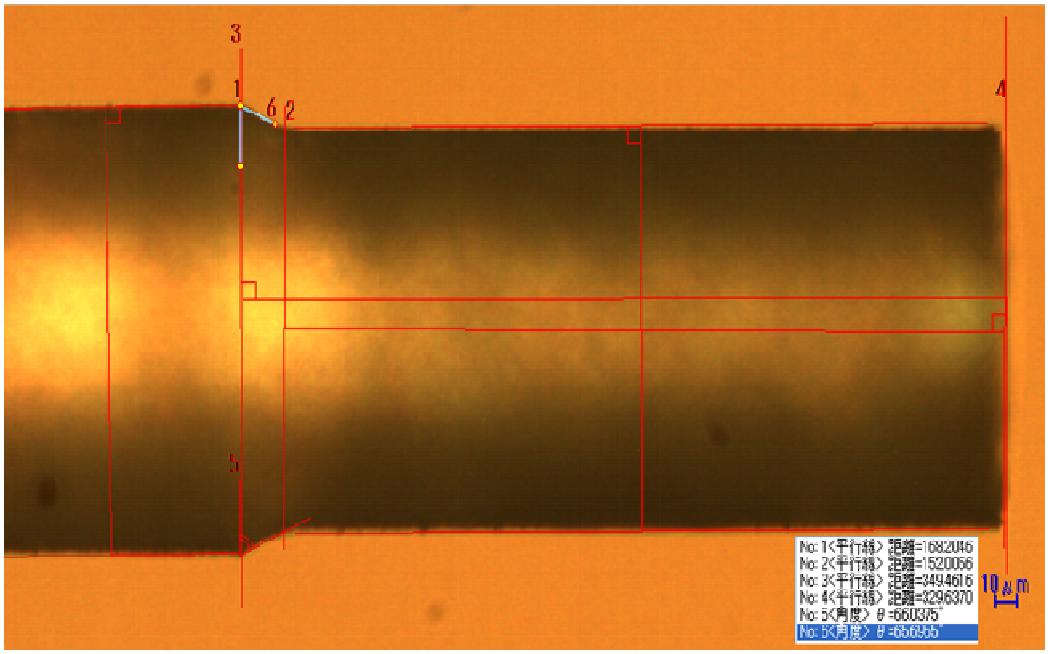

a. An example image of the machined Cu rod using micro EDM which was captured using an optical microscope

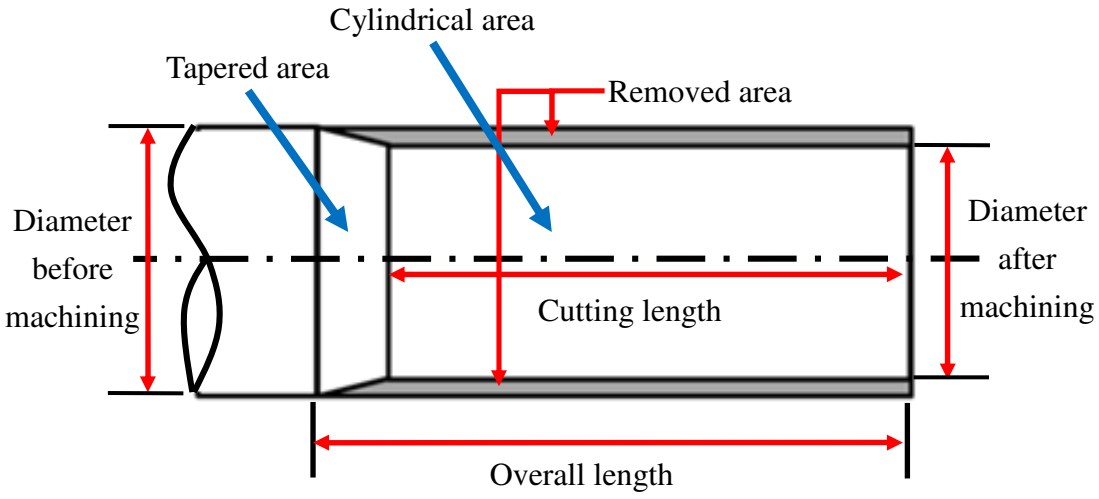

b. Cross-sectional area of Cu rod

Figure 2.13: Machining of Cu rod to obtain *V*

2.4.2 Calculation of ratio of energy carried away by debris

The ratio of energy carried away by debris, X_{deb} is calculated by dividing total amount of energy carried away by debris with the discharge energy as follows:

$$X_{deb} = (E_{debv} + E_{debm}) / (i_e \cdot u_e \cdot t_e) \quad (2.6)$$

The amount of energy carried away by debris due to vaporization and melting is calculated based on the total removal volume per pulse, V, $V_v = g \cdot V$ and $V_m = (1-g) \cdot V$, where g is an assumed value ranging from 0 to 1:

$$E_{debv} = \rho V_v [c(T_v - T_s) + L_m + L_v] \quad (2.7)$$

$$E_{debm} = \rho V_m [c(T_m - T_s) + L_m] \quad (2.8)$$

Here,
ρ: density = 8880 [kg/m^3].
c: specific heat = 386 [J/(kg K)].
T_v: boiling point = 2835 [K].
T_m: melting point = 1357.62 [K].
T_s: average temperature of electrode surface in steady state during machining
L_m: heat of fusion = 2.05 x 10^5 [J/kg].
L_v: evaporation heat = 5.03 x 10^6 [J/kg]

From **§ 2.4**, it is also known that part of the molten area is removed towards the end of discharge duration. This means, the molten area which is removed from electrodes may heat up to boiling point by the heat flux during discharging. Therefore, the temperature of the removed molten area which is used in Equation 2.8 should range from T_m to T_v. However, in this chapter T_m is used for simplicity. In the next chapter the range of temperature for the removed molten area will be considered. Furthermore, temperature dependent thermophysical properties will also be considered in the following chapter to determine X_{deb}.

Figure 2.14 shows the relationship between X_{deb} and g for anode and cathode rod workpiece which was obtained in this work. When g was changed from 0 to 1 the ratios of energy carried away by debris from anode and cathode rod workpiece increase from 1.07 to 5.77% and from 0.11 to 0.58%, respectively.

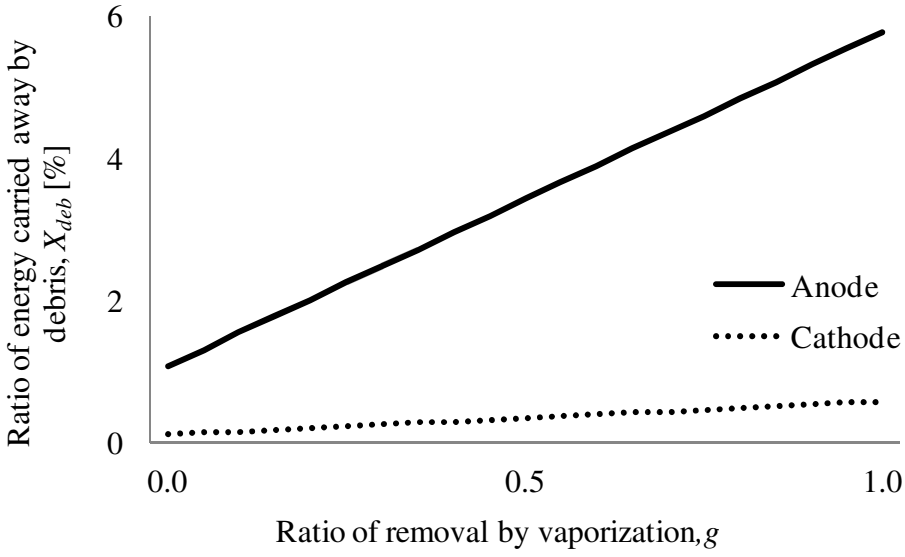

Figure 2.14: Relationship between X_{deb} and g

2.5 Relationship between energy distribution ratio and removal mechanism

It was explained in the previous sections that the energy distribution ratio into electrodes is the summation of the ratio of energy that is lost due to heat conduction and the ratio of energy carried away by debris. The equation is as follows:

$$X = X_{con} + X_{deb} \tag{2.9}$$

The ratio of energy loss due to heat conduction, X_{con} within micro EDM electrodes was explained in **§ 2.3** and it was a fixed value. On the other hand, in **§ 2.4**, it was found that the ratio of energy carried away by debris, X_{deb} depends on the removal mechanism. However, there is no comprehensive information regarding the removal mechanism in the case of micro EDM, as well as in macro EDM. In macro EDM, the ratio of removal by vaporization, g does not affect the measurement of the energy distribution ratio X, because X_{deb} is negligible compared with X. Hence, there has been no comprehensive research to obtain g so far. In micro EDM however, g is critical in the measurement of X because X_{deb} is not negligible. Thus, the range of X_{deb} with respect to the assumed ratio of removal by vaporization, g was first determined in this work. Thus, the relationship between X and g was obtained as shown in **Figure 2.15**.

Figure 2.15 shows that the energy distribution ratio into anode is greater than that of cathode and the ranges are 7.09 to 11.79% and 3.36 to 3.83%, respectively. In total, energy distribution ratio into anode and cathode is between 10 and 16%. This means at least 84% of discharge energy was lost into the electrodes' gap. **Figure 2.16** shows the distribution of energy in micro EDM process with respect to the ratio of removal by vaporization, g.

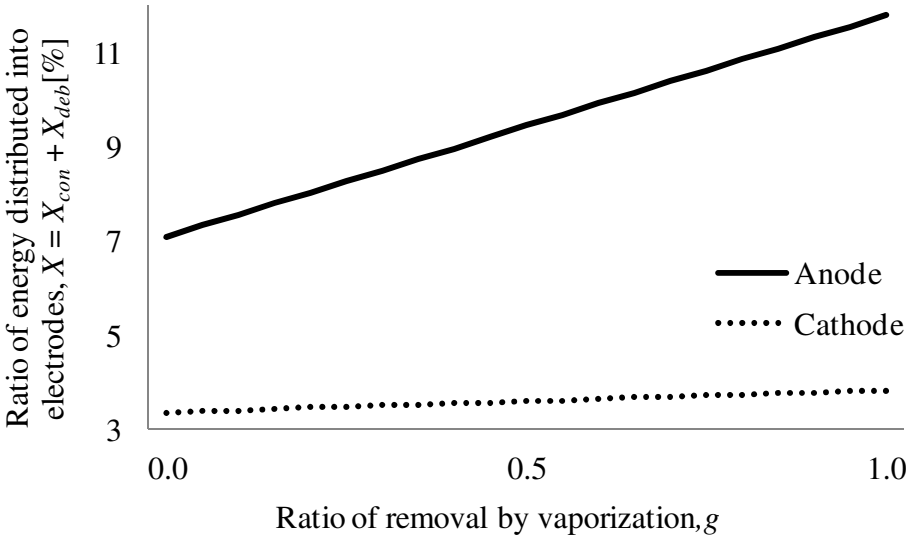

Figure 2.15: Relationship between X and g

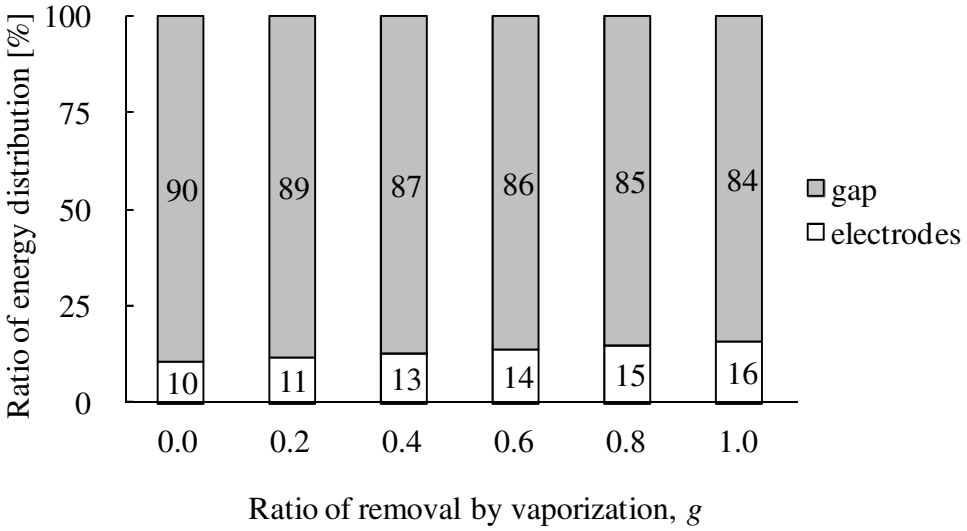

Figure 2.16: Energy distribution during micro EDM process

The relationship between discharge durations and energy distribution ratio into electrodes in total is shown in **Figure 2.17**. Xia et at. [29] reported that under normal EDM conditions 65% of the discharge energy was delivered into electrodes in total. Hayakawa et al. [31] used extraordinarily long discharge durations and found that almost all discharge energy was distributed into anode and cathode.

The energy distribution ratio into electrodes obtained in this work was comparatively lower than that was reported in [29] and [31]. **Figure 2.17** shows a linear relationship of those results with respect to logarithm of discharge duration. This validates the result which was obtained in this work.

Based on the idea reported in [31], the result measured in micro EDM indicates that much larger fraction of the discharge energy is consumed for the generation and enthalpy increase of the plasma in the case of micro than in the macro EDM, because the discharge durations are significantly short.

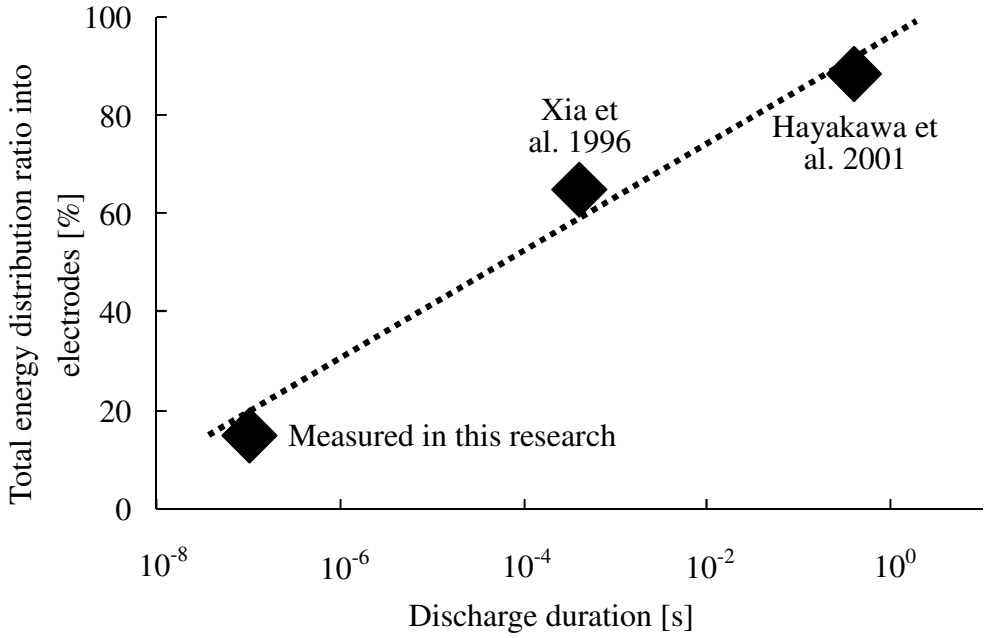

Figure 2.17: Total energy distribution ratio into electrodes vs. discharge durations

2.6 Conclusions

In this chapter a method to determine energy distribution ratio into micro EDM electrodes was explained. Discharge energy distributed into electrodes was dominated by the energy loss due to heat conduction and the energy carried away by debris. The ratio of energy lost due to heat conduction was determined by comparing the measured and calculated temperature rise on electrode. On the other hand, the ratio of energy carried away by debris was calculated based on the measured removal volume from electrode.

In micro EDM, single discharge cannot sufficiently heat up the electrode surface, and thus multiple discharges were ignited at sufficiently long distance relative to the thermocouple junction so that temperature peak could be measured and compared with the calculated temperature rise in order to increase the reliability of the result. Two types of workpiece were used and it was found that the ratio of energy loss due to heat conduction which was obtained using Cu wire is more reliable than that of Cu foil because the temperature peak could be measured, eliminating the effect of electromagnetic noise. Furthermore, measurement accuracy using Cu wire was better because the calculation result was not influenced by the assumed plasma diameter. However, there was no significant difference in the obtained ratio between the case of Cu wire and Cu foil, meaning the result obtained in the case of Cu wire was correct.

The energy distribution ratio into micro EDM Cu electrodes was significantly lower than that of macro EDM. This indicates that, the significantly short discharges durations of micro EDM leads to a much larger fraction of the discharge energy to be consumed for the generation and enthalpy increase of the plasma than in macro EDM. This result also suggests that plasma is still growing during discharge duration in the case of micro EDM. The result that energy distribution ratio into anode was higher than that of into cathode is consistent with macro EDM. However, one difference from macro EDM is that the energy carried away by debris is not negligibly small compared with the energy loss due to heat conduction within the electrodes of micro EDM. The main reason can be thought that the power density of micro EDM plasma is significantly high.

At this stage, only the range of energy distribution ratio into electrodes with respect to the ratio of removal by vaporization, g was obtained. In order to determine the value of heat source that erodes the workpiece surface during micro EDM process, further discussion on removal mechanism is required. In the next chapter, removal mechanism of micro EDM process will be discussed.

Chapter 3 Removal mechanism analysis

The exact ratio of energy distributed into workpiece, X in micro EDM cannot be obtained because the volumes of removal by vaporization and by melting under each discharge are unknown. In this chapter removal mechanism analysis will be discussed to obtain the exact value of X. At the same time, the heat source or plasma diameter, d which is also required to calculate the power density at workpiece during EDM will be obtained. The analysis method proposed in this chapter is considered to be useful to analyze the removal mechanism of macro EDM as well, where the volumes of removal by vaporization and by melting have never been obtained separately either.

3.1 Principle of removal mechanism analysis

During discharging, the plasma heats and thermally erodes a limited portion of the workpiece surface. The power density at the workpiece is calculated using the following equation;

$$P_e = X \cdot i_e \cdot u_e / (\pi \cdot d^2/4) \tag{3.1}$$

Here, i_e and u_e are discharge current and discharge voltage, respectively which can be measured during discharging using an oscilloscope. On the other hand, energy distribution ratio into the workpiece, X and plasma diameter, d are unknown parameters and have never been reported by other researchers especially in the case of micro EDM.

The range of X with respect to the ratio of removal by vaporization, g was obtained in this work, and the method to find their relationship was previously explained in **Chapter 2**. However, an exact value of X is required to calculate P_e. Therefore, the value of g should be obtained to determine X, and this is done in this work by analyzing the removal mechanism of the micro EDM process.

Another unknown parameter which is required to calculate P_e is the plasma diameter, d. In macro EDM, d expands to a maximum value within the first 2 μs of the discharge durations [43]. However, in this work t_e was less than 70 ns which is significantly shorter than 2 μs. Thus, in this work d was assumed to be time dependent and linearly increase during discharge duration. The value of d is also obtained in this

work by analyzing the removal mechanism of the micro EDM process which involves the study of temperature distribution at the vicinity of the workpiece removal area.

Basically, the removal mechanism analysis of micro EDM process is a work to analyze the relationship among ratio of removal by vaporization (g), energy distribution ratio into workpiece (X), and plasma diameter (d). It involves iterative calculations of temperature distribution within the workpiece based on a physical model of the micro EDM Cu workpiece. Based on the calculation, the simulated crater diameter and simulated vaporization volume are obtained and compared with the measured crater diameter and experiment based vaporization volume in order to decide the values of g, X and d. Finally, the energy input can be understood thoroughly including the heat source which is represented by the power density at workpiece, P_e, the time dependent plasma expansion, and the amount of material removal by vaporization and by melting.

It is important to clarify the definition of several terms which are required for the removal mechanism analysis. **Figure 3.1** a. shows an image of distribution of discharge energy at workpiece. Initially, $X\%$ of discharge energy is distributed into the workpiece. Then, $X_{deb}\%$ of the discharge energy is consumed for material removal and carried away by debris. During discharging $X_{con}\%$ of the discharge energy is lost due to heat conduction within the workpiece.

During discharging, the extremely high P_e immediately increases the workpiece's temperature and part of this heated area exceeds boiling point and it is assumed to vaporize immediately from the workpiece's surface. As shown in **Figure 3.1** b. the volume of removal by vaporization is equal to V_v, and its relationship with the total removal volume per pulse, V is shown in the figure. The relationship between V_v, V and g was explained in **§ 2.4**.

On the other hand, the area whose temperature is above melting point (including the vaporized area) is known as molten area and the volume is equal to V_s. During discharging, only a limited portion of V_s is removed from the electrode's surface by melting action and the volume is equal to V_m.

The temperature of V_m during removal might range between melting point and boiling point of the workpiece material, and it will be considered in this work. The remaining of V_s which is not flushed away from the crater solidifies to form a white layer. The diameter of the white layer which is observed from the top surface of the workpiece using a microscope indicates the diameter of the crater.

It is difficult to determine g, even if the cross section of the crater can be observed. Although the white layer can be observed, V_m cannot be obtained from the cross section only. In addition, there is a difficulty in measuring the volume of removal from the cross section because of the following reason. Araie et al. [71] used a white light interference measuring machine to measure the crater shape. Unlike the case of macro EDM, they found that the surface on the crater was not sunken but rather swollen, when a single pulse discharge was ignited on a virgin surface of workpiece material.

On the other hand, Murray et al. [63] found that crater due to micro EDM contains pores of a range 10 nm to 200 nm. This may result in the increasing volume of the molten area due to micro EDM single discharge as reported in [71]. This means physical observation of the crater cross section due to micro EDM single discharge is extremely difficult and may not be possible to be used in determining g. Therefore, a different method to determine g is introduced in this work.

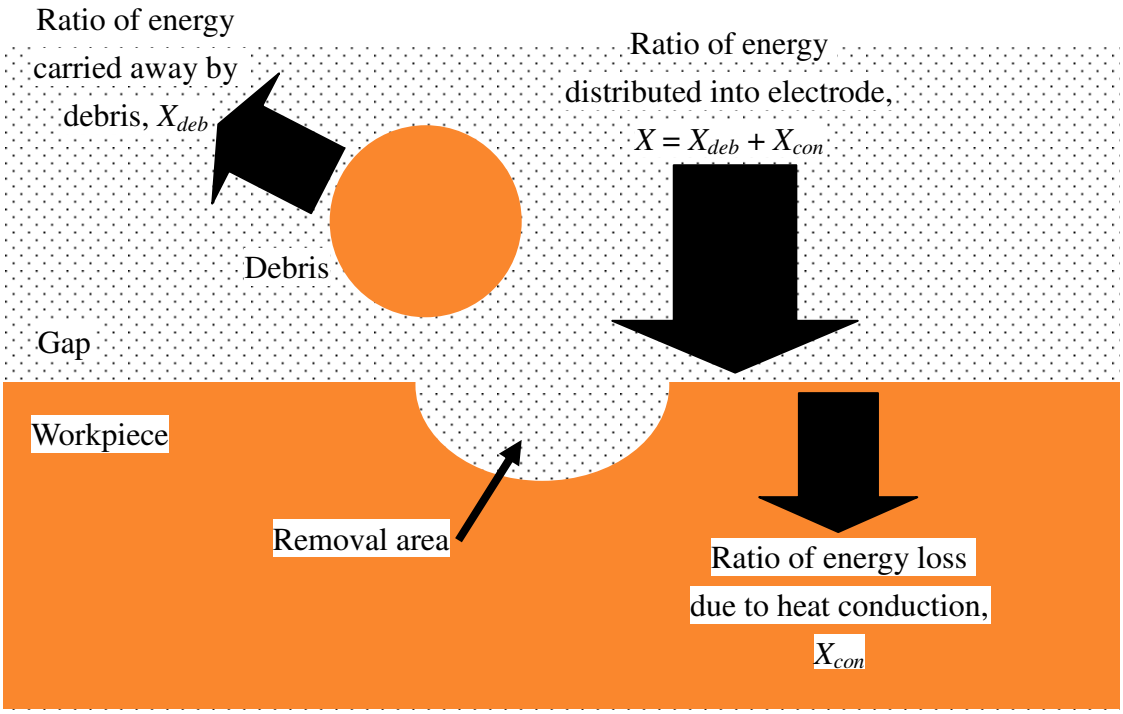

a. Energy distribution at workpiece

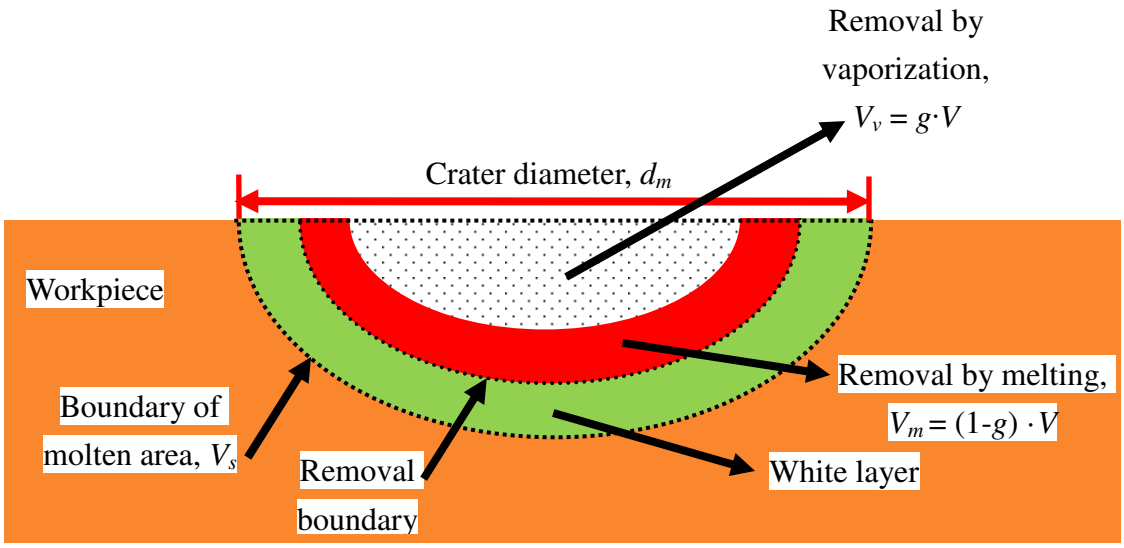

b. Removal mechanism

Figure 3.1: Energy distribution at workpiece and mechanism of material removal

Figure 3.2 shows a flowchart of the removal mechanism analysis. In this analysis, there are three main experiments involved. The first experiment was conducted to determine the ratio of energy loss due to heat conduction within workpiece, X_{con} as explained in **Chapter 2**.

The second experiment was conducted to obtain the total removal volume per pulse, V. In the third experiment, single pulse discharge was ignited on a Cu workpiece to determine the crater diameter, d_m. Those three experiments (experiments to obtain X_{con}, V and d_m) were conducted separately under similar machining conditions except the gap width between tool electrode and workpiece. It was difficult to control the gap width because tool electrode was manually fed towards workpiece during the experiment to obtain X_{con}. In this work the effect of the gap width between electrodes on the results was ignored.

In this analysis, two main parameters namely X and d must be decided to determine the power density on workpiece, P_e. Those parameters are depending on the ratios of removal by vaporization, g and by melting, $1 - g$ as explained in **§ 2.4**. Given the assumed value for g, two experiment based results namely removal by vaporization, V_v and measured crater diameter, d_m will be compared with simulated vaporization volume, V_{vap} and simulated crater diameter, d_c, respectively to decide the value of g, X and d, and then determine P_e.

As shown in **Figure 3.2**, the analysis began by assuming the unknown g between 0 and 1. Remember that the assumed value of g; 0 and 1 means the removal action is accomplished 100% by melting and by vaporization, respectively. This means the energy carried away by debris is maximum at $g = 1$ and minimum at $g = 0$, based on the fact that more energy is consumed to vaporize the material than to melt it.

Then g is multiplied with V to obtain the volume of removal by vaporization, V_v. Using the same value of g, X is obtained from the relationship between X and g as shown by **Figure 3.3**. In this work, it was assumed that during discharging, the temperature of debris which was removed by melting action was between melting and boiling point of the Cu workpiece. However, as shown in **Figure 3.3**, at higher g, where the removal by vaporization is dominant, this assumption is less significant on the value of X.

Then, experiment is conducted to measure the crater diameter, d_m. During the experiment the discharge current, i_e and discharge voltage, u_e are measured. Here, the plasma diameter, d is assumed, and now all parameters to calculate P_e are available, and thus the heat conduction within Cu workpiece due to single discharge can be modeled.

Figure 3.4 is the illustration of the heat conduction model due to single discharge of micro EDM at Cu workpiece. Plasma was modeled as a circular disk heat source and remains at the same vertical location until ends of discharge. The heat source radius was assumed to increase linearly with time during discharge duration. Cu workpiece was modeled sufficiently large so that temperature at the edge and the bottom surface remains at initial value within the simulation time. All surfaces of the Cu workpiece within the model were assumed adiabatic except below the circular disk heat source. The setting of thermophysical properties of Cu workpiece will be explained in **§ 3.2**.

From the heat conduction model of the Cu workpiece, the simulated crater diameter, d_c can be obtained based on the result of temperature distribution. Here, d_c is compared with d_m. The calculation is repeated by varying the assumed plasma diameter, d until $d_c = d_m$. When d_c coincides with d_m, d may equal to the plasma diameter.

Using the same simulation result, the volume of area where temperature is above the boiling point of the workpiece material so-called the simulated vaporization volume, V_{vap} is obtained and compared with the experiment based volume of removal by vaporization, V_v. Here, g is varied and the routine as shown in **Figure 3.2** is repeated until V_{vap} coincides with V_v which means g is equal to the ratio of removal by vaporization, d is equal to the plasma diameter and corresponding value of X is the energy distribution ratio into workpiece. Here, the power input, P_e that is used to model the heat conduction within the Cu workpiece during the analysis is equal to the power density at workpiece.

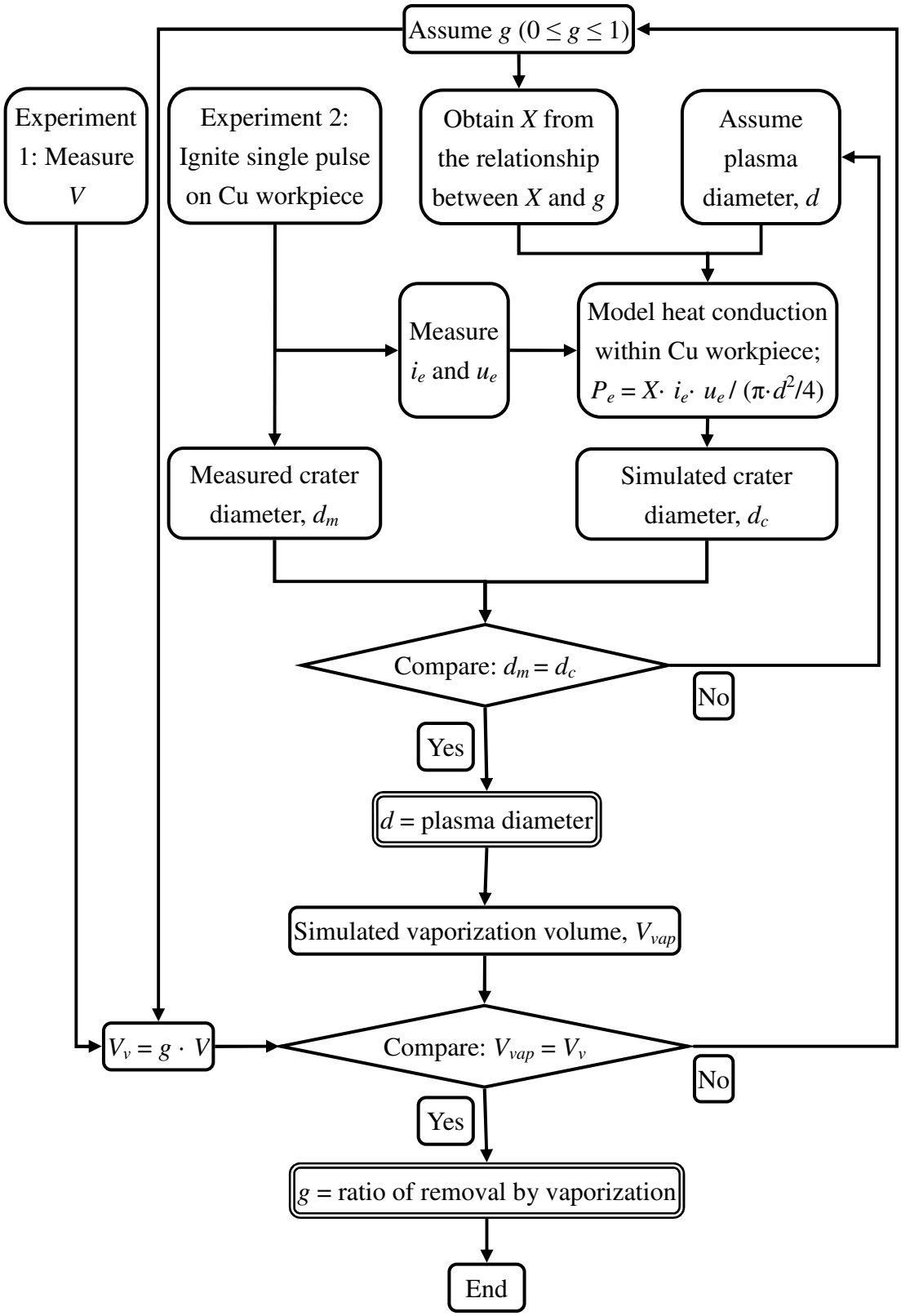

Figure 3.2: Overview of removal mechanism analysis

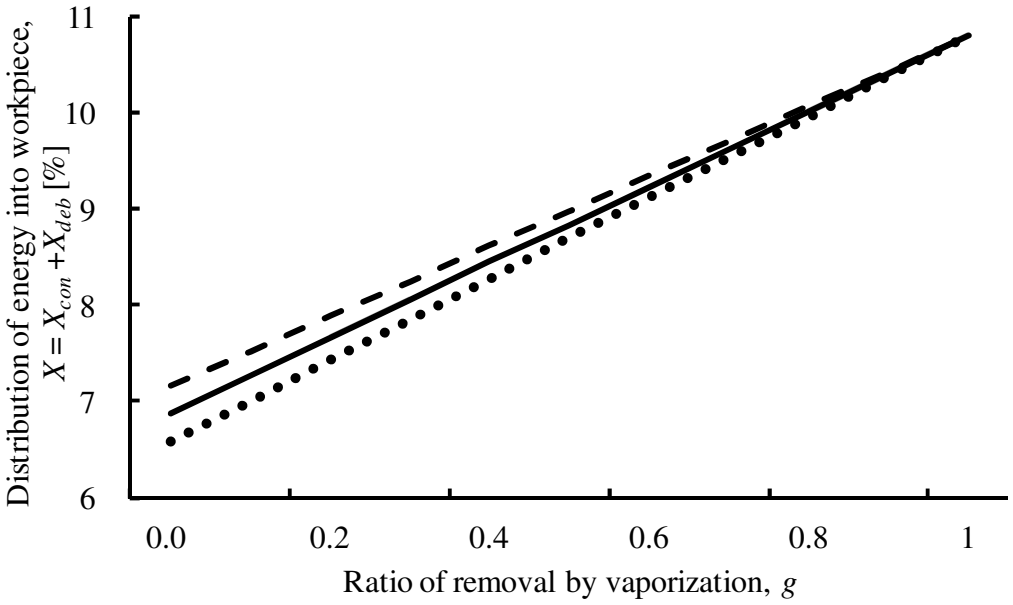

Figure 3.3: Relationship between X and g under various assumptions of removed molten area temperature

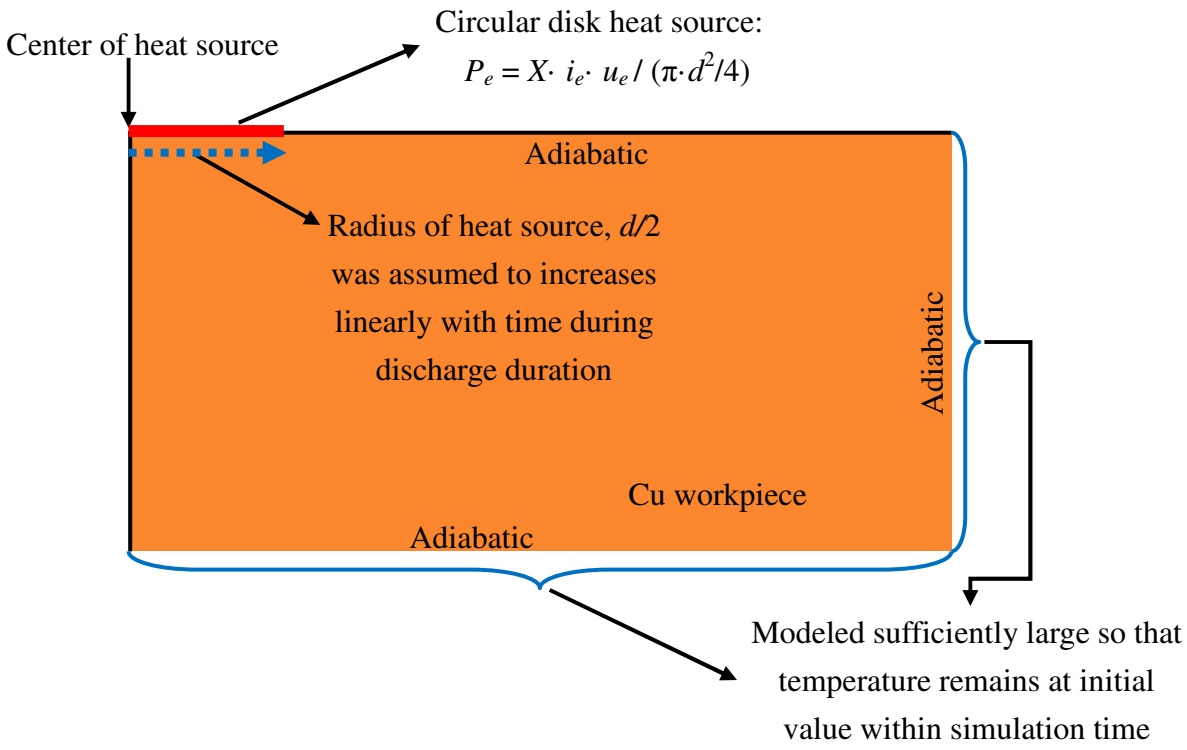

Figure 3.4: Heat conduction model at Cu workpiece to calculate crater diameter and material removal by vaporization

3.2 Thermophysical properties of workpiece

In the removal mechanism analysis of micro EDM, temperature distribution in the vicinity of discharge location on the Cu workpiece surface was studied. It involves significantly high temperature rise and the changes of the workpiece material phase from solid to liquid and gas in an extremely short period. Therefore, temperature dependent thermophysical properties of the workpiece material should be considered. In this work, the values of thermophysical properties of Cu workpiece were referred to [72-76].

In order to develop a physical model of micro EDM Cu workpiece to calculate the temperature distribution, there are three main thermophysical properties involved; Cu density, ρ [kg/m^3], specific heat, C [J/ (kgK)], and thermal conductivity, k [W/ (mK)]. Furthermore, in this work the area on workpiece where temperature is above the boiling point of Cu during discharging was assumed immediately removed from the workpiece. Therefore, moving boundary was also considered by setting those properties equal to zero or extremely high value (10^{10}) as indicated in **Figure 3.5**.

As shown in **Figure 3.5**, within the area where temperature is above the boiling point of Cu and below the plasma, the setting was $\rho = C = 0$ and $k = 10^{10}$. This was to model removal area, and thus no mass and no heat absorption here. However, k was set extremely high so that heat from the circular disk heat source can be transferred directly to the new surface below the area where temperature is above the boiling point of Cu.

On the other hand, in the area where temperature is above the boiling point of Cu, but beyond the plasma, the setting was $\rho = C = k = 0$. This was to model vaporized area and to assure the heat flux only transferred in the vertical direction below the plasma and no heat was transferred from this area to the new surface beyond the area where temperature is above the boiling point of Cu.

During discharging, a part of molten area where temperature is between melting and boiling points also might be removed from the workpiece. However, unlike the vaporized area, the removal may not occur immediately. The removal of this area may occur towards the end of discharge duration or after the end of the discharge. Hence, in the removal mechanism analysis, for simplicity this area is not considered as moving boundary. At higher g, where the removal by vaporization is dominant, the assumption of moving boundary is less significant because the thickness of the layer which is removed by melting might be significantly thinner than the depth of crater.

For the removal mechanism analysis, finite difference method was used to simulate the temperature profile in the workpiece, and the simulation period was equal to the discharge time. On the other hand, later in **Chapter 5**, for thermal stress analysis due to single discharge which involves thermal and structural analyses, finite element method was used. The simulation period was made several times longer than the discharge duration to allow molten area that remains over the workpiece surface to cool down before determining the thermal stress. To simulate the moving boundary in the thermal stress analysis, method of element death is used and will be explained in **§ 5.3.3**.

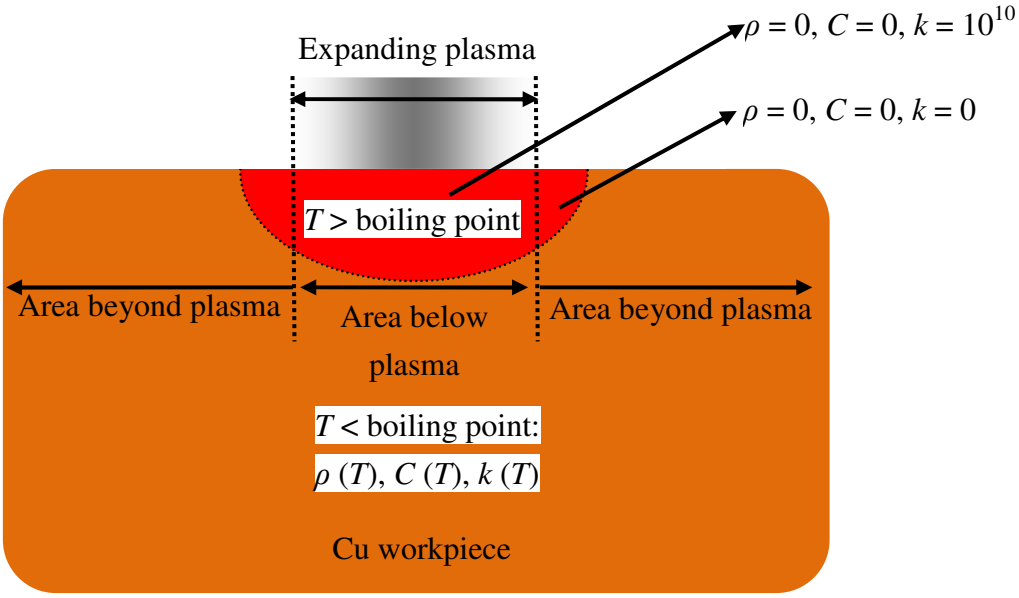

Figure 3.5: Cu workpiece thermophysical properties setting

In the area where temperature is below the boiling point of Cu, temperature (T) dependent thermophysical properties were considered, and the values were referred from [72-76]. In order to define the thermophysical properties within the calculation model, following approximate equations which were made based on those referred values were used:

- Cu density, ρ at the area on workpiece where temperature is ranging between room temperature and boiling point;

$$\rho = - 0.82 \cdot T + 9187.14$$

Figure 3.6 shows the comparison of the referred values and the approximation for Cu density.

- Cu specific heat, C was set constant at 516.85 J/(kgK) if the temperature was between 1300 K and boiling point. On the other hand, at workpiece temperature less and equal to 1300 K;

$$C = 0.11 \cdot T + 349.06$$

Figure 3.7 shows the comparison of the referred values and the approximation for Cu specific heat at the area.

- The third property was the thermal conductivity, k;

  At workpiece temperature between 2300 K and boiling point:

$$k = 155.16 + 0.029 \cdot T - 0.0000067 \cdot T^2$$

  At workpiece temperature between 1300 K and 2300 K:

$$k = 70.13 + 0.1 \cdot T - 0.000022 \cdot T^2$$

  At workpiece temperature below 1300℃;

$$k = 417.13 - 0.063 \cdot T$$

Figure 3.8 shows the comparison of the referred values and the approximation for Cu thermal conductivity.

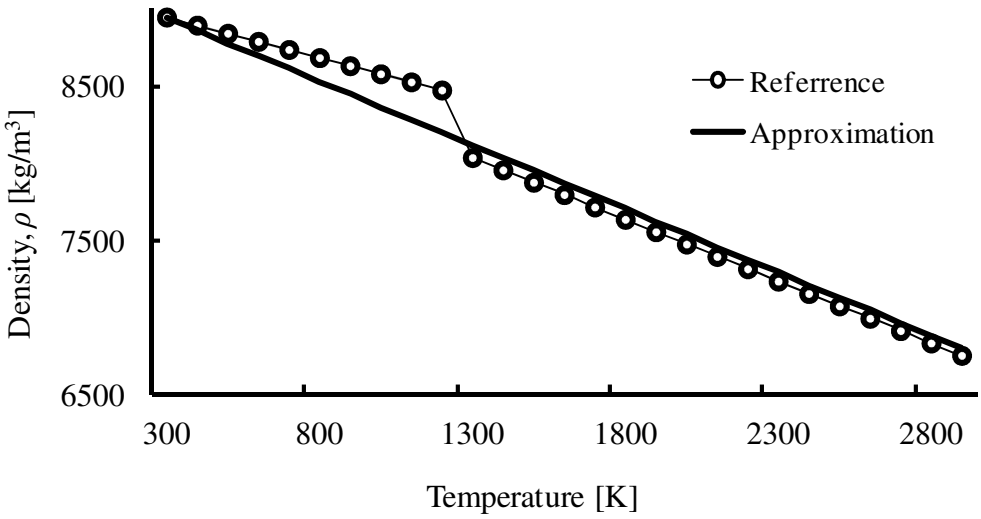

Figure 3.6: Temperature dependent Cu density, ρ
(Room temperature to boiling point)

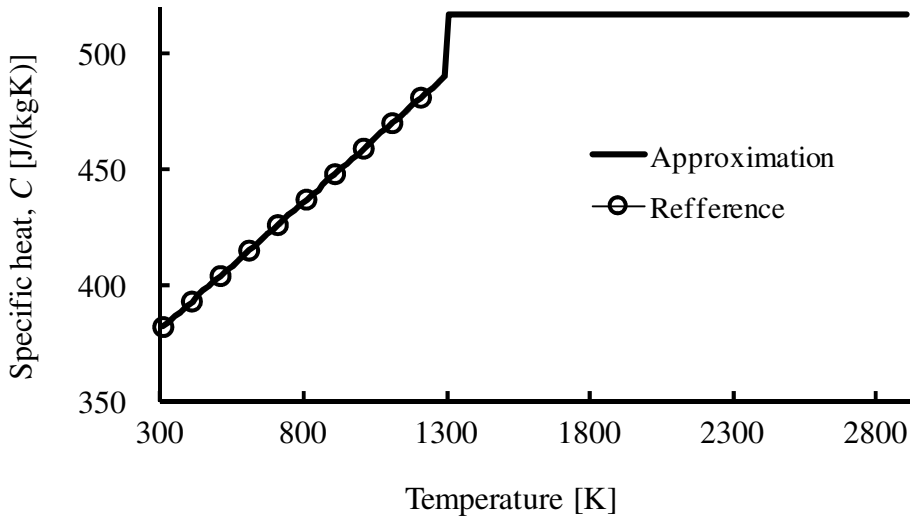

Figure 3.7: Temperature dependent Cu specific heat, C
(Room temperature to boiling point)

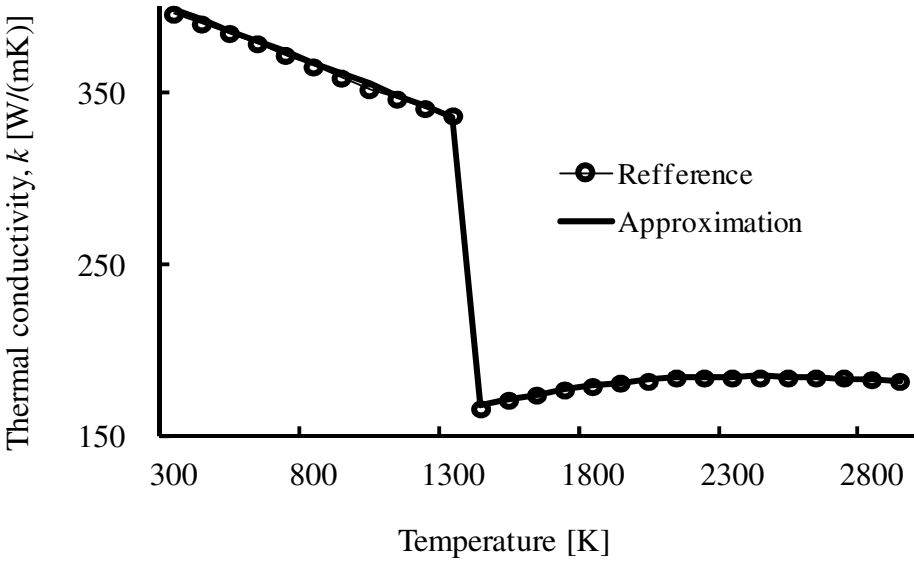

Figure 3.8: Temperature dependent Cu thermal conductivity, k
(Room temperature to boiling point)

3.3 Method to determine energy input at Cu workpiece

As shown in **Figure 3.2**, the removal mechanism analysis began by conducting an experiment to determine the total removal volume per pulse, V. Then, the ratio of removal by vaporization, g was assumed, for example $g = 0.9$. This means, 90% of the total removal volume per pulse is assumed to be removed by vaporization, and another 10% is removed by melting. At this stage, experiment based removal by vaporization, V_v can be calculated by multiplying g and V.

The next step was igniting a single pulse discharge on a Cu workpiece by using similar discharge conditions which were used to obtain V. In this experiment, the crater diameter, d_m was measured using an optical microscope. Discharge current, i_e and discharge voltage, u_e were also measured during this experiment using an oscilloscope.

The product of i_e and u_e is the discharge power per pulse. In this work, the power density at workpiece is desired, and therefore the concern here should be the power that is distributed at the workpiece only, which can be obtained by multiplying the energy distribution ratio into workpiece, X with the discharge power ($i_e \cdot u_e$).

Under the same value of g which was mentioned above, from **Figure 3.3** the value of X can be obtained and it is approximately 10.41% (at $g = 0.9$). Based on the measurement result of i_e and u_e, and the value of X the power distributed at workpiece can be determined. **Figure 3.9** shows an example curve of power distributed into workpiece ($X \cdot i_e \cdot u_e$) during discharge duration, t_e. These values were approximated using polynomial equation. The equation was then used to develop the heat conduction model.

Another assumption is the plasma diameter, d. In this work, d was assumed to increase linearly with time (t) during discharging. If the plasma diameter at the end of discharge duration is equal to d_{max}, the time dependent plasma diameter can be written as follows:

$$d = (d_{max} / t_e) \cdot t \tag{3.2}$$

From Equation (3.1), (3.2) and 3rd degree polynomial approximation of power distributed into workpiece, the power density, P_e can be calculated as follows:

$$P_e = (a_0 + a_1 \cdot t + a_2 \cdot t^2 + a_3 \cdot t^3) / [\pi \cdot ((d_{max} / t_e) \cdot t)^2 / 4] \tag{3.3}$$

Now, the heat conduction model as shown in **Figure 3.4** can be simulated. Based on the simulation result of the temperature distribution within the Cu workpiece, the simulated crater diameter, d_c was determined. Then, d_c was compared with d_m and the assumed value of the plasma diameter was varied until $d_c = d_m$, which means the assumed value is equal to the plasma diameter.

When d_c coincides with d_m, under the same simulation result, the volume of the area where temperature is above the boiling point was obtained by counting the mesh elements. This volume is known as simulated vaporization volume, V_{vap}. Here, V_{vap} was compared with V_v which was obtained in the earlier stage of this analysis. If $V_{vap} \neq V_v$, the assumed value of g is changed and the following routines as shown in **Figure 3.2** are repeated. When, $V_{vap} = V_v$ the assumed value of g is now equal to the ratio of removal by vaporization. This also means that, the assumed d is equal to the plasma diameter, X is the energy distribution ratio into workpiece, and P_e is the power density at workpiece. Here, the power density and complete information on removal mechanism can be used to obtain the residual stress due to discharge based on thermal stress analysis in **Chapter 4**.

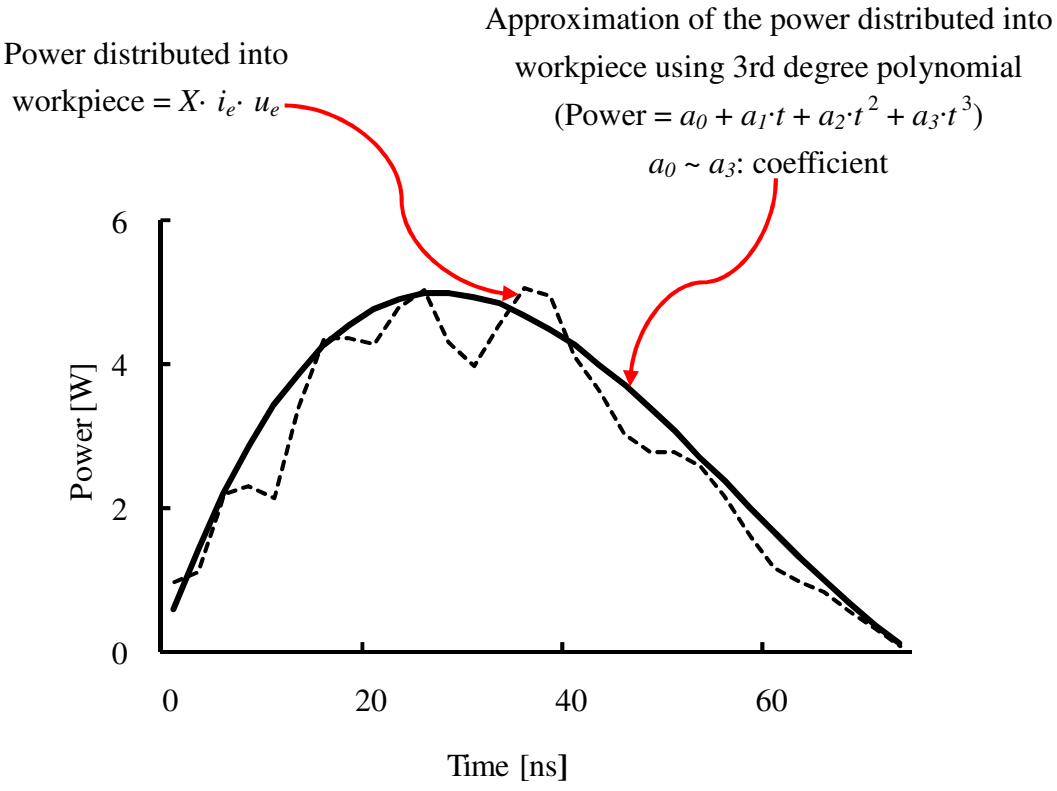

Figure 3.9: Power distributed on workpiece (= $X\cdot\ i_e\cdot\ u_e$) during discharging

3.4 Results of energy input

The total workpiece removal volume per pulse, V was found to be 1.9 ± 0.1 μm^3 under the conditions; peak discharge current, i_e = 1.14 ± 0.02 A, average discharge voltage, u_e = 24 ± 1.5 V, discharge duration, t_e approximately 70 ns, and the discharge energy per pulse approximately 1.9 μJ. Under similar discharge conditions, single pulse discharge was ignited on a Cu workpiece. It was found that the measured crater diameter, d_m = 4.3 ± 0.3 μm. Pictures of several examples of crater due to micro EDM single discharge are shown in **APPENDIX C**.

Based on the above experimental results, a heat conduction model of Cu workpiece due to single discharge was developed. When the ratio of removal by vaporization, g was fixed at 0.89 and plasma diameter, d was made to expand to 13.7 μm (about 3 times of crater diameter) at the end of the discharge duration, the simulated crater diameter, d_c = 4.3 μm. This means the calculated crater diameter almost coincided with the measured crater diameter, d_m where error between d_c and d_m was less than 1.5%. The simulated and measured crater size is shown in **Figure 3.10**.

Furthermore, under the same model the simulated vaporization volume, V_{vap} = 1.67 μm^3 also almost coincides with the experiment based removal by vaporization, V_v = 1.69 μm^3 where error between V_{vap} and V_v was also less than 1.5%. Thus, the ratio of removal by vaporization, g was equal to 0.89, which means 89% of the total removal volume per pulse, V was removed by vaporization and another 11% of V was removed by melting in the case of micro EDM. The simulated temperature distribution result which was used to determine V_{vap} is shown in **Figure 3.11**.

From **Figure 3.3**, at g = 0.89 the corresponding energy distribution ratio into workpiece, X was 10.37%, and from **Figure 2.9** the ratio of energy lost due to heat conduction, X_{con} within anode workpiece was 6.02%. This means, from Equation 2.9 the ratio of energy consumed for material removal and carried away by debris, X_{deb} from the workpiece was equal to 4.35% of the discharge energy.

From the above results and Equation 3.1 the power density at Cu workpiece, P_e can be calculated and it was found to be in the order of 10^{10} W/m^2. However, it was difficult to define plasma size and power density at 0 s. Thus, during calculation the initial value of plasma diameter and the power density at electrode was made equal to the value at 0.7 ns of discharging time. Discharge duration was 70 ns, and divided into 100 time steps during calculation, which means 0.7 ns is the 2nd step of the total time steps. The power density at Cu workpiece during calculation is shown in **Figure 3.12**.

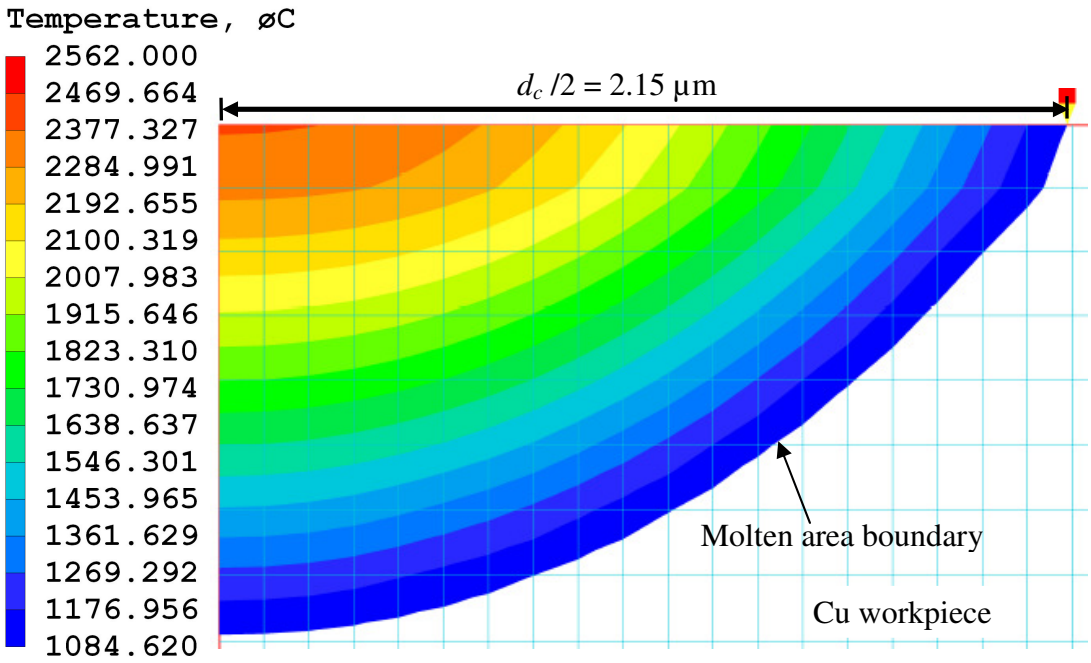

a. Calculated diameter, d_c

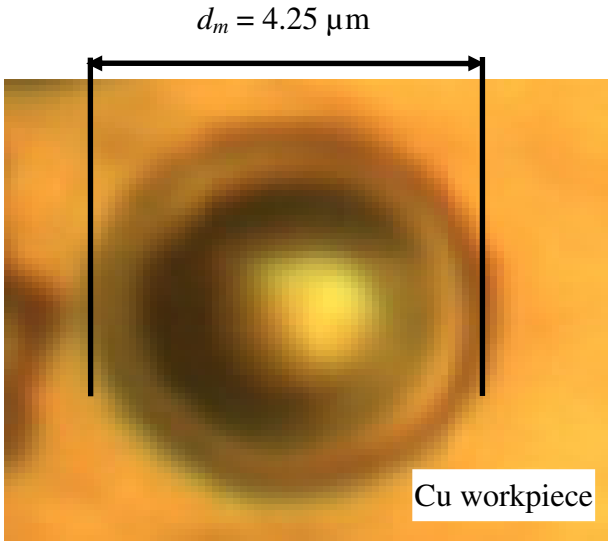

b. Picture of crater

Figure 3.10: Measured and simulated crater diameter due to micro EDM single pulse discharge
(i_e = 1A, u_e = 24 V, t_e = 70 ns, discharge energy per pulse = 1.9 µJ)

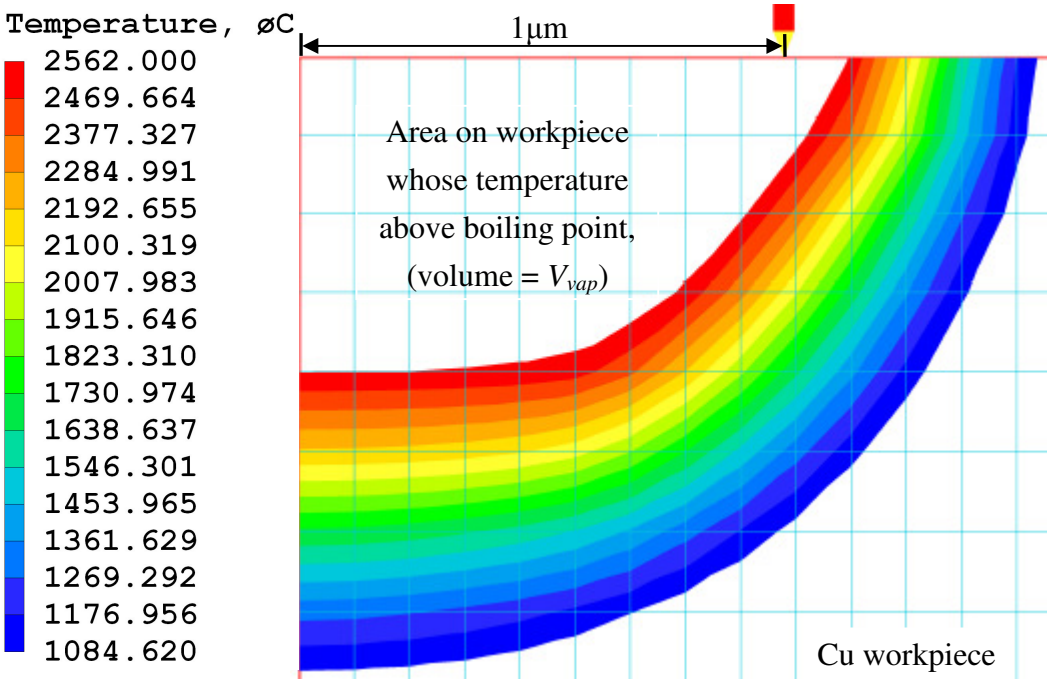

Figure 3.11: Calculated temperature distribution to determine area on workpiece that exceeds boiling point

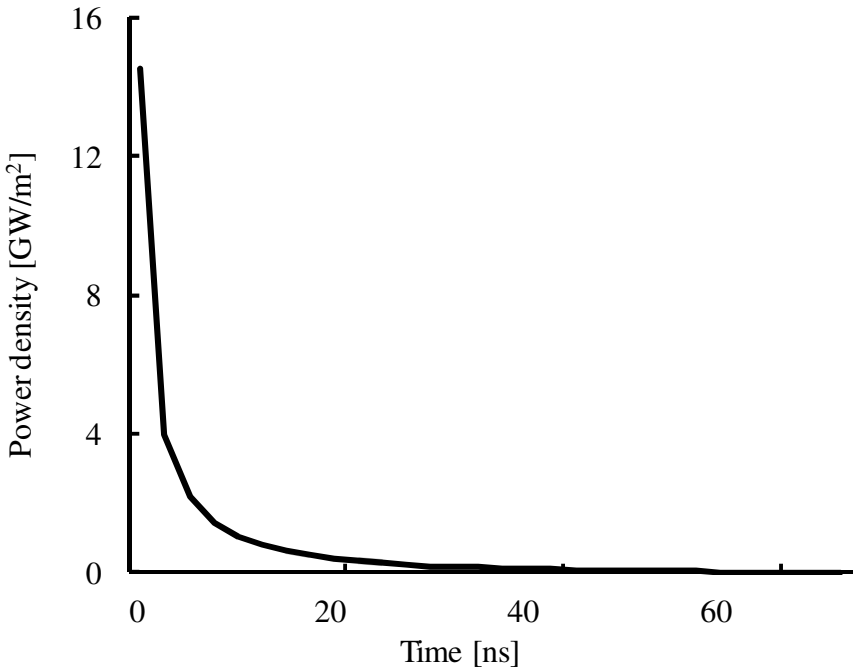

Figure 3.12: Time dependent power density at Cu workpiece during discharge duration

3.5 Comparison between micro and macro EDM

Most researchers observe performances of EDM by varying the discharge energy levels. In this work, in order to explain the physics of EDM process more clearly, instead of the energy, the correlation between power density at workpiece and the EDM efficiencies is discussed.

Table 3.1: Comparison of micro and macro EDM parameters

Parameters	micro	macro
Discharge current, i_e [A]	1.14±0.02	10.36
Discharge voltage, u_e [V]	24 ±1.5	17
Discharge duration, t_e [μs]	0.07	17
Crater diameter, d_m [μm]	4.3±0.3	68.4
Total removal volume per pulse, V [μm^3]	1.9±0.1	973
Plasma diameter, d [μm]	13.7	342 [43]
Energy distribution ratio into workpiece (anode), X [%]	10.37	34 [28]
Ratio of energy lost due to heat conduction, X_{con} [%]	6.02	30 [28]
Ratio of energy carried away by debris, X_{deb}[%]	4.35	1 [28]
Ratio of removal by vaporization [%]	89	-
Ratio of removal by melting [%]	11	-
Molten Area volume [μm^3]	10	-
Power [W]	27±1.5	178
Power density distributed into workpiece (anode) [GW/m^2]	19	0.7
Energy Efficiency, E_e [%]	42	3 [28]
Removal efficiency, R_e [%]	19	1~10 [16]

3.5.1 Measured and calculated results of micro and macro EDM

Table 3.1 shows the measured and calculated results of micro and macro EDM which were obtained in this work and referred from other researchers. The table shows several parameters which are important to understand the fundamental phenomena of EDM processes especially for the thermal stress analysis. The first five parameters are

the measurement results, and the remaining parameters are based on calculations. In the following sections how the machining conditions affect the performances of micro and macro EDM will be discussed. The parameters and performances to be discussed in this chapter are as follows:

i) The distribution of energy during discharging.
ii) Power density, P_e; energy per unit time that is distributed into workpiece per unit area of the plasma cross-sectional area.
iii) The ratio of removal by vaporization, g and the ratio of removal by melting, 1 - g with respect to the total removal volume per pulse.
iv) Removal efficiency, R_e; the volumetric ratio of material removed from workpiece with respect to the area in the workpiece where temperature is above the melting point of Cu during discharging.
v) Energy efficiency, E_e; the ratio of energy consumed for material removal and carried away by debris from the workpiece with respect to the energy distributed into the workpiece.

3.5.2 Machining conditions

The machining conditions were measured at the discharge gap in this work in both micro and macro EDM, and the results are shown in **Table 3.1**. Discharge current, i_e was time dependent and the average of i_e during discharging was equal to 1.14 A. The discharge duration, t_e was determined based on the measured i_e which was approximately 70 ns. The discharge voltage, u_e was approximately 24 V; slightly higher than that of macro EDM. This indicates that the plasma in micro EDM is in transient state until the end of t_e. Under this condition, the discharge energy of a single pulse in the case of micro EDM was not higher than 2 μJ.

On the other hand, in macro EDM, discharge current and discharge duration used in medium-finish machining are, for example 10 A and 17 μs, respectively. The discharge energy per pulse of macro EDM was approximately 3000 μJ (more than 1000 times greater than that of micro EDM). Under these machining conditions, the measured crater diameter due to single discharge of micro and macro EDM was found to be approximately 4.3 μm and 68.4 μm, respectively. Furthermore, the measured total removal volume per pulse, V in the case of micro and macro EDM was found to be approximately 1.9 μm^3 and 973 μm^3, respectively.

3.5.3 Energy distribution and plasma diameter

Figure 3.13 shows the relationship of the energy distribution ratio into tool electrode and workpiece in total with discharge durations, which was obtained in **§2.5**. It was measured in this work that the total ratio of energy distributed into tool electrode and workpiece of micro EDM was 15% of the discharge energy, and another 85% was lost within the gap between the electrodes. In the case of macro EDM only 35% of the total discharge energy was lost within the gap [29], and at extraordinarily long discharge durations most of the discharge energy was distributed into tool electrode and workpiece [31].

The results shown in **Figure 3.13** verify the idea of Hayakawa et al. [31] where in the early stage of discharging, a large fraction of discharge energy was consumed for the generation of plasma channel. This means almost 85% of the discharge energy was lost within the gap between electrodes of micro EDM to generate the plasma. The results also agree with the findings in [31] and [43] that plasma expands only in the early stage of discharging, and after the plasma stops expanding, most of the discharge energy is distributed into tool electrode and workpiece.

The significant difference of discharge durations between micro and macro EDM affects the distribution of energy during discharging. Large fraction of the discharge energy was lost within the gap between tool electrode and workpiece of micro EDM. The discharge energy was consumed for the generation of plasma channel only in the early stage of discharge duration. When the plasma stops growing within the first 2 μs of discharge duration and the discharge still continuing, the energy is mainly distributed into the tool electrode and the workpiece. Thus, larger fraction of discharge energy is distributed into the electrodes at longer discharge durations.

Figure 3.14 illustrates the plasma and crater of micro and macro EDM. As shown in **Figure 3.14** b., in the case of macro EDM plasma diameter, d expands to a maximum value about 5 times of its crater diameter, d_m during the first 2 μs of discharge durations and remains at that size until the end of the discharge. On the other hand, the plasma diameter of micro EDM was assumed to increase with time until the end of discharge durations. From the removal mechanism analysis, it was found in micro EDM that at the end of discharge duration, the plasma diameter was about 3 times of its crater diameter. The values of crater and plasma diameters in the case of micro and macro EDM were shown in **Table 3.1**.

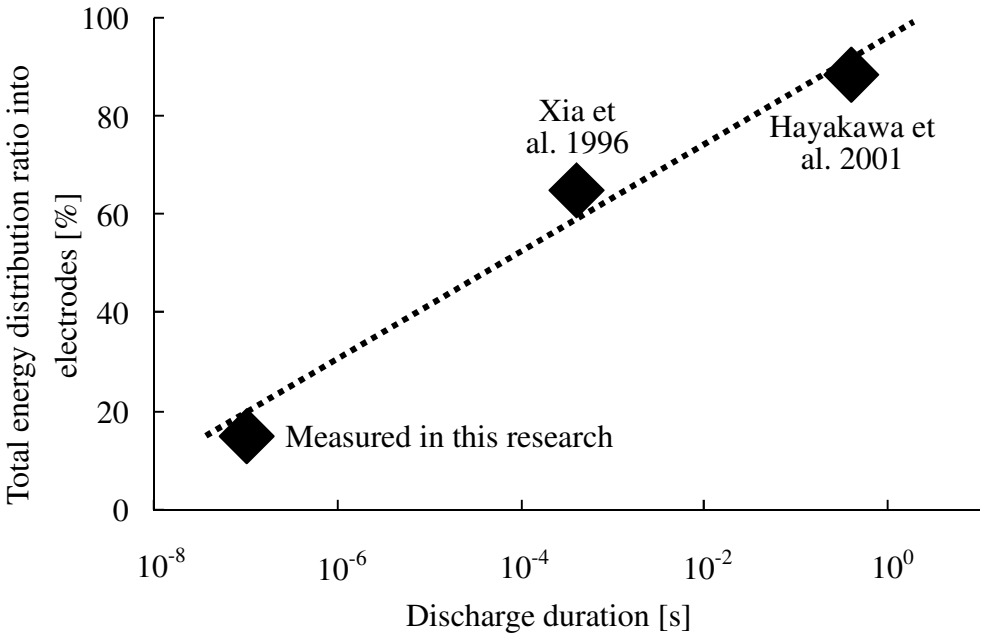

Figure 3.13: Relationship between total energy distribution ratios into electrodes and discharge durations

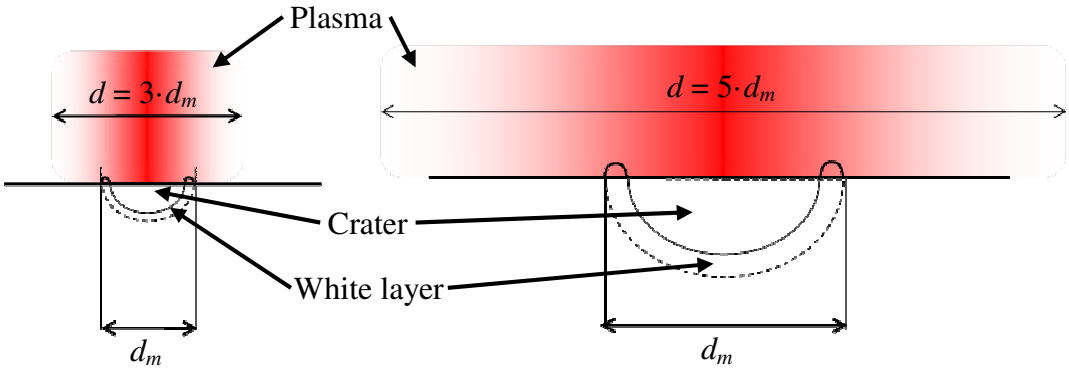

a. Micro EDM workpiece

b. Macro EDM workpiece

Figure 3.14: Comparison of plasma size between micro and macro EDM and its relationship with crater size

3.5.4 Power density

The power input from the plasma which is represented by the power density at workpiece, P_e is determined by the energy distribution ratio into the workpiece, discharge current, discharge voltage and the diameter of the cross-sectional area of the plasma as shown in Equation 3.1.

As previously shown in **Table 3.1**, it was found in this work that in average during discharge duration the power density on the micro EDM workpiece was in the order of 10^{10} W/m^2. On the other hand, the power density on the macro EDM workpiece was calculated using the results of energy distribution ratio into workpiece from the reference [29], and the value was in the order of 10^8 W/m^2. As explained in **§ 3.5.1**, although the amount of discharge energy in the case of macro EDM was about 1000 times greater than that of micro EDM, the power density of micro EDM was about 30 times higher than that of macro EDM. The significantly short discharge durations of micro EDM limit the plasma from expanding immediately, and thus contribute to smaller cross-sectional area and higher power density compared to the case of macro EDM.

3.5.5 Removal mechanism

The high density of discharge power immediately increases workpiece surface temperature at discharge location and removes a fraction of the area that exceeds melting point by vaporization and melting. Another fraction of molten area remains to form a white layer.

However, the amounts of removal by vaporization and by melting in order to calculate the energy consumed for material removal and carried away by debris during discharging were unknown. Hence, the ratio of removal by vaporization, g was introduced, and then it was determined based on the removal mechanism analysis.

In this work, as shown in **Table 3.1**, it was found that about 89% of the total removal volume per pulse was removed by vaporization, and another 11% was removed by melting. However, no such information regarding macro EDM has been reported.

It is reasonable to say that the ratio of removal volume by vaporization in micro EDM should be higher than that in macro EDM, because the power density at micro EDM workpiece is significantly high compared with macro EDM as described in the previous section. This can be inferred from the theory of high power density beam

processes such as laser and electron beam processes, where high peak with ultra-short pulse duration results in removal of material so quickly that surrounding material absorbs little energy, so-called ablation.

In addition, the flowchart as shown in **Figure 3.2** can be simplified to determine g in the case of macro EDM. **Figure 3.15** shows the flowchart to determine g in macro EDM. As shown in the figure, only one loop is left in this analysis. This is because the plasma in the case of macro EDM can be observed and it is measurable [31, 43]. This indicates that the ratio of material removal by vaporization and by melting with respect to the total removal volume per pulse can be determined more easily compared to the case of micro EDM.

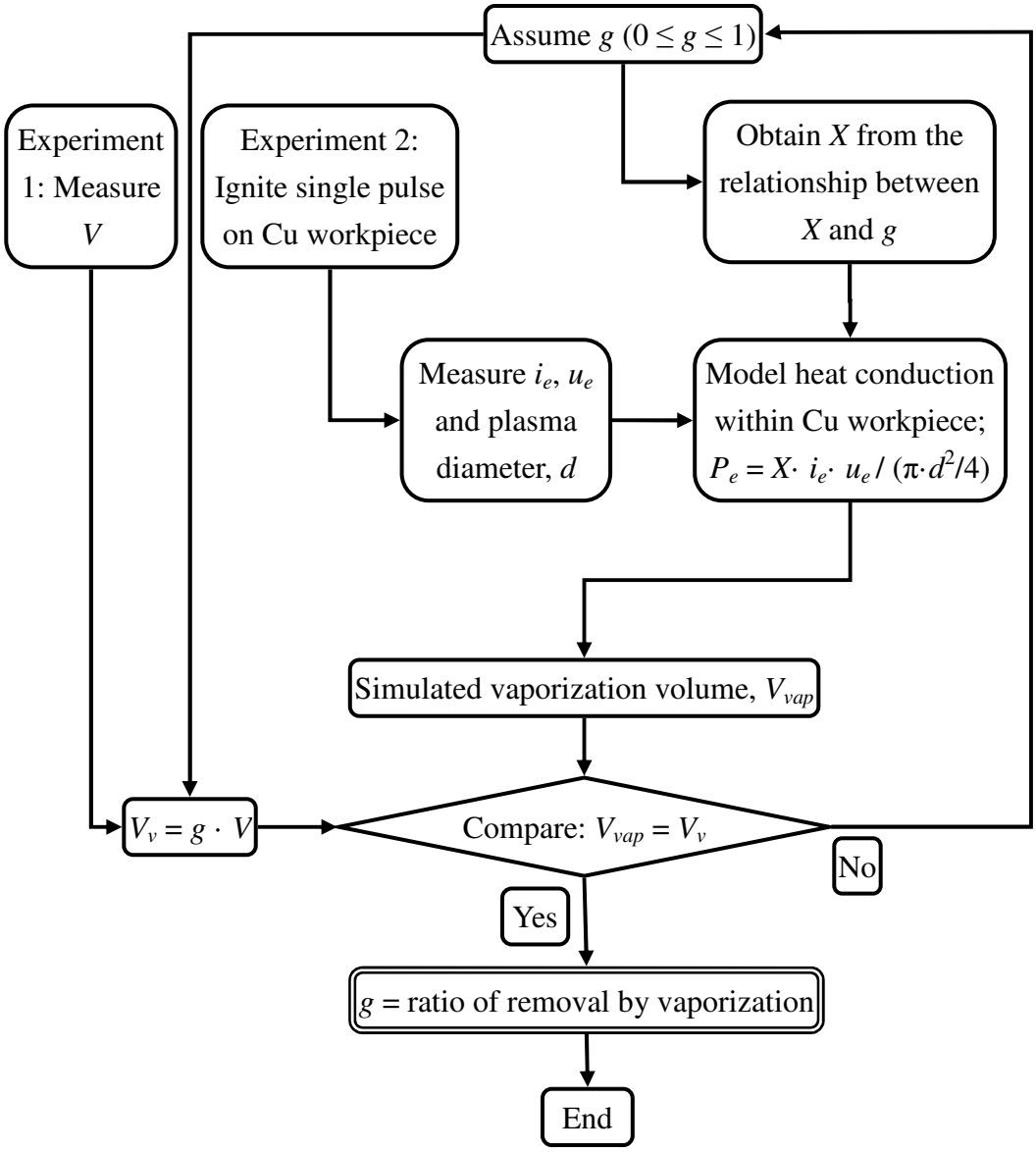

Figure 3.15: Removal mechanism analysis in macro EDM

3.5.6 Removal efficiency

In EDM, it was known that not all area on workpiece where temperature is above the melting point is removed from the workpiece surface during discharging. **Figure 3.16** describes the heated area on a workpiece. The ratio of the total removal volume per pulse, V ($=V_m + V_v$) with respect to the area where temperature is above the melting point, V_s (including the vaporize area) was named removal efficiency, R_e.

$$R_e = V / V_s \tag{3.4}$$

In this work, about 19% of the area on micro EDM workpiece where temperature is above the melting point was removed during discharging. On the other hand, removal efficiency was about 1 to 10% in the case of macro EDM [16]. As mentioned above, the reason for the difference in R_e between macro and micro EDM is analogous to that of the difference between the nanosecond and the femtosecond pulse lasers.

Higher R_e in the case of micro EDM compared to that of macro EDM means less fraction of the area where temperature is above the melting point remains at the discharge location to form the white layer. Generally, white layer is brittle and includes micro cracks, reducing the strength of the area. In some applications white layer is not desirable, and thus need finishing operation such as grinding and polishing.

The different thickness of white layer between micro and macro EDM may affect the formation of residual stress within the workpiece. Although the thickness of white layer is thin in micro EDM, it is not negligible compared with the thickness of the micro part machined by micro EDM, thereby causing deformation of the micro part.

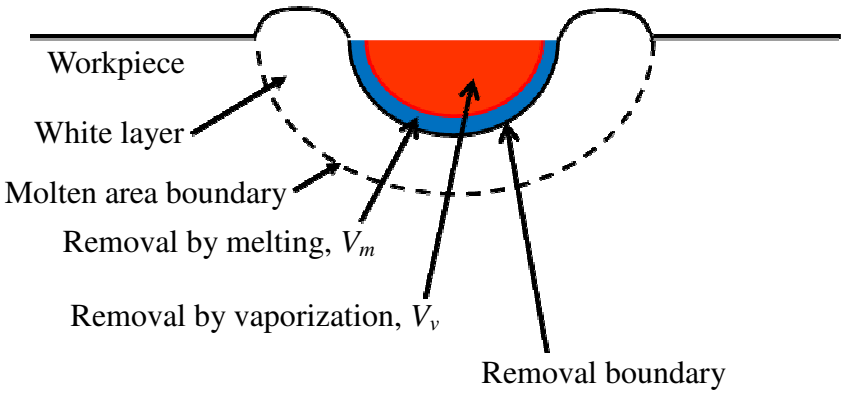

Figure 3.16: Heated area on EDM workpiece and removal mechanism

3.5.7 Energy efficiency

Figure 3.17 describes the distribution of energy into micro EDM workpiece. In this work, energy that is distributed into the workpiece is then consumed for material removal and carried away by debris, and lost due to heat conduction within the workpiece. The ratio of energy consumed for material removal and carried away by debris with respect to the energy distributed into the workpiece was named energy efficiency, E_e. Energy efficiency was calculated in this work as follows:

$$E_e = X_{deb} / X \tag{3.5}$$

Here, X_{deb} and X ($=X_{con} + X_{deb}$) is the ratio of energy carried away by debris and the ratio of energy distributed into workpiece, respectively. **Figure 3.17** describes X_{deb} and X_{con}. As shown in **Table 3.1**, the energy efficiency in the case of micro EDM was found to be about 40%. On the other hand, in the case of macro EDM, the energy efficiency was not higher than 3% [28].

In micro EDM, X_{con} and X_{deb} was 6.02% and 4.35%, respectively. Almost half of the energy distributed into workpiece was consumed for material removal. On the other hand, X_{deb} was only 1%, while X_{con} was 30% in macro EDM as shown in **Figure 2.1**. Most of the energy distributed into macro EDM workpiece was lost due to heat conduction within the workpiece. This result correlates with the result of removal efficiency which explains the reason of larger fraction of the molten area on macro EDM workpiece remains to form white layer compared to that of micro EDM.

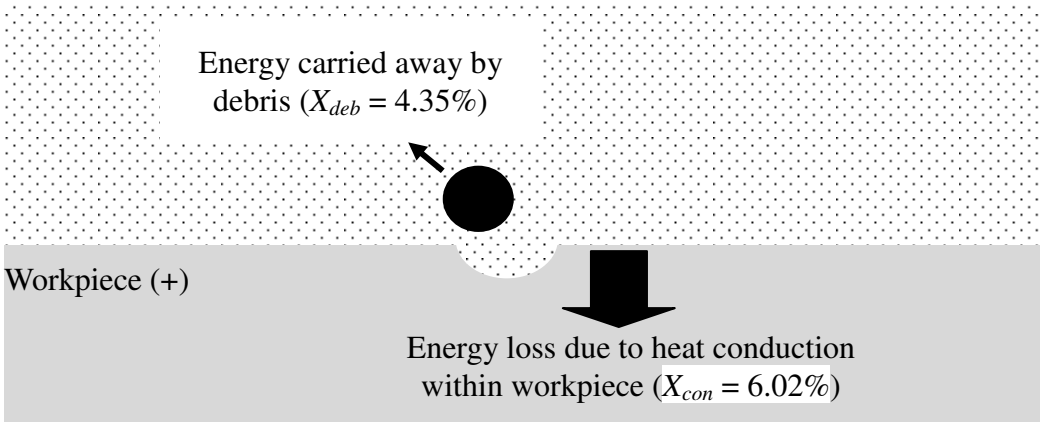

Figure 3.17: Energy distribution ratios in micro EDM workpiece

3.6 Conclusions

Material removal in EDM is complicated. It involves melting and vaporization of electrodes surface. A part of molten area remains on EDM workpiece, resolidifies and forms a white layer, and its amount is unknown. This makes the analysis of removal mechanism in EDM difficult especially in the case of micro EDM due to low discharge energy, low removal volume per pulse, and lack of fundamental information including power density, energy distribution ratio and plasma diameter.

In this work, to determine the power density in micro EDM, energy distribution ratio and plasma diameter have been obtained by analyzing the distribution of energy at workpiece and the removal mechanism. From the removal mechanism analysis the volumes of removal by vaporization and by melting during micro EDM have been obtained separately. However, those volumes have never been obtained in the macro EDM separately. Thus, the analysis method proposed in this chapter is considered to be useful to analyze the removal mechanism of macro EDM as well.

The performances between micro and macro EDM were compared. In micro EDM, the energy distributed into workpiece is small. However, since the plasma is always in the transient state and its diameter is being expanded during the discharge duration, the plasma diameter is still small. Hence, the power density on micro EDM workpiece is significantly higher than that of macro EDM where the plasma expansion is almost finished in the early state of the discharge duration. Consequently, removal and energy efficiencies of micro EDM were higher than those of macro EDM. The efficiencies of micro and macro EDM explain the easiness of formation of white layer within the workpiece of both processes. The formation of white layer and heat affected zone is critical in EDM. This kind of information is important especially to produce high quality components using this process. For example, as explain in **§ 1.2.3**, the formation of residual stress due to discharge is influenced by the white layer. Although the white layer is thinner in micro EDM than in macro EDM, the thermal stress may cause electrodes deformation especially at micro dimensions, which may affect the dimensional accuracy and stability of the parts. In the following chapter, an example regarding thermal stress analysis will be discussed to determine the residual stress due to micro EDM single discharge.

Chapter 4 Thermal stress due to micro EDM

Thermal stress analysis of macro EDM has been studied by other researchers [35, 46-52]. However, there is no such work that used accurate thermal boundary conditions to calculate the residual stress. In most cases, the energy distribution ratio and plasma diameter were assumed, not based on theory or experiment. In the case of micro EDM, it is further difficult to find papers relevant to the residual stress analysis. The main reason is no comprehensive information regarding the heat source that heats the workpiece and the removal mechanism of the micro EDM. Although micro and macro EDM share the same machining principle, residual stress formed below their crater may not be the same. This is because the power density at micro EDM workpiece is significantly different from the case of macro EDM as discussed in **Chapter 3**. Consequently, the formation of white layer in micro EDM which is related to the formation of the residual stress below each crater differs from that of macro EDM. In this chapter, thermal stress analysis to determine the residual stress due to micro EDM single discharge will be discussed. The work begins by simulating temperature distribution in a workpiece due to the single discharge. Residual stress is then calculated from the result of the temperature distribution.

4.1 Principle of thermal stress analysis

Generally, a material tends to expand and contract freely due to heat, when temperature is uniform in the body. In EDM however, temperature distribution within the workpiece is not uniform. Thus, stress is produced by the restraining action among the elements to prevent the workpiece from expanding and contracting freely during temperature change. The restraining actions will cause compressive stress on the heated surface and tensile stress on the cooling surface.

While the area near the discharge crater is in molten state, no residual stress will be formed because elements in the area can move freely. However, after the white layer solidifies, cooling process begins. At cooling area, tensile residual stress is formed, causing the area near the crater to contract [35, 46-52].

In order to determine the residual stress, a heat conduction model should be built. Here, accurate model for the heat source during micro EDM is required. In micro EDM,

as explained in **Chapter 3**, discharge energy per unit time distributed at workpiece under each unit area of circular surface heat source so-called power density, P_e was used as a measure of power input during discharging. P_e is calculated using Equation 3.1.

All the parameters that are required to determine P_e in micro EDM have been explained in **Chapter 3**, and they are summarized in **Table 4.1** below. A physical model of heat conduction in the workpiece was built using a finite element analysis software namely ANSYS. Then, the temperature distribution result is used to estimate the residual stress due to micro EDM single discharge. In this work, Cu was used as the workpiece because its high thermal conductivity makes it suitable to function as a tool electrode in micro EDM drilling. To make the micro rod electrode made of copper, a copper rod is machined by micro EDM with reversed polarity that the copper rod is positive. In this situation, since toughness of Cu is not sufficiently high, Cu rods are vulnerable to thermal deformation.

Table 4.1: Micro EDM power input

Parameters	Value
Discharge current, i_e [A]	1.14
Discharge voltage, u_e [V]	24
Discharge duration, t_e [μs]	0.07
Energy distribution ratio into workpiece, X [%]	10.37
Plasma diameter at end of t_e , d [μm]	13.7
Power density on workpiece, P_e (t_e) [GW/m^2]	4045~1.4

4.2 Overview of heat conduction model

Figure 4.1 shows an overview of the heat conduction model of Cu workpiece. In this work, the heat input from the plasma was modeled as a circular disk heat source with a uniform power density. The plasma diameter, d was assumed to increase linearly with time within the discharge duration, t_e = 70 ns. From removal mechanism analysis which was discussed in **Chapter 3**, it was found that plasma expands to a maximum diameter of 13.7 µm at the end of t_e.

Since d = 0 at t_e = 0, from Equation 3.1, the initial power density, P_e is infinity. This will cause an unstable calculation. Thus, for calculation purposes the minimum diameter was set 1/10 of maximum plasma diameter which is equal to 1.37 µm. As shown in **Table 4.1**, under this condition P_e decreases from 4.0 x 10^{12} to 1.4 x 10^9 W/m^2 during discharge duration. The model was made axisymmetric, with 50 µm in radius and 40 µm in thickness. All surfaces were assumed adiabatic except the discharge area.

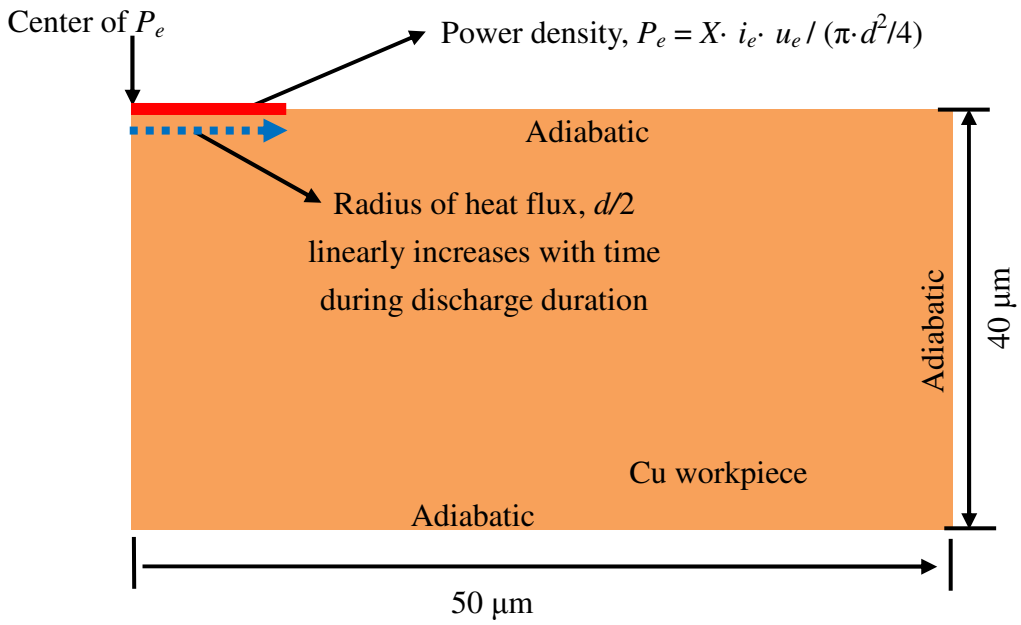

Figure 4.1: Overview of heat conduction model on Cu workpiece to calculate residual stress due to micro EDM single discharge

Figure 4.2 shows magnification of the discharge area. High power density in the beginning of discharge immediately removed portion of the heated area on the workpiece. As explained in the previous chapter about 40% of the energy distributed into micro EDM workpiece was consumed for the material removal. From the removal mechanism analysis, approximately 19% of the molten area on workpiece (comprising 89% of removal by vaporization and 11% of removal by melting) was removed during discharging. Therefore, moving boundary was considered in this work and will be discussed in later section. Accordingly, the surface heat flux location was changed during simulation as shown in **Figure 4.2**.

Then, with the passage of time during discharging the decreasing power density continues to heat the workpiece even though the surface temperature may decrease. About 60% of the energy distributed into the micro EDM workpiece is lost due to heat conduction. As a result, the thermal stress not only in the melted area but also in the thermally softened area is released. Therefore, for residual stress calculation, temperature dependent yield stress and modulus of elasticity were considered.

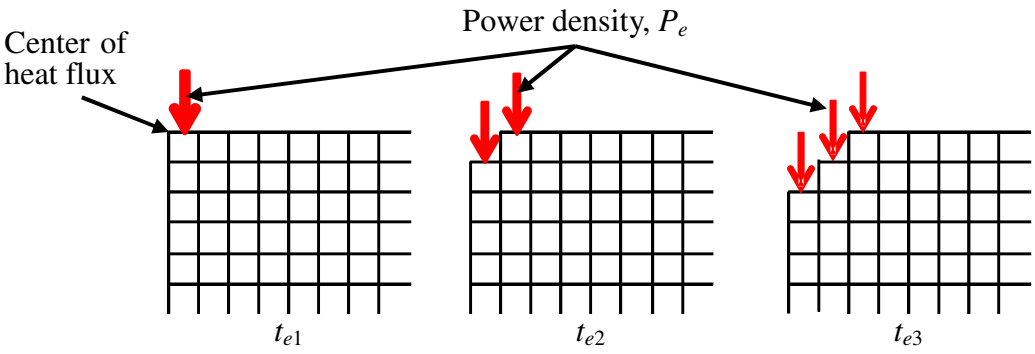

Figure 4.2: Magnification of discharge area considering moving boundary

4.3 ANSYS modeling

In this work, ANSYS Mechanical APDL program that has many finite element analysis capabilities including thermal and structural analyses was used to determine residual stress due to single discharge, and then to perform the beam deformation analysis in the next chapter. The overview of the heat conduction model of Cu workpiece is previously shown in **Figure 4.1.** This model was divided uniformly into more than 116 thousands square elements for the finite element analysis and the size of an element was equal to 0.2278 μm.

4.3.1 Modeling assumptions

During EDM process, a large fraction of molten area remains at the crater and solidifies to form a white layer. The thickness of the white layer in the case of macro EDM might differ from that of micro EDM based on the fact that discharge energy in macro EDM is more than one thousand times greater than that normally used in micro EDM and a larger fraction of the energy is lost due to heat conduction into macro EDM electrodes compared to that of micro EDM. This also can be explained using the removal efficiency, R_e which was discussed in **Chapter 3.**

R_e is between 1 and 10% in the case of macro EDM [16]. This means 90 to 99% of molten area remains in the crater and forms a white layer during macro EDM. On the other hand, it was found in this work that only 80% of molten area remains as white layer in micro EDM. This means, the white layer in micro EDM can be expected to be thinner relative to the crater depth compared to that of macro EDM.

As explained in **§ 4.2** it is important to consider temperature dependent structure properties of the workpiece material. Therefore, elastic-perfectly plastic model was considered in this work. **Figure 4.3** shows the structure properties which were used in the calculation. Furthermore, based on the removal mechanism analysis which was explained in **Chapter 3**, 19% of the molten area was removed during discharging, and thus material removal is also considered in the calculation of residual stress due to micro EDM single discharge. Other important assumptions that have been made regarding the model are as follows:

i) The workpiece material is homogeneous and isotropic
ii) Thermophysical properties of the material are temperature dependent as explained in **§ 3.2**.
iii) The workpiece is stress-free before EDM

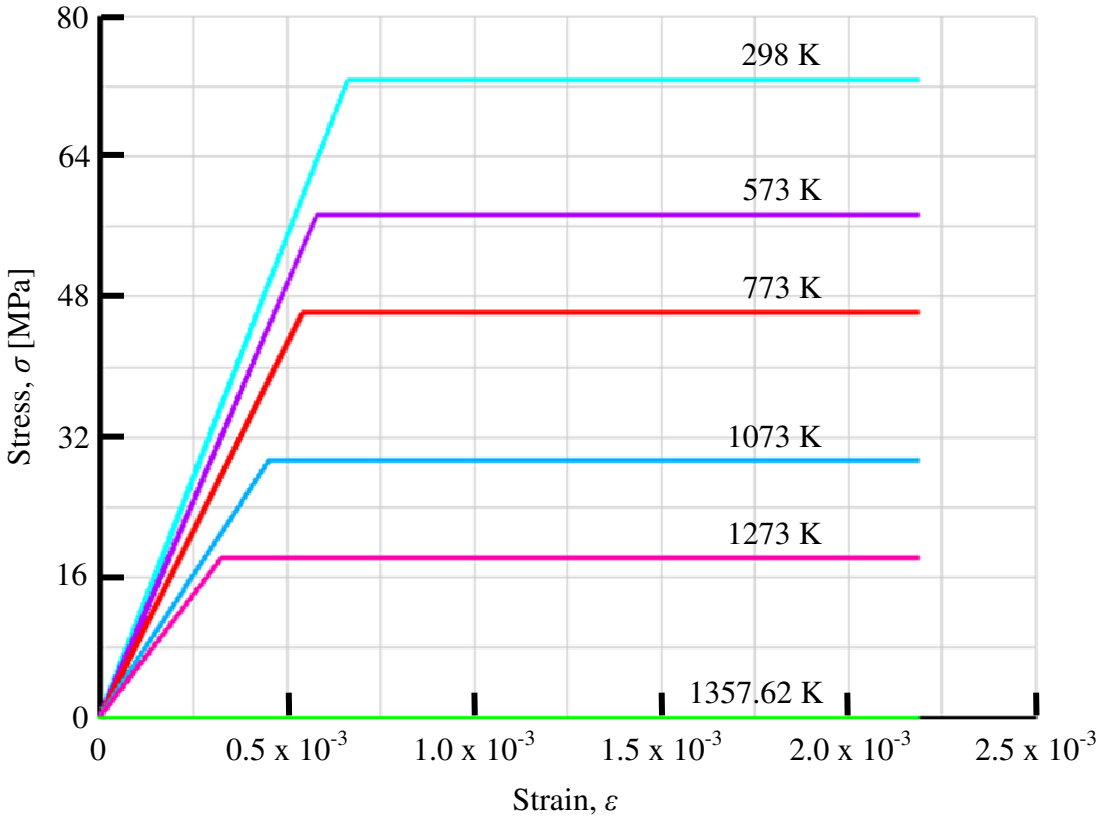

Figure 4.3: Temperature dependent stress/strain relationship

4.3.2 Coupled-field analyses and element types

In this work, residual stress is calculated based on the results of temperature distribution within the workpiece. This means thermal and structural analyses are required in the calculation of the residual stress. A convenient method to perform such analysis is known as coupled structural-thermal analysis which is one of the coupled-field analyses in ANSYS. A coupled-field analysis is a combination of analyses from different engineering disciplines (in this case structural and thermal) that interact to solve global engineering problem which is commonly known as a multiphysics analysis. To perform this analysis a couple-field element should be selected.

There are more than 150 different element types in ANSYS. The selection of the type of element is important to assure that the desired model can be developed and the desired output results can be obtained. In this work, 2-dimensional 8 nodes coupled-field solid element (PLANE223) has been selected.

PLANE223 is provided in ANSYS so that it can be used for thermal and structural analysis. All thermophysical and mechanical properties that are required to calculate the residual stress due to discharge can be imposed within the element, and it is also good for transient analysis. Furthermore, several types of surface load can be applied when using PLANE223 including power density. The solution outputs associated with this element include stresses, strains and temperature.

4.3.3 Surface heat flux and element death

ANSYS is capable of simulating material removal by means of element death. To achieve the effect of element death, the ANSYS program does not actually remove the elements. Instead, it deactivates them by reducing their stiffness significantly in structural analysis. **Figure 4.4** shows an example of material removal simulation using the element death feature in ANSYS.

In the figure, temperature distribution at the beginning of micro EDM single discharge is shown. **Figure 4.4** a. shows the result before employing the element death procedure. In this example, the boiling point of the workpiece is equal to 2562℃ and area on workpiece where its temperature exceeds the boiling point is assumed to vaporize immediately. Thus, elements where their temperature exceeds boiling point should be deactivated. **Figure 4.4** b. shows the result after deactivation of the elements.

In this work, as explained earlier the power density diameter, d (t_e) is assumed to increase linearly within the discharge duration (= 70 ns). As shown in **Table 4.1**, the power density, P_e (t_e) is also time dependent and decrease significantly toward the end of the discharge duration. Therefore, temperature started to decrease not after the end of discharge but during the discharging.

Because deactivation of elements need to be executed during calculation, the discharging simulation was separated into 10 parts with simulation period 7 ns for each part in order to employ the element death feature in between. For example, **Figure 4.5** shows the method to apply the power density on a workpiece. **Figure 4.5** a. shows the 1st part of the discharging. The diameter of the heat flux expands to 1/10 of maximum plasma diameter within this period. 7 ns after igniting a discharge, temperature distribution result is obtained and deactivation of elements is executed.

Figure 4.5 b. shows the 2nd part where the heat flux diameter expands to 2/10 of maximum plasma diameter. The result of the 1st part is used as initial state for the 2nd part of discharge. Here, the current value of P_e (t_e) is applied on the new elements surface. The process was repeated until the end of discharge time. Then, additional one model to simulate cooling process is built. Here, the result of 10th part of the discharging model is used as initial state and the simulation period is set equal to 300 ns to allow sufficient cooling period before obtaining the residual stress.

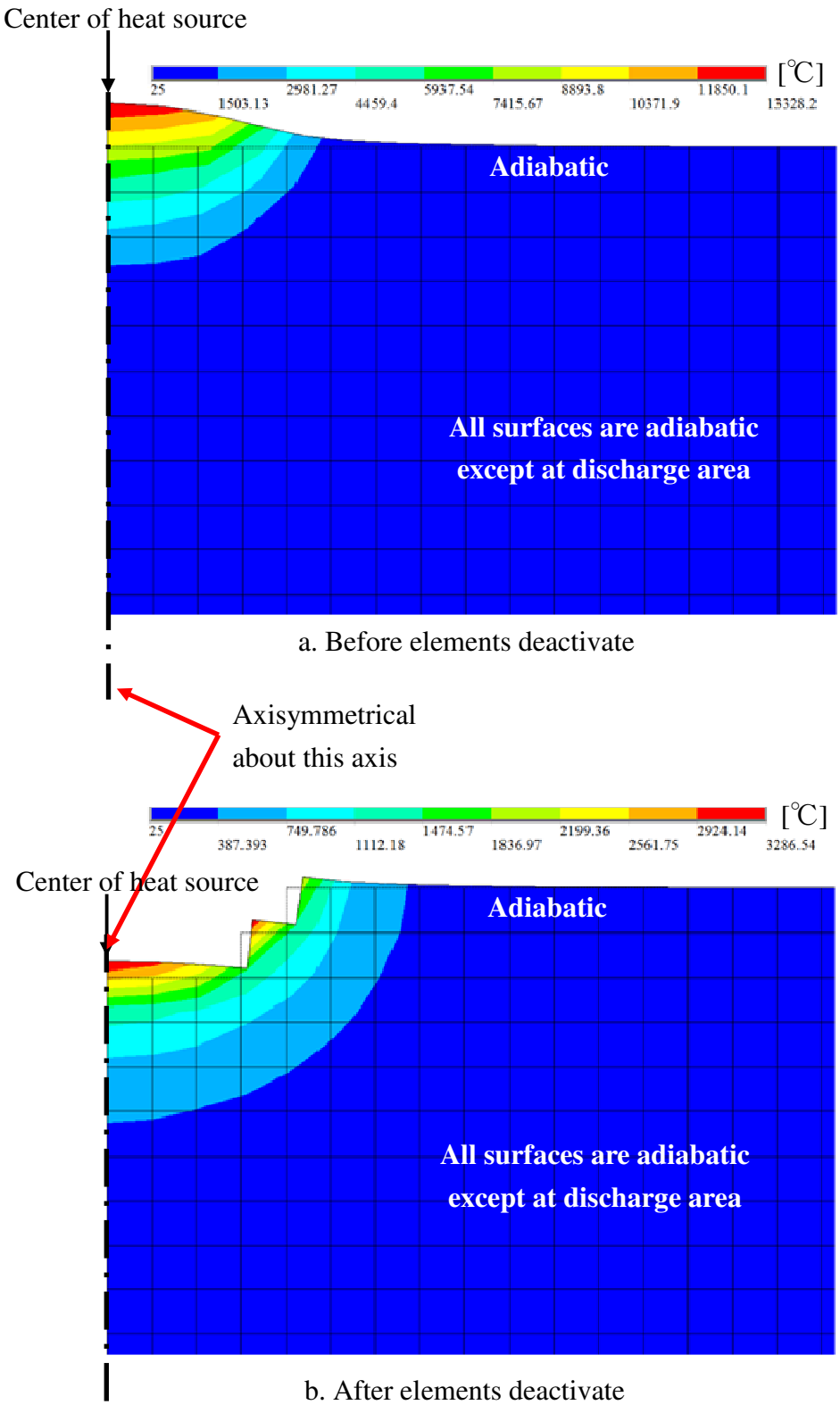

Figure 4.4: Method to simulate material removal with respect to temperature rise

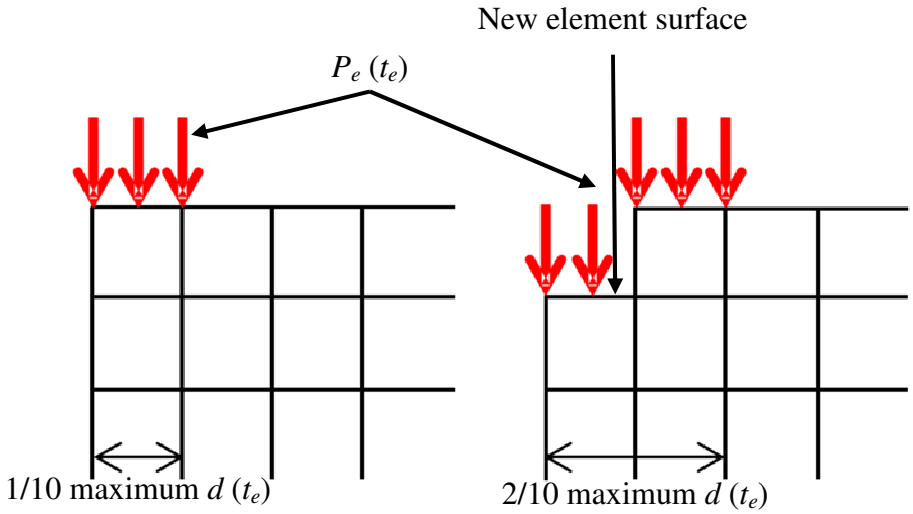

a. 1st part
(0 ~ 7 ns discharge duration)

b. 2nd part
(7 ~ 14 ns discharge duration)

Figure 4.5: Power density on workpiece surface

4.4 Results

Figures 4.6 and **4.7** show the temperature distribution results with and without considering the material removal, respectively. As shown in **Figures 4.6** a. and **4.7** a. at the end of discharge duration (t = 70 ns after the ignition of discharge), the maximum temperature near the discharge crater was approximately 300 ℃ in both cases. In **Figure 4.6** b. and **Figure 4.7** b. at the end of cooling time (t = 370 ns after the ignition of discharge), the maximum temperature of the workpiece model drops to about 40 ℃ in both cases. This means, maximum temperature was approximately 15 ℃ above the initial temperature after cooling. This can be considered sufficiently low for the residual stress calculation. In the case of macro EDM, maximum temperature at the end of cooling time of approximately 100 ℃ was considered sufficiently low [47].

The distributions of temperature with respect to time during discharge duration in the case of considering material removal are shown in **APPENDIX D**.

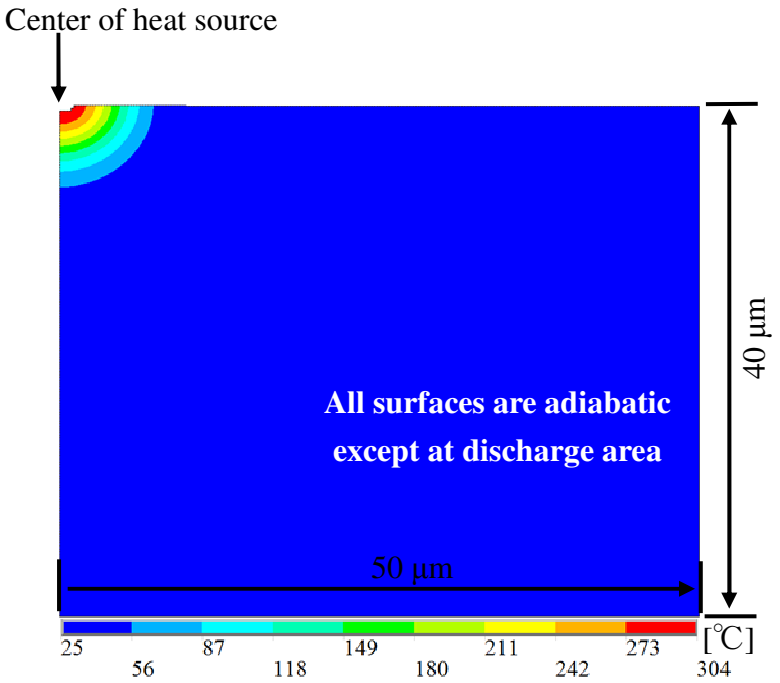

a. At the end of discharge

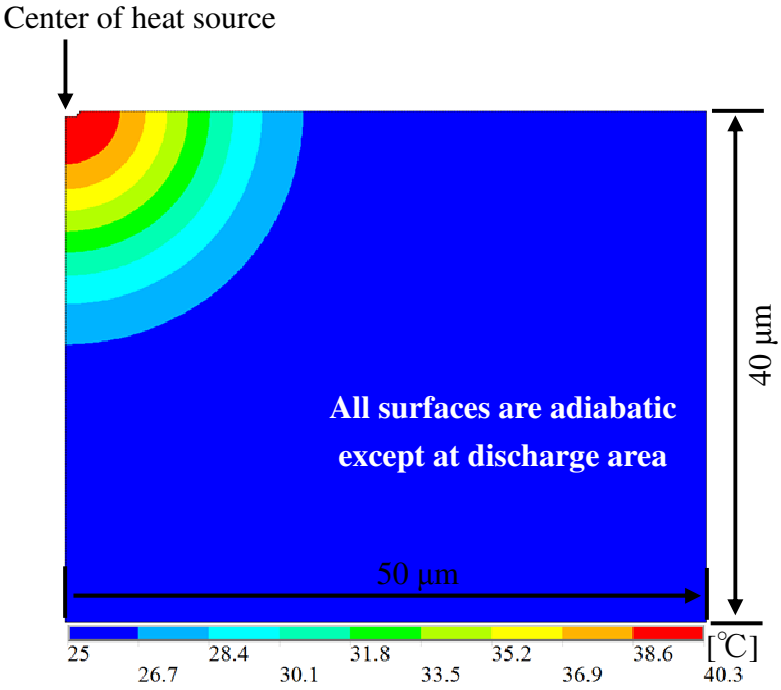

b. At the end of cooling time

Figure 4.6: Temperature distribution result considering material removal

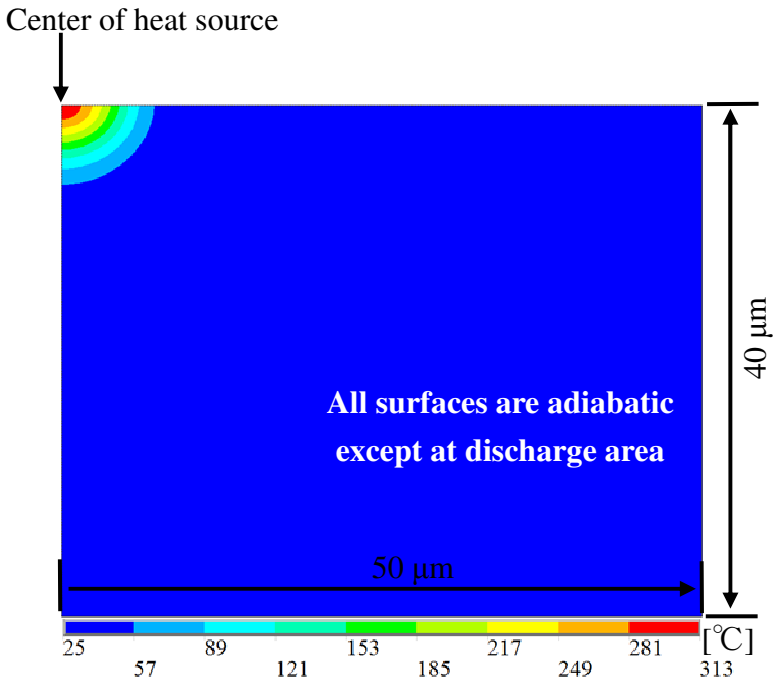

a. At the end of discharge

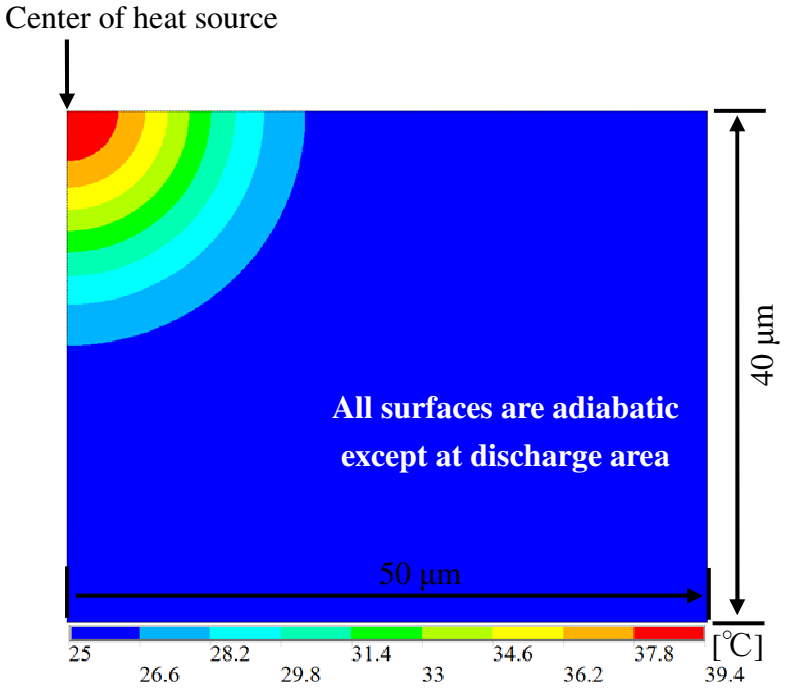

b. At the end of cooling time

Figure 4.7: Temperature distribution result without considering material removal

From this model, the residual stress distribution along the center axis of a crater due to micro EDM single discharge was calculated. **Figure 4.8** shows the results of the residual stress in the radial direction, $\sigma_r(z)$ with and without considering the material removal. In the case of considering material removal, elements where temperature is above 2562 ℃(boiling point of copper) were removed from the workpiece model. The distribution of residual stress at the end of cooling time in the case of considering material removal is shown in **APPENDIX E**.

According to the result of removal mechanism analysis in **Chapter 3**, 11% of the total removal volume per pulse is removed by melting. However, the temperature of the material which is removed by melting was unknown, and in **§ 3.1**, the material was assumed to be removed above 1823 ℃ (average between melting and boiling points of copper) to calculate the energy carried away by debris. Thus, to calculate the thermal stress in this chapter, in a separate model, after removing elements where temperature is above boiling point of copper, elements where temperature is above 1823 ℃ were also removed from the workpiece model. The simulated volume of removal was slightly larger compared to that of the model considering material removal at boiling point. As shown by solid grey line in **Figure 4.8**, there is no significant difference in thermal stress result compared to the case of considering material removal at boiling point of copper.

As shown in the figure, the distribution of $\sigma_r(z)$ in depth direction is non-linear. At the area near the crater tensile residual stress was formed, and at deeper area in depth direction $\sigma_r(z)$ changes to compressive residual stress. Although the peak and the depth of $\sigma_r(z)$ are different from the case of macro EDM, the distribution of $\sigma_r(z)$ in the depth direction coincides with the calculation results obtained by other researchers in the macro EDM [46-52].

In the figure, tensile residual stress peaks near the surface. In this work, temperature dependent structure properties were considered and the values are lower at higher temperature as previously shown in **Figure 4.3**, and as shown in **Figure 4.6** and **APPENDIX D**, temperature at surface always higher than that of deeper area. This might be the main reason that the peak of tensile residual stress appears below the surface. In the next chapter the influence of the $\sigma_r(z)$ distribution in depth direction on micro fin deformation will be discussed.

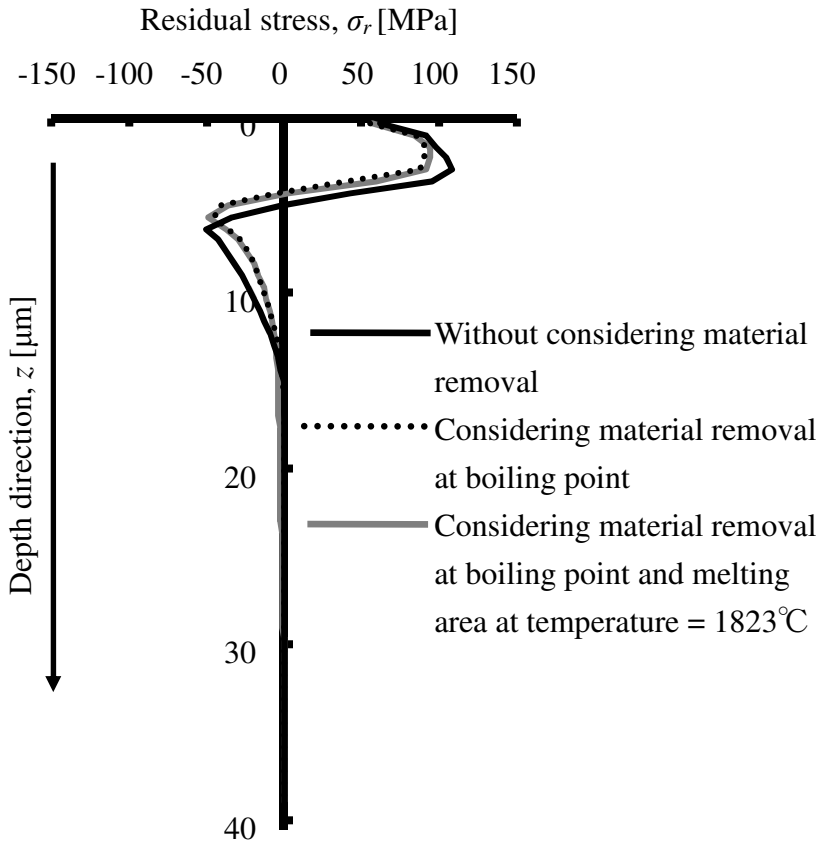

Figure 4.8: Residual stress due to micro EDM single discharge

4.5 Conclusions

A model has been developed using accurate thermal boundary conditions based on the results of thermal phenomena analysis which were obtained in this work to calculate thermal stress due to micro EDM single discharge. In the model, power density at workpiece and heat source diameter were made to change with time during discharge duration. Besides, material removal was also considered during the calculation. The calculation result shows that the peak and the depth of thermal stress in the center axis of a crater due to micro EDM single discharge were smaller than those of macro EDM [47]. However, the distribution of the thermal stress along the center axis of the crater was similar to that of macro EDM [47].

Chapter 5 Deformation of micro EDM workpiece

In the previous chapter, residual stress due to micro EDM single discharge has been obtained using the accurate heat source model which was made based on the experimental and analytical results obtained in **Chapters 2** and **3**. Although the formation of the stress below the micro EDM crater was not as deep as that of macro EDM, the distribution of the residual stress in depth direction was similar to the case of macro EDM [46-52]. The residual stress due to micro EDM discharges may cause the workpiece deformation. However, as explained in **§ 1.2**, the deformation also could be caused by residual stress that exists within the workpiece prior to micro EDM process. In this chapter, the main purpose is to discuss the effect of the residual stress due to micro EDM on workpiece deformation. Therefore, the influence of pre-existing residual stress should be eliminated prior to micro EDM. If the influence of the stress on deformation of workpiece is significant, all the workpieces should undergo stress-release treatment before the micro fins fabrication.

5.1 Method to cut the workpiece

In wire EDM, fabricated fins started to bend when the fin thickness was less than 100 μm in rough cutting condition, and it was considered that the occurrence was due to the thermal effect of EDM [32]. Compared to macro EDM, as explained in **Chapters 2** and **3**, the micro EDM process involves lower discharge energy, lower energy distribution ratio into workpiece, and forms thinner white layer. However, the deformation of micro EDM workpiece occurs more often than macro EDM, because the diameter or thickness of micro parts is comparable to the depth of the heat affected zone. In order to observe the deformation and the influence of the pre-existing residual stress, various methods to cut micro fin using micro EDM will be conducted. In this work, two types of workpiece namely Cu plate and Cu wire will be cut into micro fin, and then physical models will be built using finite element analysis software in order to understand the deformation.

5.1.1 Thin plate cutting using micro EDM

Figure 5.1 shows methods to cut Cu thin plate. The methods shown in **Figure 5.1** a. and b. are similar, except the plate workpiece was held horizontally and vertically, respectively. In order to explain the method, **Figure 5.1** b. is referred. First, the tool was moved downward to the starting position in the direction of cutting depth, *Cd;* approximately 1000 μm for the workpiece which was held vertically. Then the tool was relatively moved towards the plate side surface perpendicularly and cutting begins. In this work, micro tool was rotated during the thin plate cutting so that excessive tool wear does not occur at only one side of the tool surface which may severely influence the cutting progress.

After the first slot cutting, the tool was returned to the starting position, and then it was moved in the *y*-direction relative to the plate. Then, the tool was moved again towards the plate side surface to begin the 2nd slot cutting. Here, movement in *y*-direction is important to control the fin thickness, *ft*. Workpiece with plate thickness, *Th* equal to 80 μm was used in this work.

Besides, to eliminate the influence of the residual stress due to cold working within the Cu plate, the residual stress releasing process was conducted by heating some samples of Cu plate before the machining at approximately 150 ℃ for 30 minutes. This is a typical condition for the stress-release treatment of copper. Then, comparison of micro fin between samples that were annealed and not annealed can be made.

In this work, a hot plate was used for the stress-release treatment. **Figure 5.2** shows setup for the stress-release treatment. First, hot plate temperature was set to 150 ℃. When the temperature of the hot plate surface reached 150 ℃, Cu plates were placed on the hot plate and three layers of Teflon sheets with 0.5 mm in thickness each were placed on the Cu plates as heat insulator. Then, a static load was used to press the samples from the top side of the Teflon sheets while the heating is in progress.

After 30 minutes, the power supply of the hot plate was turned off. Then, after temperature of the Cu plate decreased to room temperature the load and Teflon sheets were removed. However, there was possibility that the residual stress due to cold working was not released completely from the Cu plate. Therefore, the plate was also cut in various orientations and the deformations of the workpiece under various conditions were observed and compared.

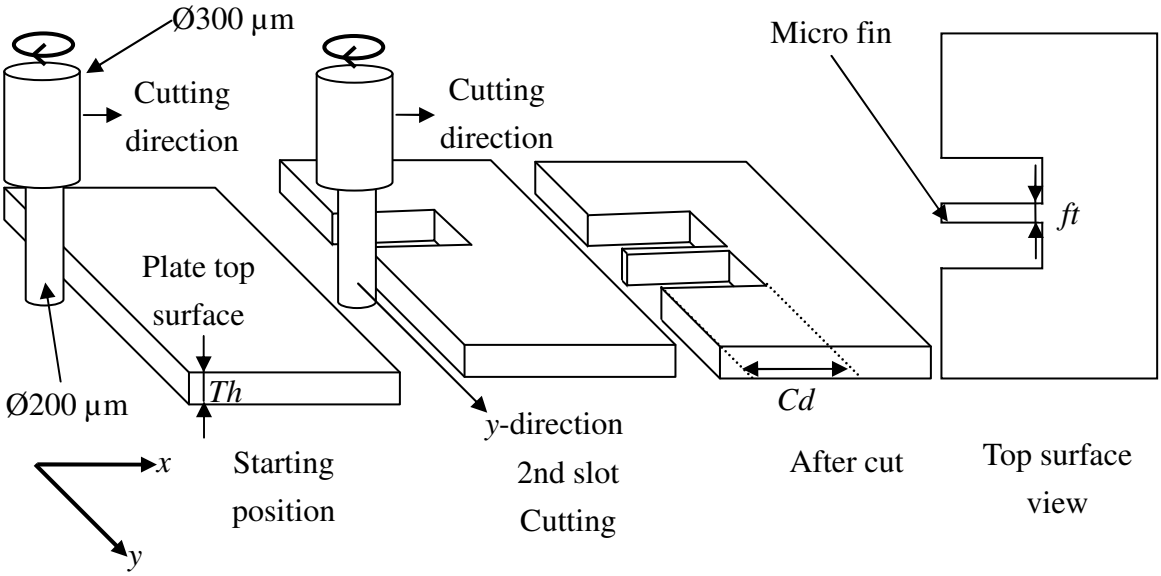

a. Cu workpiece held horizontally

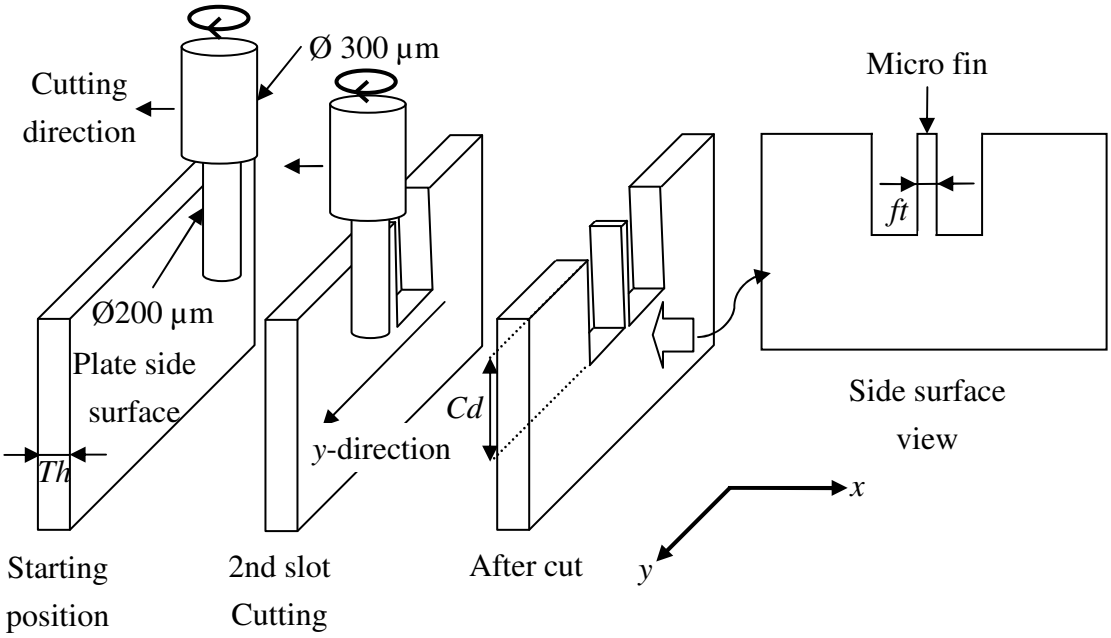

b. Cu workpiece held vertically

Figure 5.1: Fabrication of micro fin from Cu thin plate

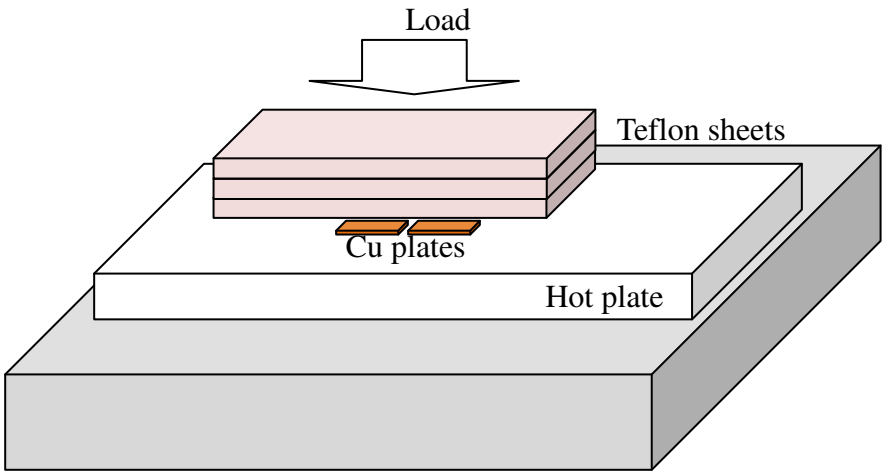

Figure 5.2: Stress-release treatment to eliminate residual stress prior to EDM

Figure 5.3 shows some examples of micro fins which were cut using the method which was previously shown in **Figure 5.1** a. In the example, discharge current and duration was equal to 4.5 A and 195 ns, respectively. As shown in **Figure 5.3** a., under a certain fin thickness, *ft* the fins deformed. However, the fins produced by this method are difficult to be modeled for the structural analysis. The reason is the fin thickness was not consistent along its length as shown in **Figure 5.3** b.

The main reason that causes the taper shape was the tool electrode worn out during cutting. By using this method, severe concentration of wear on a limited area of the tool can be observed. This is because only a small area on the tool confronted the workpiece during cutting for a long period.

In order to reduce the concentration of tool wear, instead of holding the workpiece horizontally, it was held vertically as previously shown in **Figure 5.1** b. By using this method, the area on the tool confronting the workpiece during cutting could be increased significantly. This means the occurrence of wear will be distributed along the tool length surface. Furthermore, since the wear becomes uniform along the tool axis, the thickness of the fin can also be machined uniformly.

Figure 5.4 a. shows micro fins which were cut using the 2nd method. In the example, discharge current and duration was equal to 4.5 A and 195 ns, respectively. The deformation of fins can be observed. However, as shown in the figure, as cutting continues the shape of fins is changed from the shape that is shown in the left picture to that of the right picture. This is because the fins are bent during cutting and the free end tip of the fins approach and cut the tool electrode. A picture of the tool electrode which was used to cut all the 6 fins is shown in **Figure 5.4** b.

The pictures in **Figure 5.4** a. also show that the fins always bend towards 2nd slot cutting. Furthermore, a similar degree of bending was observed during micro fins fabrication although the cutting orientation of the Cu plate was changed, and with or without the stress-release treatment in **Figure 5.2**. This means the pre-existing residual stress was not affecting the deformations in this work. This also means that residual stress due to micro EDM is the dominant factor to cause the deformation. However, the fins produced by this method were also difficult to be analyzed because the fin thickness along its length was not consistent. Thus, a different method of fin fabrication using micro EDM should be considered for more reliable thermal stress analysis.

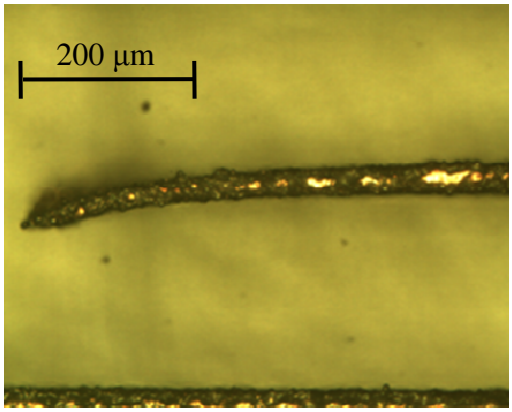

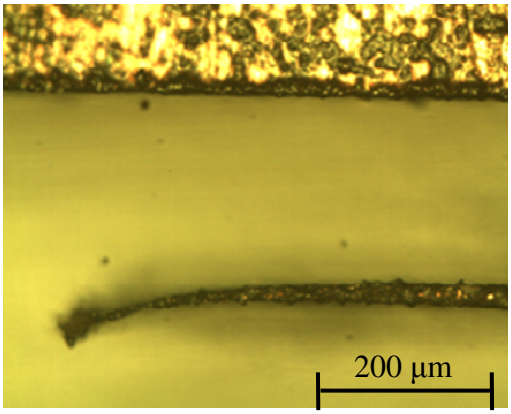

a. Micro fins started to deform under a certain fin thickness

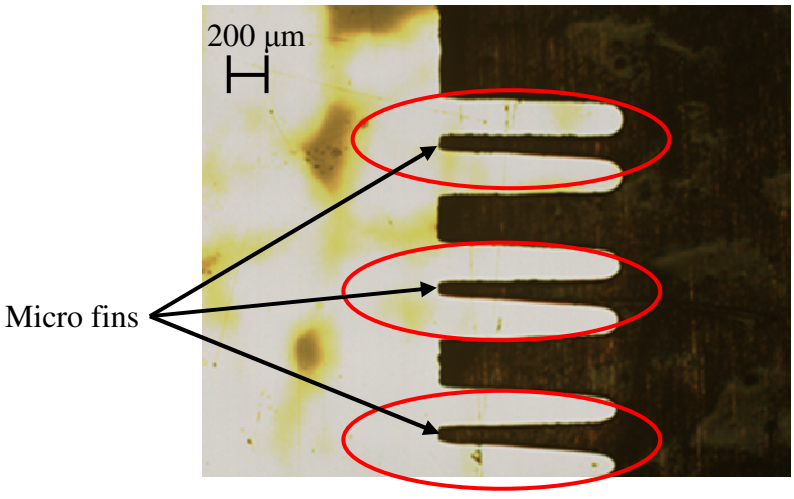

b. Fins thickness not consistent along its length

Figure 5.3: Micro fins (Cu workpiece was held horizontally)
Machining conditions; i_e = 4.5 A, t_e = 195 ns

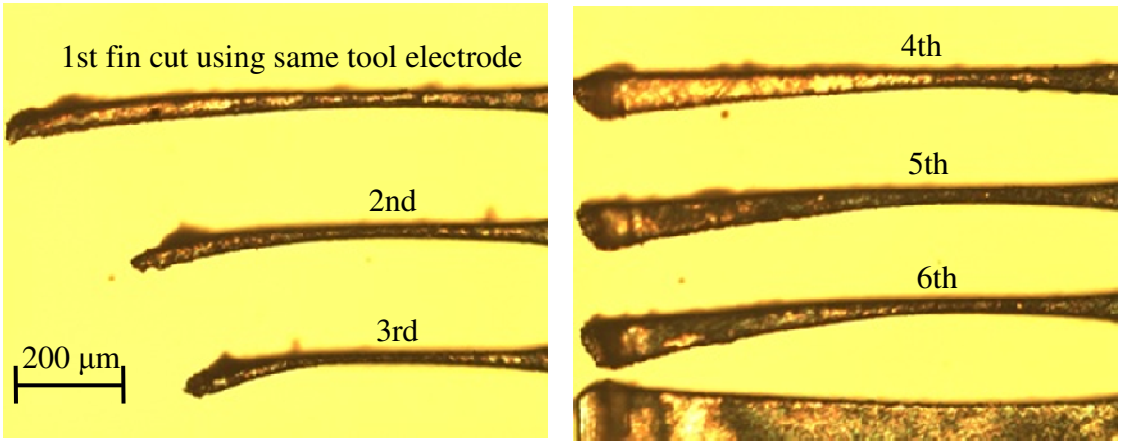

a. Micro fins cut by micro EDM

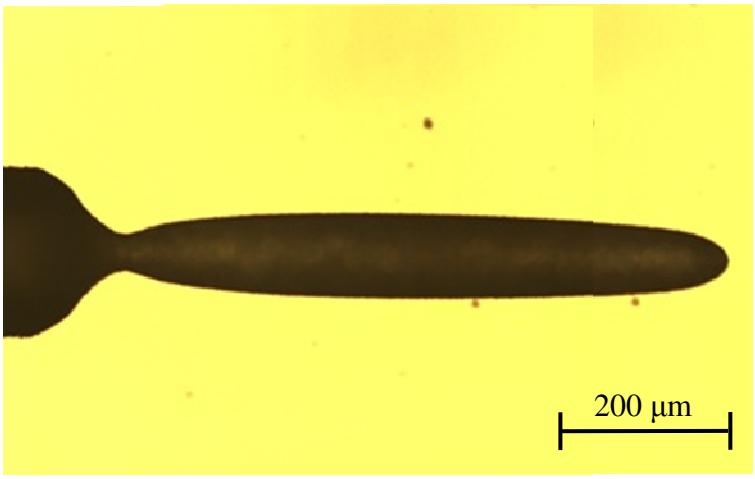

b. Micro EDM tool that was used to cut the above 6 fins

Figure 5.4: Micro fins (Cu workpiece was held vertically)
Machining conditions; i_e = 4.5 A, t_e = 195 ns

5.1.2 Copper wire machining using WEDG

In this experiment, the machined micro fin thickness along its length should be consistent otherwise it will be difficult to be modeled. In order to obtain a consistent fin thickness along its length, the influence of tool electrode wear is not allowable. Thus, wire-electro discharge grinding, WEDG [9] was used in this work because the wire tool electrode continuously travels during machining, and thus the wire wear does not affect the machining precision. Furthermore, since discharge occurs only at the root of the micro fin, the end of the bent fin does not interfere with the tool electrode. Therefore, the fin can be deformed freely according to the distribution of residual stress.

Figure 5.5 shows the method to machine Cu wire workpiece using WEDG. **Table 5.1** shows the WEDG setting. First, diameter of a rotating Cu wire workpiece was reduced from Ø300 μm to Ø100 μm. The preparation of Ø100 μm cylinder was done under a finishing condition to assure no significant effect of thermal stress on the micro fin deformation [56]. Then, its surface was machined in the subsequent steps as shown in **Figure 5.5** b. and c.

As shown in **Figure 5.5** b., the rotation of Cu wire workpiece was stopped, and one side of the Cu workpiece was machined using low discharge energy; 55 V open circuit voltage and stray capacitance (< 10 pF), in order to minimize the thermal effect on this side surface. Stray capacitance was used to obtain the minimum discharge energy which can be provided by the pulse generator of the WEDG. As shown in **Figure 5.5** c., the Cu workpiece was manually rotated by 180°, and then the other side of the workpiece was machined using high discharge energy; 110 V open circuit voltage and 1000 pF capacitance to generate thermal stress on this surface. Capacitance of 1000 pF was used for rough machining in micro EDM.

As shown in **Figure 5.5** d., the deformation of Cu workpiece with consistent fin thickness along its length can be observed. In all machining results, fins always bent towards the 2nd side cutting surface. It was also found that the fin always deformed at fin thickness below 30 μm. Further observation on the comparison of deformation results between samples annealed and not annealed prior to micro EDM process also indicated that the effect of pre-existing residual stress due to cold working was not significant. Thus, only thermal stress due to micro EDM influences the deformation of the Cu workpiece in this experiment.

Table 5.1: Cu wire WEDG setting

Operation	Open circuit voltage [V]	Capacitor [pF]
a. Reduce Cu wire diameter to Ø100 µm	60	100
b. Cut 1st side	55	< 10
c. Cut 2nd side	110	1000

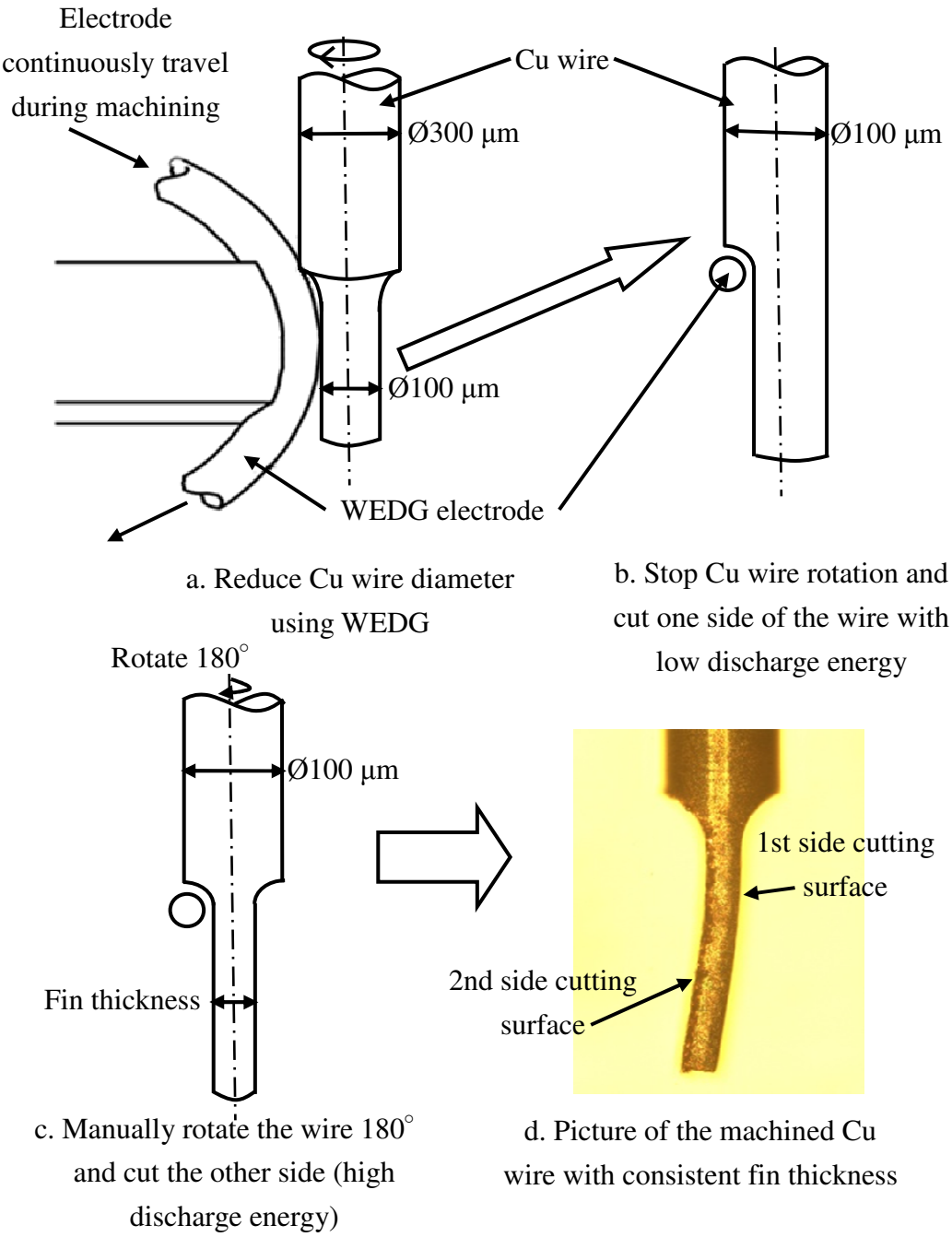

Figure 5.5: Experiment to observe the Cu wire workpiece deformation

In actual machining, thousands of discharges are ignited during micro fin machining at random locations, and the residual stress distribution due to each discharge is axisymmetrical with respect to the discharge spot. Therefore, to apply the stress distribution to the machined surface randomly, three-dimensional analysis is required. Moreover, linear superimposition of the stress distribution due to single discharge does not give the stress field as a result of consecutive discharges because the stress distribution caused by a single discharge is released to some extent by melting, softening and removing of the material due to the subsequent discharges. Furthermore, change in phase and microstructure may also occur.

However, three-dimensional and time-dependent simulation by imposing the thermal stress due to sequential discharges is very complicated and time-consuming. Hence, considering the purpose of the present example, for simplicity, it was assumed that the residual stress is two-dimensional, and the stress result considering material removal at boiling point and melting area at temperature = 1823℃ as shown by solid grey line in **Figure 4.8** was applied to the beam uniformly along the axis as shown in **Figure 5.6**. The dimension of the model was based on the machined micro fin as shown in **Figure 5.5** d. Young's Modulus and Poisson ratio was set equal to 1 x 10^{11} Pa and 0.33, respectively.

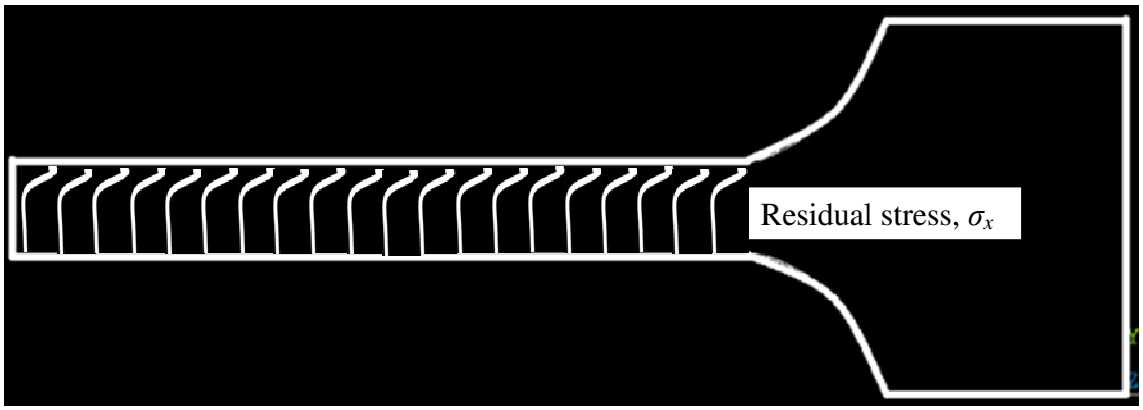

Figure 5.6: Applied residual stress, σ_x within the model

5.2 Method to impose residual stress

ANSYS provides several types of element that can be used for the structural analysis. **Figure 5.7** a. shows a picture of micro fin which was machined by micro EDM in this work. As shown in the figure, the deformation of micro fin is not uniform along the axis. The fin looks straight near the tip and curvature is larger near the root. One of the element types in ANSYS which are suitable to model curvature is PLANE 183. Therefore, PLANE 183 was selected as an element to build the micro fin model.

Furthermore, the element can be used for axisymmetric modeling and well suited for large deflection and large strain capability. Another capability of this element is allowing the application of 'initial state'. This is required in this work to impose the residual stress within the micro fin model. To impose the residual stress, ANSYS uses INISTATE command. This command need to be typed manually within the ANSYS program for each element. The syntax is as follows:

'INISTATE, define, element #, , , , residual stress value'

For example, 'INISTATE, define, 304, , , , -2e+8' means compressive residual stress of 2 x 10^8 Pa is imposed at element number 304. Here negative sign indicates compressive, and to impose tensile stress within an element no particular sign is required. In later section uniform rectangular beam model will be developed to understand the effect of the residual stress which is non-linearly distributed in the thickness direction on the fin deformation. The model size will be 26.4 μm x 200 μm and mesh size is made equal to 0.66 μm. This means all together 12160 elements are involved, and thus 12160 syntaxes must be typed manually within the ANSYS program to define residual stress at each element.

5.3 Comparison between machined and modeled workpiece

Figure 5.7 shows machined and simulated micro fin. The fin thickness is 26.4 μm. As shown in **Figure 5.7** b., when residual stress due to single discharge was uniformly imposed along the fin length, the change in displacement at its tip so-called deflection, λ = 30.3 μm, which was 19 μm smaller than the measurement. This is because the model was two dimensional and interaction between thermal stress fields caused by sequential discharges was ignored. Hence, sequential discharges must be considered.

After the first deformation as shown in **Figure 5.7** b., the residual stress distribution will be released to some extent. Then, the next sequential discharges will be ignited over the surface continuously. Hence, using the deformed shape of the fin and the residual stress distribution inside the fin, another same residual stress due to discharge should be applied only in the area near the top surface. That is, the residual stress near the top surface only is replaced by the residual stress distribution due to discharge which is the same as the first deformation process. Residual stress distribution in other area should be left the same as that was generated after the first deformation.

Then, the second deformation due to the newly applied residual stress is calculated. As a result, the fin will be deformed furthermore, thereby the residual stress distribution will be renewed. In the second deformation, the increment of λ will be smaller than that in the first deformation. This is because another deformation in the second process will increase the tensile stress on the bottom surface of the micro fin further.

Then, using the newly deformed shape of the fin and residual stress distribution inside the fin as the initial conditions, the third deformation process is calculated. Since the top surface is again covered by the new discharge craters for the third time, the residual stress distribution near the top surface is replaced by the same distribution that was distributed on the virgin surface in the first process. Thus, the fin will be deformed further. However, the increment of λ will be smaller than the one in the second process.

In the same way, the deformation process is repeated until the shape of the fin deformed does not change in the steady state. Hence, the calculation of the deformation process should be repeated until the change in the shape of the fin does not occur. In the steady state, the residual stress before bending should be equal to that after bending. That means the original residual stress distribution due to discharge on the top surface should balance with the residual stress distribution in the bottom side of the fin.

However, it is difficult to use the deformed shape of micro fin as initial condition for the next sequence of discharges. Therefore, for simplicity, the deformation of straight micro fin with the stress fields caused by the previous sequential discharges is obtained. This means, the value of λ based on this calculation method will indicate the increment of micro fin deflection in the ideal calculation which was explained above. Thus, the summation of all λs which are calculated using straight micro fin as an initial condition should be equal to the final λ obtained from the ideal calculation.

Figure 5.7 c. and d. show the results of calculation models that used straight micro fin as initial condition imposed with the stress field due to the two and three sequential discharges, respectively. As shown in the figures, λ was equal to 13.2 and 3.9 μm, respectively. In the example, λ decreased and theoretically it will equal to zero at steady

state, which means residual stress distribution due to discharges on the top surface is balanced with the residual stress distribution in the bottom side of the micro fin. From **Figure 5.7** b., c. and d., the total values of λ was almost equal to the measured deflection. This indicates the deformation of micro fin in the example was the result of stress fields caused by sequential discharges.

As shown in **Figure 5.7** a. and b., although λ was different, experimental and simulation results show similar curvature which is not uniform along the axis. The fin looks straight near the tip and curvature is larger near the root. Theoretically, to form a uniform bending, the distribution of stress in thickness direction must be linear and symmetrical about the boundary between compressive and tensile region. However, as shown in **Figure 4.8**, the distribution of stress in thickness direction, $\sigma_r(z)$ was not linear, and this may cause the non-uniform bending. Therefore, in order to explain the deformation, additional models using a uniform straight beam were built and will be explained in **§ 5.4**.

In addition, as shown in **Figure 5.8**, λ of micro fin increased when the fin thickness was reduced. This is because the tensile residual stress distributed within 4 μm in depth from the workpiece top surface as shown in **Figure 4.8** causes the fin to contract. At deeper area within 30 μm, compressive residual stress acts oppositely. Therefore, when the fin thickness was reduced approximately under 30 μm, the moment generated by the residual stress distribution in the thickness direction causes the deflection of micro fin.

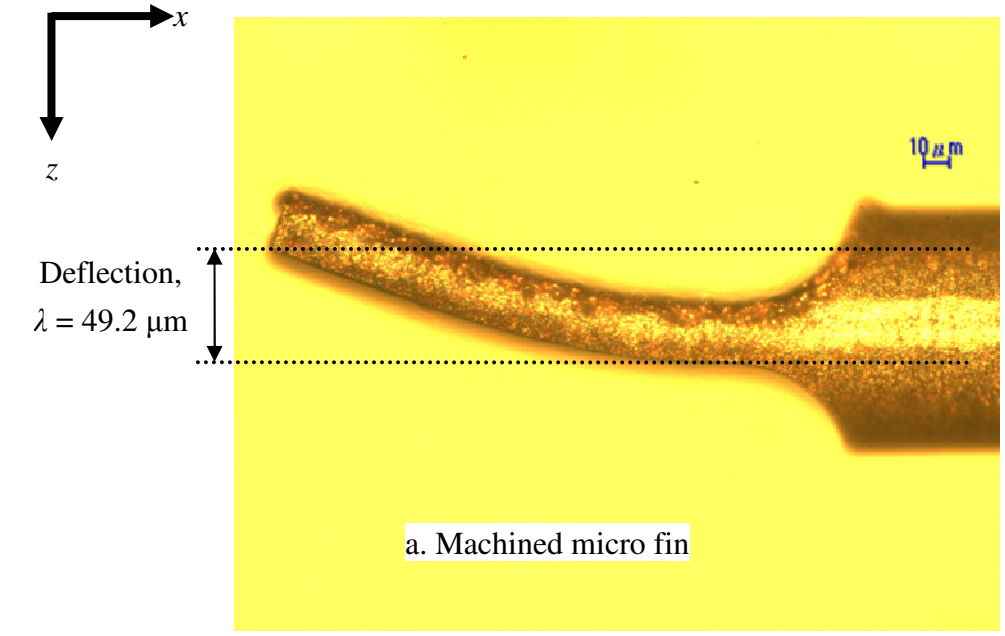

a. Machined micro fin

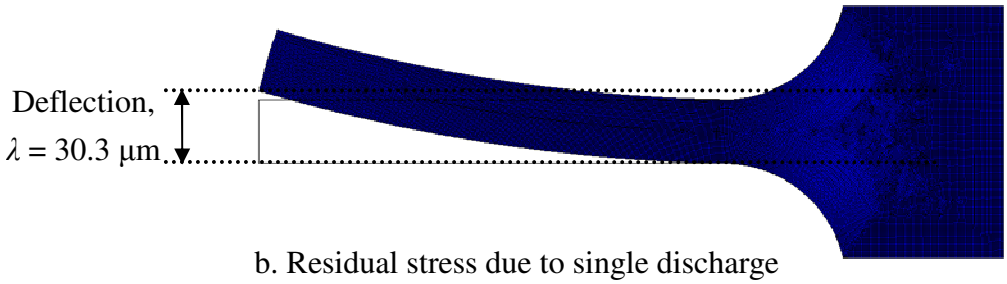

b. Residual stress due to single discharge uniformly imposed along the fin length

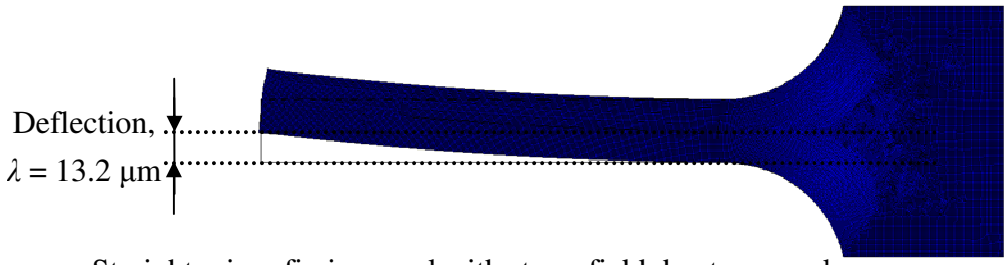

c. Straight micro fin imposed with stress field due to second sequential discharges

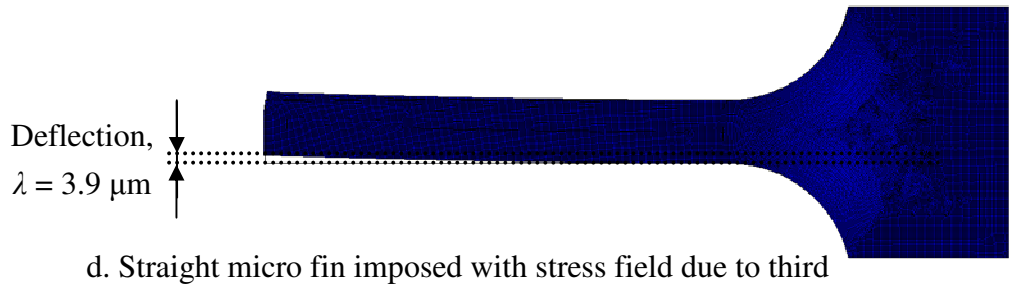

d. Straight micro fin imposed with stress field due to third sequential discharges

Figure 5.7: Deformation of machined and simulated micro fin

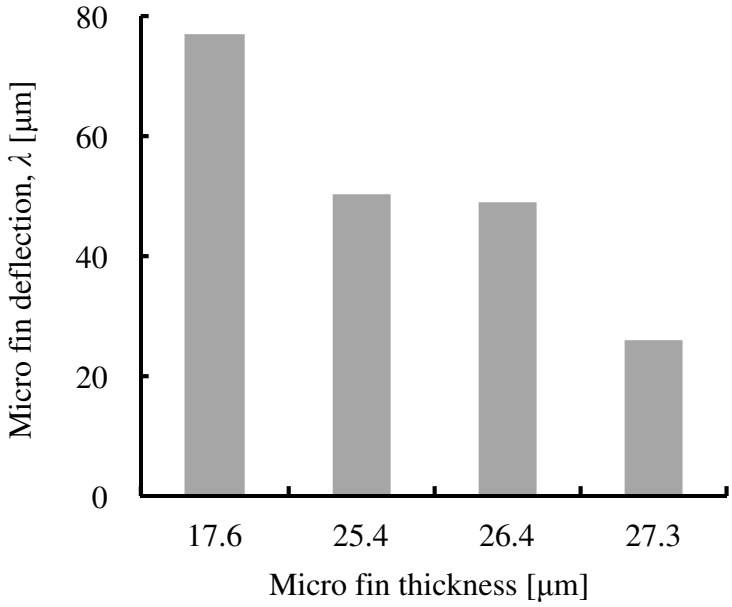

Figure 5.8: Measured deflection of micro fin with respect to its thickness

5.4 Uniform rectangular models

The uniform rectangular beam models were used to investigate the effect of residual stress in the longitudinal direction, $\sigma_x(z)$ varying in thickness direction on the beam curvature. Either $\sigma_x(z)$ distributed linearly or $\sigma_x(z)$ due to discharges is imposed within the uniform straight beam model to observe the effect of $\sigma_x(z)$ distribution. For simplicity, it is assumed that $\sigma_x(z)$ due to multi discharges is equivalent to $\sigma_r(z)$ generated by a single discharge. Two results to be observed from these models in order to explain the non-uniform bending are the straightness of beam end surface and the radius of curvature at beam top surface. For this purpose, four additional models were built as follows:

i) Simple beam support with $\sigma_x(z)$ varying linearly in thickness direction.
ii) Rigidly fixed at one side with $\sigma_x(z)$ varying linearly in thickness direction.
iii) Simple beam support with $\sigma_x(z)$ due to discharge
iv) Rigidly fixed at one side with $\sigma_x(z)$ due to discharge

Figure 5.9 and **Figure 5.10** show the types of support and the distribution of $\sigma_x(z)$, respectively.

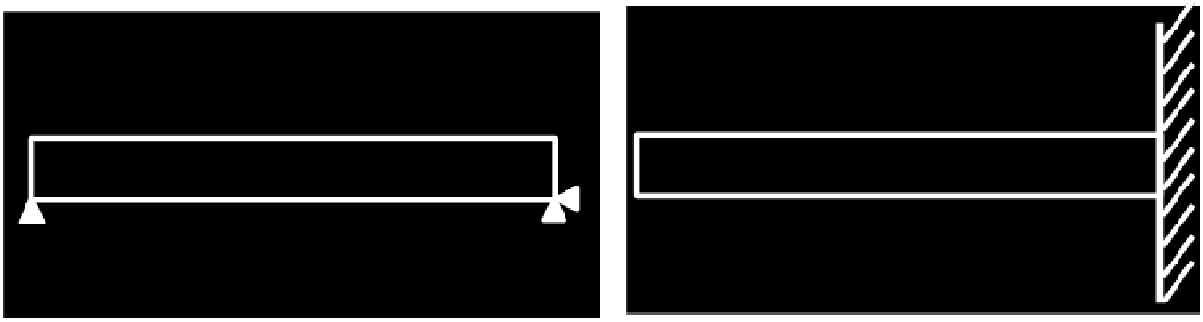

a. Simple beam support

b. Rigidly fixed at one side

Figure 5.9: Types of uniform rectangular beam

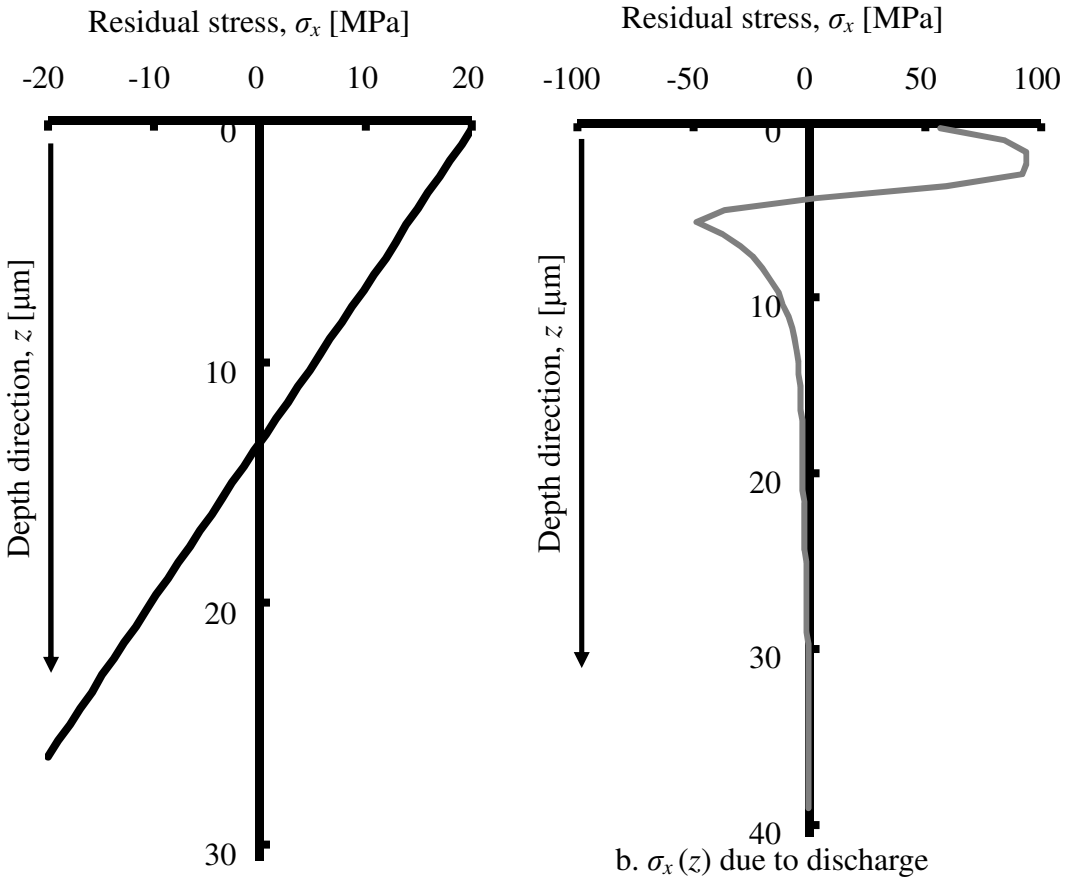

a. $\sigma_x(z)$ varies linearly in thickness direction

b. $\sigma_x(z)$ due to discharge (Considering material removal at boiling point and melting area at temperature = 1823℃)

Figure 5.10: Linear and non-linear distribution of $\sigma_x(z)$ in fin thickness direction

5.5 Results and discussions

First, the straightness of free end surface (left end surface in **Figure 5.9**) of simulated uniform rectangular beam models was observed. Theoretically, if $\sigma_x(z)$ varies linearly in thickness direction, the free end surface of a rectangular beam in both simple support and one side rigidly fixed should remain straight. **Figure 5.11** shows the displacement of the free end surface in x-axis direction after imposing $\sigma_x(z)$. **Figure 5.11** a. and b. are results in the cases of linear $\sigma_x(z)$ with simple support and rigidly fixed at one side, respectively.

As shown in both figures, displacement of end surface perfectly coincided with the least square linear approximation line, which means when linear $\sigma_x(z)$ was imposed within the beam in both types of support, the free end of the uniform rectangular beam remains straight. On the other hand, when the non-uniform distribution of $\sigma_x(z)$ due to discharge was imposed within the uniform rectangular beam, the end surface was not straight in both types of support as shown in **Figure 5.11** c. and d.

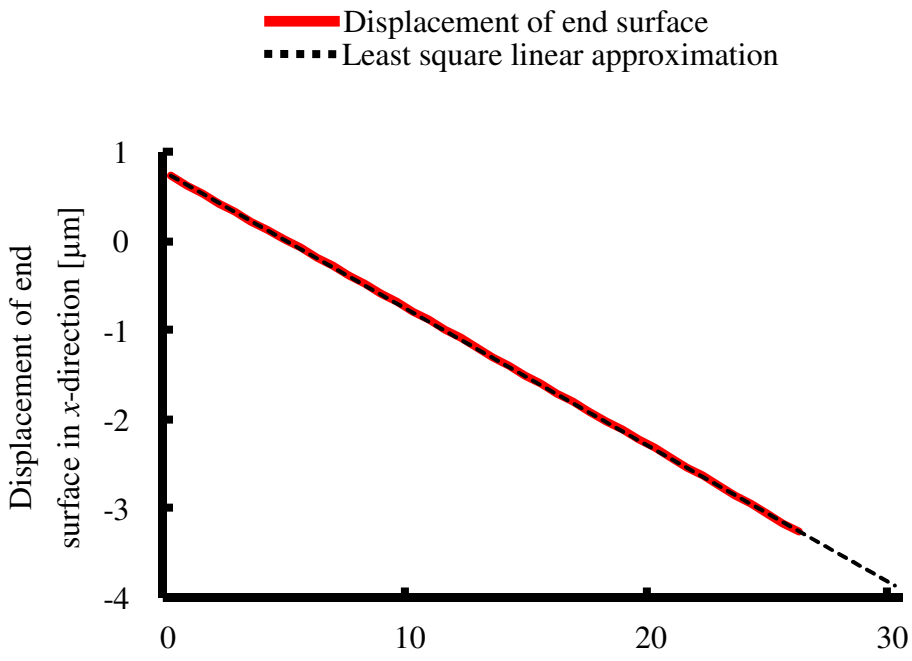

a. Simple beam support with linear $\sigma_x(z)$

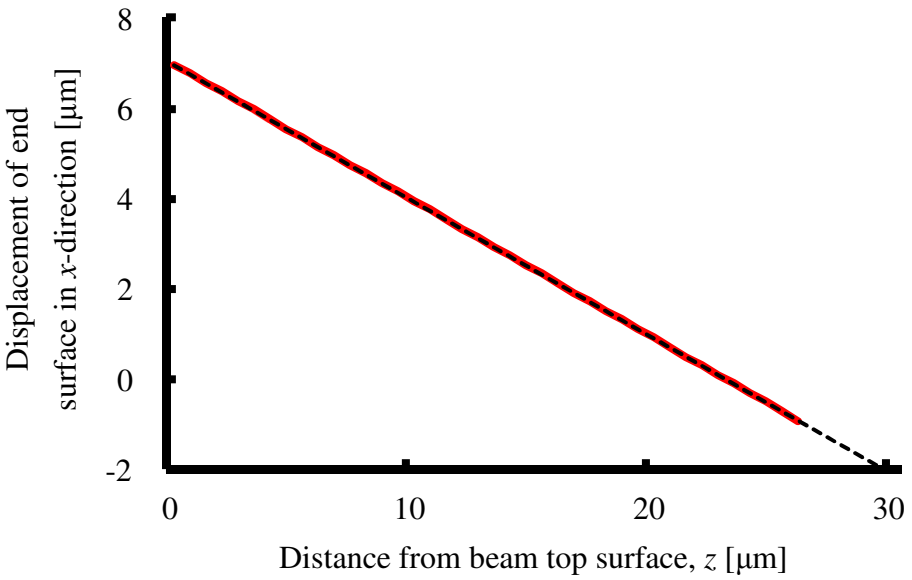

b. Rigidly fixed at one side with linear $\sigma_x(z)$

Figure 5.11: Observation of beam end surface after imposed with residual stress

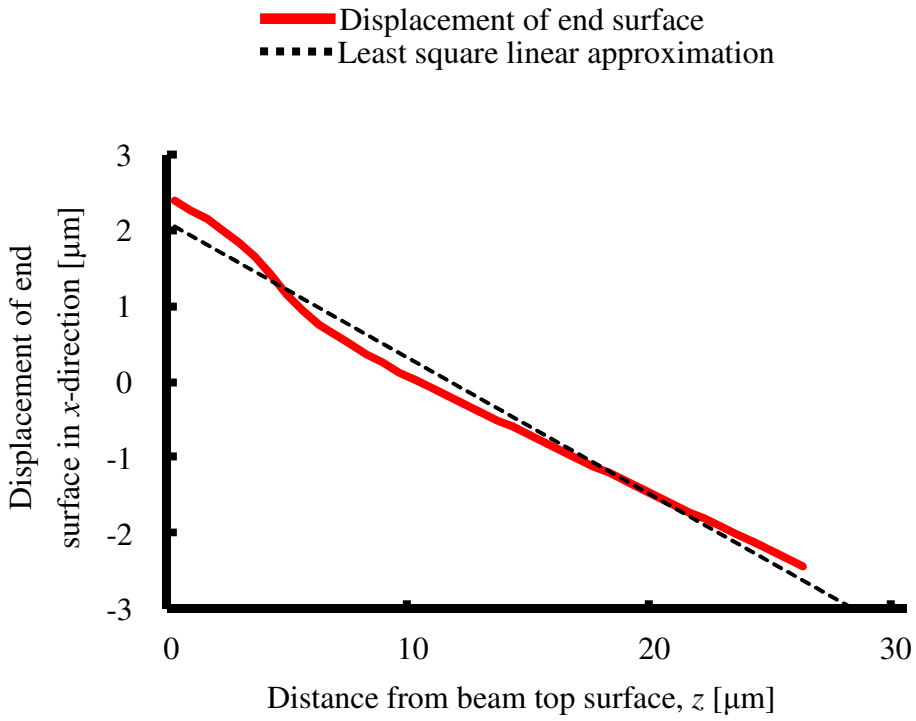

c. Simple beam support with $\sigma_x(z)$ due to discharge

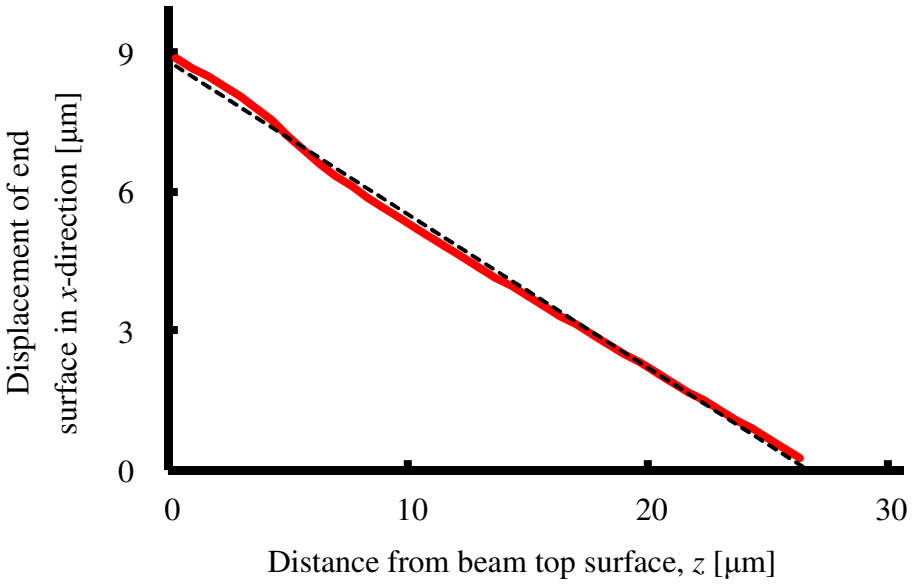

d. Rigidly fixed at one side with $\sigma_x(z)$ due to discharge

Figure 5.11: Observation of beam end surface after imposed with residual stress

Furthermore, in **Figure 5.12** the comparison of $\sigma_x(z)$ between before and after bending was made, and it is shown that the imposed $\sigma_x(z)$ was released completely after deformation in the case of linear distribution of $\sigma_x(z)$. Thus, the beam should bend uniformly, and this can be seen in **Figure 5.13** where the top surface of rectangular beam models which are imposed with linear distribution of $\sigma_x(z)$ is forming an arc of a perfect circle with radius equal to 652 μm. In other words, radius of curvature of the beam at any point on the top surface should be constant. The radius of curvature on top surface of the beam was calculated at several places and it was constant in both support types. **Figure 5.13** also shows the stress is uniformly zero within the beam.

In the case of rectangular beam models imposed with non-linear distribution of $\sigma_x(z)$, the bending of the beam was not uniform in both types of support. In the case of simple support shown in **Figure 5.14** a., both ends of the beam surfaces were almost free from residual stress. At the center of the beam however, residual stress was not released after bending. Similarly, in **Figure 5.14** b. if one end was rigidly fixed, residual stress at the fixed end was not released because the end surface must be kept straight.

Figure 5.15 shows the residual stress distribution after deformation. The tensile stress on the top surface of the simple support beam is not released except for the free ends. Hence, distortion at the center of the beam is larger than both ends. In the case of the rigidly fixed at one side, the tensile stress in the root area is not released. Hence, distortion is significant within the root area of the beam. In contrast, near the free end surface, tensile stress on the top surface is almost released. Therefore, area near the free end is straighter than the root side.

This is the reason why the beam deformation was not uniform when the beam was imposed with non-linear distribution of $\sigma_x(z)$. In **Figure 5.16**, radius of curvature at the top surface of a beam model with rigidly fixed at one end was observed. In **Figure 5.16** a., near the free end the radius of curvature was 616 μm, it drops to 588 μm near the fixed end.

This explains the results of experiment and simulation in this work as shown previously in **Figure 5.7**. During the experiment, one side of Cu workpiece was rigidly supported, and micro EDM results in non-linear residual stress distribution within the workpiece as shown in **Figure 4.8**. Thus, non-uniform deformation as shown in **Figure 5.7** can be observed.

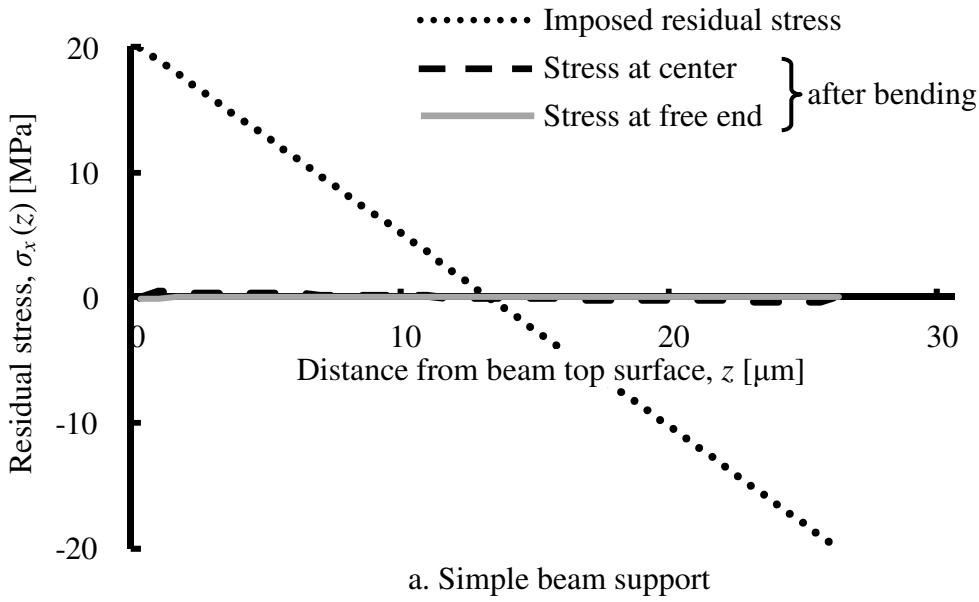

a. Simple beam support

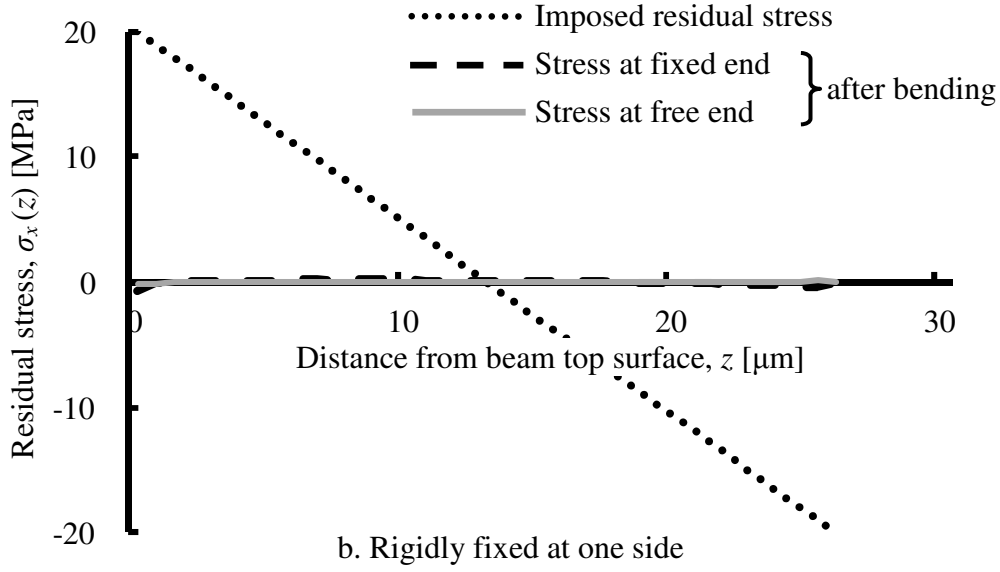

b. Rigidly fixed at one side

Figure 5.12: Comparison between imposed linear distribution of $\sigma_x(z)$ and the $\sigma_x(z)$ after bending

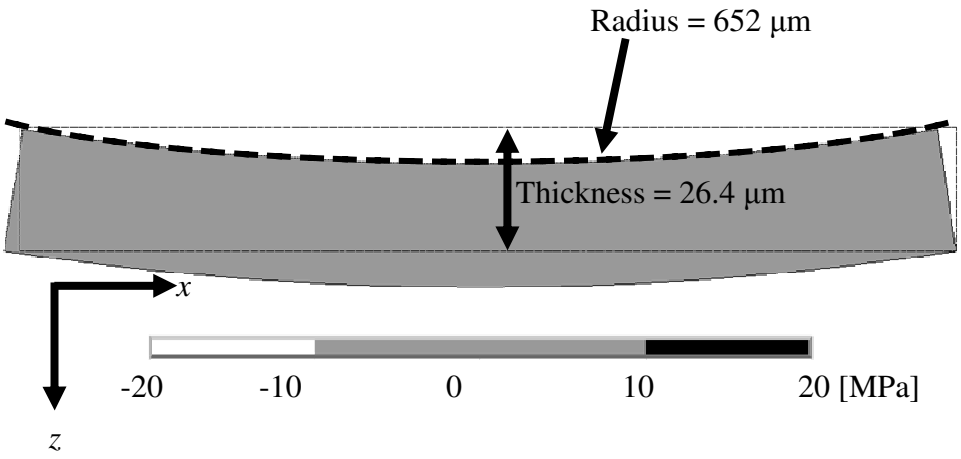

a. Simple beam support

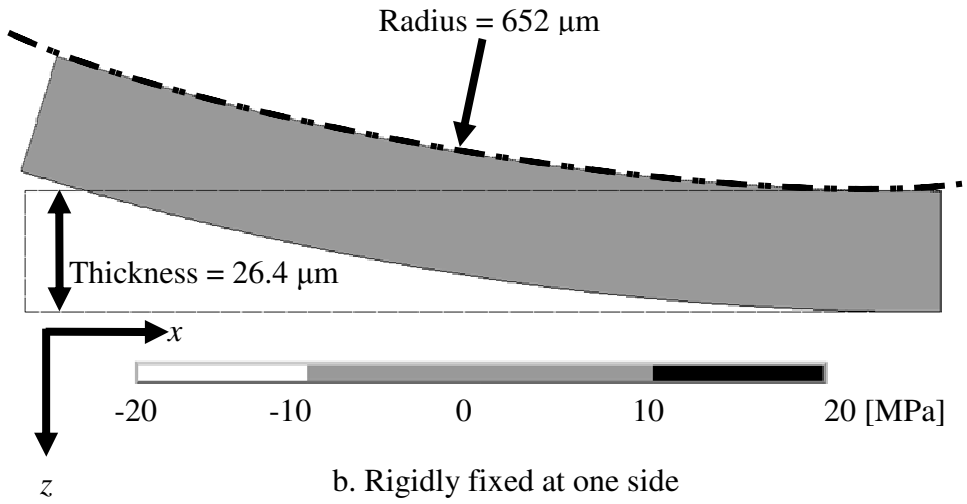

b. Rigidly fixed at one side

Figure 5.13: Observation of top surface curvature of beam imposed with linear distribution of $\sigma_x(z)$, and distribution of the $\sigma_x(z)$ within beam after deformation.

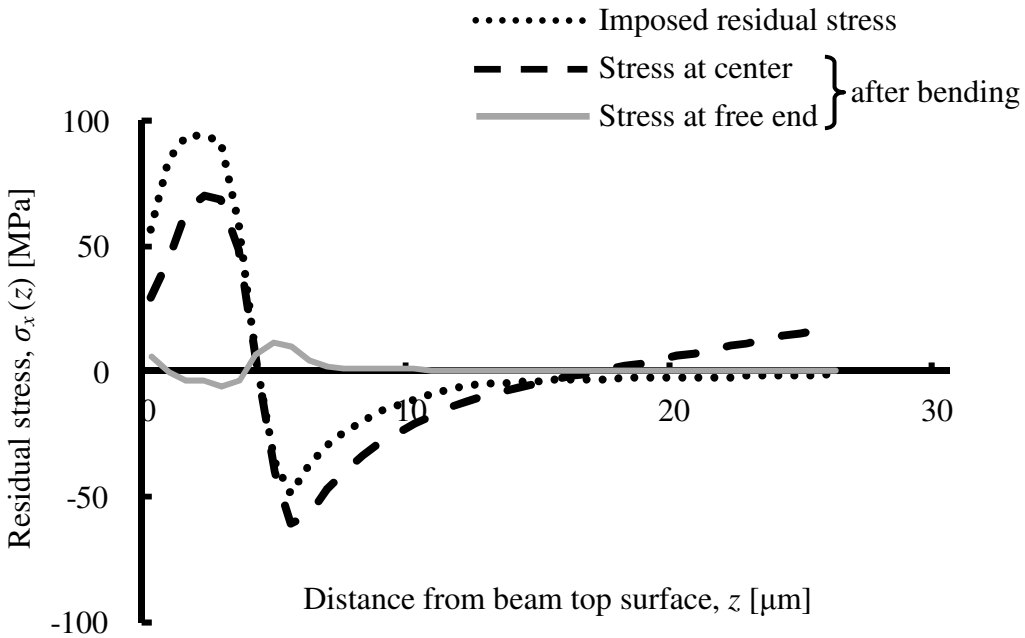

a. Simple beam support

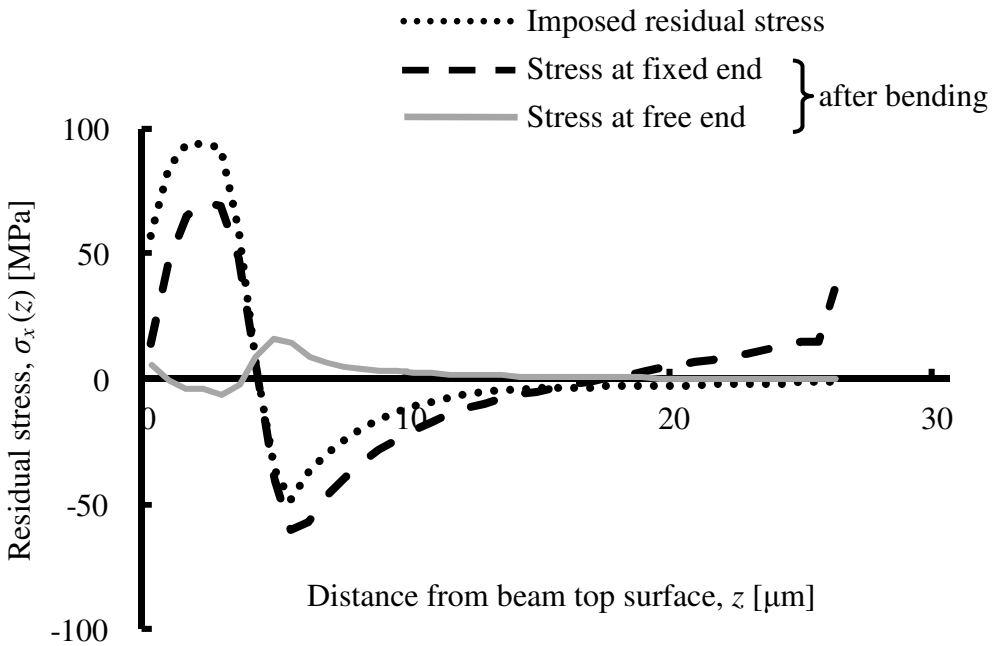

b. Rigidly fixed at one side

Figure 5.14: Comparison between imposed non-linear distribution of $\sigma_x(z)$ and the $\sigma_x(z)$ after bending

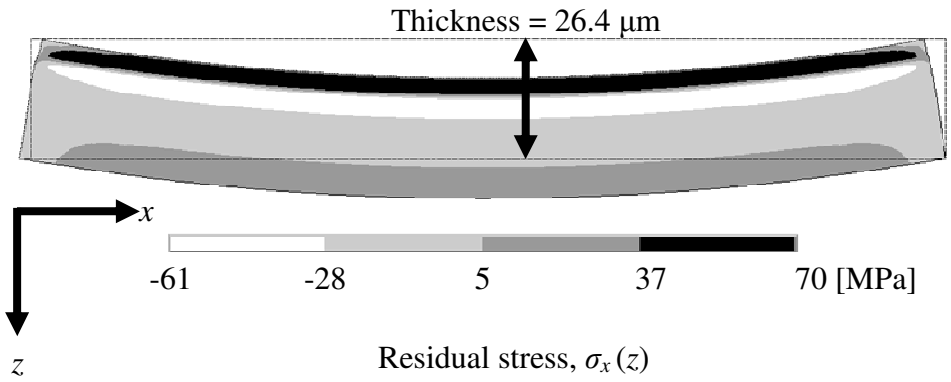

a. Simple beam support

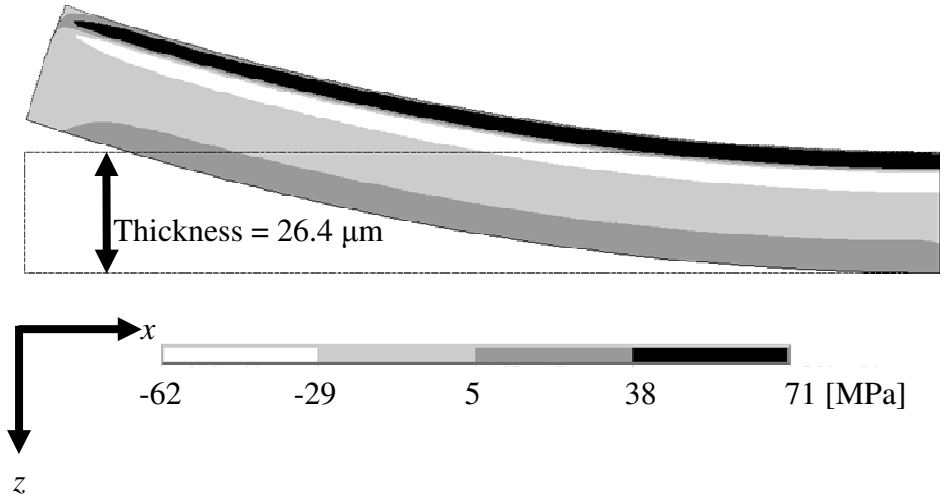

b. Rigidly fixed at one side

Figure 5.15: Distribution of $\sigma_x(z)$ after deformation when the non-linear distribution of $\sigma_x(z)$ was imposed

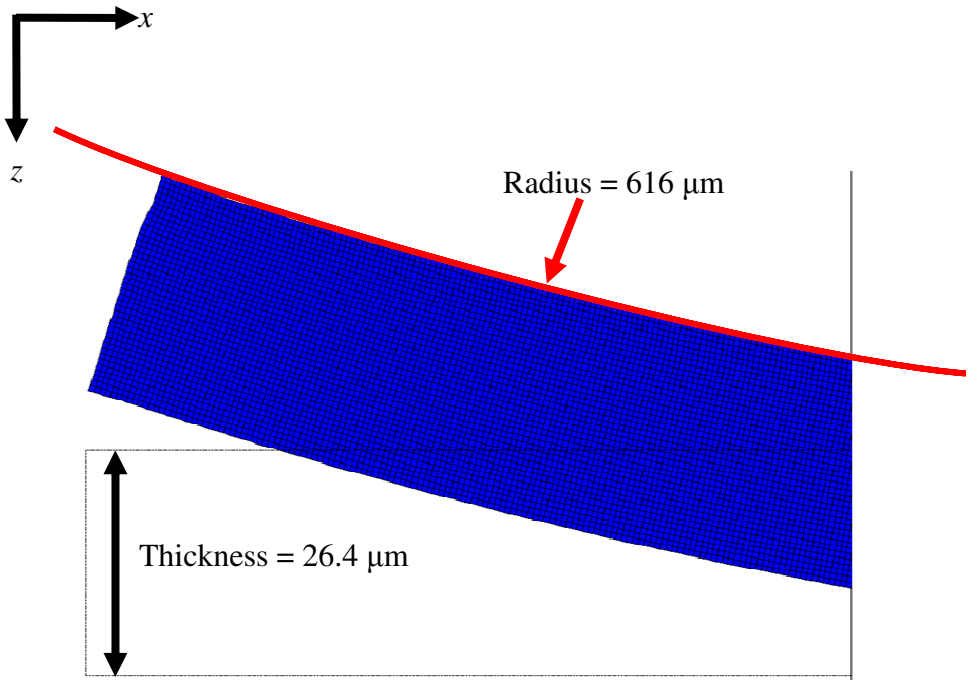

a. Near free end

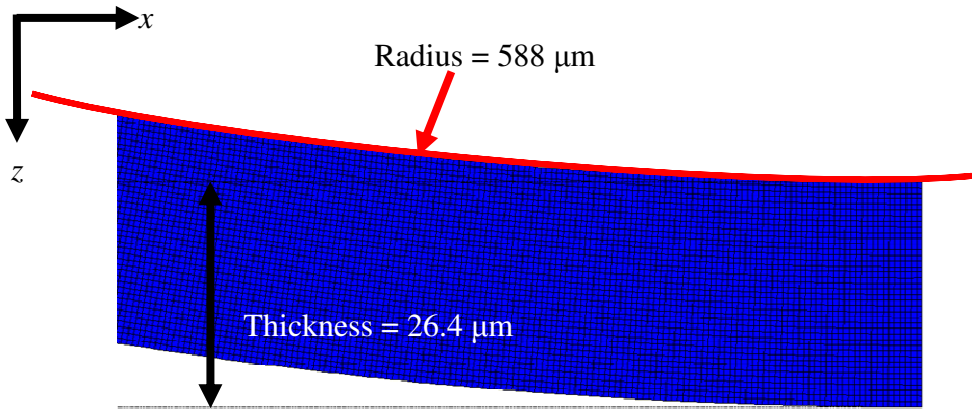

b. Near fixed end

Figure 5.16: Observation of beam top surface curvature
(Non-linear distribution of $\sigma_x(z)$ and rigidly fixed at one end model)

5.6 Conclusions

In this chapter deformation of micro fin caused by residual stress due to micro EDM has been discussed. To understand the deformation of micro fin due to micro EDM, thermal stress and structural analyses were conducted based on the results of thermal phenomena which were explained in **Chapters 2** and **3**. The work began by estimating residual stress, $\sigma_r(z)$ beneath the crater due to micro EDM single discharge based on the accurate model of power density, P_e at workpiece. Then, the result of $\sigma_r(z)$ was imposed in the micro fin model.

Assuming that $\sigma_r(z)$ due to single discharge is equal to the residual stress distribution $\sigma_x(z)$ in multi discharges, $\sigma_x(z)$ was imposed within the two-dimensional micro fin model uniformly along the fin length. As a result, calculated deflection was smaller than the measurement. Thus, superposition of residual stress generated by sequential discharges was considered. Ideally, the deformed shape of micro fin should be used as initial condition for the next sequence of discharges. However, for simplicity, the deformation of rectangular micro fin with the stress fields caused by the previous sequential discharges was obtained. It was found that, after three sequential discharges, the deflection approaching zero, and the total deflection values calculated after first, second and third deformations almost equal to the measured deflection. This indicates that the deformation of micro fin may result from interaction of stress field due to approximately three sequential discharges.

Although the calculated deflection was lower than the measurement, after the first deformation, a similar non-uniform curvature compared to the machined micro fin was observed. Therefore, to understand the curvature, additional uniform rectangular beam models were built and imposed with linearly distributed $\sigma_x(z)$ and the $\sigma_r(z)$ due to single discharge. It was found that the non-linear distribution of residual stress due to single discharge in micro fin thickness direction was the main reason to cause the non-uniform curvature of the fin when the stress was applied to the beam with one of its ends rigidly fixed.

The similar curvature between simulated and machined micro fins indicates that the use of residual stress due to single discharge was sufficient to explain the non-uniform curvature of micro fin which was machined by multi discharges. Hence, it is considered that the distribution of residual stress $\sigma_x(z)$ generated by multi discharges in the depth direction is similar to $\sigma_r(z)$ generated by single discharge.

Chapter 6 Conclusions and future works

In general, although there is no difference in principle and mechanism of material removal in micro and macro EDM, performances of micro EDM differ from those of macro EDM. Therefore, in this work fundamental of micro EDM with respect to thermal phenomena has been studied. The main parameters of thermal phenomena in micro EDM including energy distribution into workpiece, plasma diameter, removal mechanism and power density at workpiece have been obtained. These parameters have been compared with those of macro EDM and how they influence the energy efficiency and removal efficiency of both processes have been discussed. Finally, as another particularity of micro EDM, thermal stress and structural analyses were conducted to understand the micro EDM workpiece deformation using the fundamental thermal parameters obtained in this work. This research can be concluded as follows:

(i) In EDM, electrical discharge occurs within a very short time, in a narrow gap which is filled with dielectric liquid and gas. Material is removed from the workpiece and tool electrodes, and the complicated removal mechanism involves both melting and vaporization. Consequently, observations based on experiment and theoretical analyses are extremely difficult. Therefore, thorough discussion on phenomena within EDM gap is important to characterize and explore fundamental knowledge of the process.

(ii) At the EDM gap only, there are several main parameters which should be known before conducting various fundamental analyses of EDM including energy distribution ratios into tool electrode, workpiece and gap, heat source or plasma diameter, and power density at electrodes. Those parameters have been reported by many researchers in the case of macro EDM. However, in micro EDM comprehensive reports on those parameters are not available. Therefore, they were obtained in the beginning of this work.

(iii) Besides, it is also important to understand the removal mechanism; ratios of removal by vaporization and by melting with respect to the total removal volume per pulse, especially to calculate thermal energy consumption during material removal to understand the energy input during electrical discharge.

(iv) In this work, two main indexes were used to compare the performances between micro and macro EDM process. They are the removal efficiency and the energy efficiency.

(v) In macro EDM, discharge durations are sufficiently long so that plasma can grow to a maximum diameter and remains at that size until the end of discharge duration. On the other hand, discharge durations in micro EDM are significantly shorter than the case of macro EDM. Thus, the plasma is not fully developed and the diameter of the plasma is limited in the case of micro EDM. Consequently, a larger power density at workpiece about 30 times, compared to that of macro EDM is generated.

(vi) When plasma expands to the maximum diameter in macro EDM, comparatively low power density is distributed over the workpiece which is not sufficiently high to cause the workpiece removal. Thus, a large fraction of the thermal energy is lost due to heat conduction within the workpiece. On the other hand, the large power density results in higher energy efficiency in micro EDM which means higher energy consumption ratio for material removal with respect to energy distributed into the workpiece compared to that of macro EDM. On the contrary, the ratio of energy loss due to heat conduction within micro EDM workpiece is lower than that of macro EDM.

(vii) Furthermore, removal efficiency was higher in micro EDM compared to that of macro EDM. This means more molten area resolidifies and remains in the crater of macro EDM than that of micro EDM. The remainder in the crater is known as white layer. This explains the reason of significantly higher energy lost due to heat conduction within macro EDM workpiece.

(viii) While the white layer is in molten state, there is no constraint on the movement of the layer's elements. This means no residual stress formation during this period. Then, after the white layer is solidified, the cooling process of the layer generates tensile residual stress near discharge crater and compressive residual stress at deeper area. This explains the contraction of micro fin at the machining surface.

(ix) Above conclusions explain correlation of efficiencies, formation of white layer and the residual stress. Therefore, results of thermal phenomena including power density at workpiece and the removal mechanism were required to estimate the residual stress due to micro EDM discharge. Based on those results, thermal stress analysis was

conducted.

(x) In this work, due to time constraint and lack of information regarding temperature dependent mechanical properties of copper workpiece, elastic-perfectly plastic behavior of workpiece material was considered during the thermal stress analysis due to single pulse discharge. It was found that residual stress was non-linearly distributed in the thickness direction below micro EDM crater which is similar to that of macro EDM, except that the formation area was shallower compared to that of macro EDM.

(xi) To simulate the micro fin deformation, a very complicated and time-consuming model should be considered. However, for simplicity, it was assumed that the residual stress is two-dimensional, and the radial residual stress generated by single discharge was applied to the beam uniformly along the axis. The dimension of the model was based on the actual size of machined micro fin.

(xii) Consequently, a non-uniform bending of micro fin along its length due to micro EDM can be observed. Structural analysis was conducted to show the residual stress which was non-linearly distributed in the fin thickness direction is the main reason that causes the non-uniform bending of the micro fin along its length.

(xiii) The curvature of simulated micro fin was similar to that of machined micro fin. This result indicates that the distribution of residual stress generated by multi discharges in the depth direction is similar to the residual stress generated by single discharge.

(xiv) However, the error in deflection between measurement and calculation can be observed. The main reason is, the superposition of residual stress generated by sequential discharges was not considered. It is ideal if the deformed shape of micro fin caused by present discharges can be used as initial condition for the next sequence of discharges. However, for simplicity, thermal stress field due to series of sequential discharges covering the fin surface was applied into the straight micro fin model, and the deflection indicates the increment of micro fin deflection if the ideal calculation is conducted. The deflection decreased with the number of series of sequential discharges and approached zero. The total value of deflections after three sequential discharges based on the simplified model was almost equal to the measurement result. This indicates that the deformation of micro fin may result from interaction of stress field

due to approximately three sequential discharges.

(xv) It was found in this work, to prevent bending of Cu workpiece, machining sizes below 30 μm should be avoided. Besides, to prevent deformation in general, several ideas can be proposed such as machining with extremely low discharge energy, appropriate selection of workpiece materials that have high toughness such as cemented carbide as proposed by Kawakami and Kunieda 2005, and use machining method that not rely on thermal removal mechanism such as electro chemical machining (ECM). Kawakami and Kunieda 2005 also reported that if the residual stress existent prior to machining is removed by annealing, the micro cylindrical rod will not be bent because the distribution of the residual stress caused by EDM is axisymmetrical.

From this fundamental study, many researches regarding EDM can be explored. Following are some recommendations for future works:

i) In this work, as an example application of thermal phenomena results and for simplicity many assumptions were made during thermal stress and structural analyses. Therefore, further improvement on the analyses will be conducted in future.

ii) Only copper was tested in this work. It is known that electrodes' material is also a significant factor that influences the process. Therefore, other types of material especially that are normally machined by EDM such as titanium and nickel based alloy should be considered. Furthermore, the results obtained in this work may not represent micro EDM in general.

iii) Wire EDM is one of the types of EDM which are widely used. However, fundamental study like what was done in this work is not reported yet because the discharge duration used in wire EDM is shorter than that in sinking EDM, although it is longer than micro EDM. A similar approach can be applied with respect to wire EDM.

iv) The removal mechanism analysis that was used in this work also can be used for macro EDM.

There are still many research topics which can be generated based on this fundamental study of the EDM process. Hopefully this research will be referred for better quality researches in the future.

References

[1] Kunieda, M., Lauwers, B., Rajurkar, K. P. and Schumacher, B. M., 2005, Advancing EDM through Fundamental Insight into the Process, Annals of the CIRP, Vol. 54, No.2, pp. 64-87.

[2] Masuzawa, T., 2000, State-of-the-art on Micromachining, Annals of the CIRP, Vol. 49, No. 2, pp. 473-488.

[3] Kalpajian, S., Schmid, S.R., Musa, H., 2010, Manufacturing Engineering and Technology, 6th edition in SI units, Prentice Hall Singapore, pp. 769-774.

[4] Kunieda, M., Nakashima, T., 1998, Factors Determining Discharge Location in EDM, IJEM, No. 3, pp. 53-58.

[5] Morimoto, K., Kunieda, M., 2009, Sinking EDM Simulation by Determining Discharge Locations Based on Discharge Delay Time, Annals of the CIRP, Vol. 58, No. 1, pp. 221-224.

[6] Masuzawa, T., Tsukamoto, J., Fujino, M., 1989, Drilling of deep microholes by EDM, Annals of the CIRP, Vol. 38, No. 1, pp. 195-198.

[7] Fleischer, J., Masuzawa, T., Schmidt, J., 2004, New applications for micro-EDM, J. of Materials Processing Technology, Vol. 149, No. 1-3, pp. 246-249.

[8] Pham, D.T., Dimov, S.S., Bigot, S., Ivanov, A., Popov, K., 2004, Micro-EDM recent developments and research issues, J. of Materials Processing Technology, Vol. 149, No. 1-3, pp. 50-57.

[9] Masuzawa, T., Fujino, M., Kobayashi, K., 1985, Wire Electro-Discharge Grinding for Micro-Machining, Annals of the CIRP, Vol. 34, No. 1, pp. 431-434.

[10] Masuzawa, T., Yamaguchi, M., Fujino, M., 2005, Surface Finishing of Micropins Produced by WEDG, Annals of the CIRP, Vol. 54, No. 1, pp. 171-174.

[11] Meek, J. M., Craggs, J. D., 1978, Electrical Breakdown of Gases, John Wiley & Sons.

[12] Palatnik, L.S., Liulichev, A.N., 1958, Investigation of the Temperature in the Vapor Phase Occurring during the Electrical Spark Treatment, Soviet Physics-Technical Physics, Vol. 1, pp. 818-824.

[13] Albinski, K., Musiol, K., Miernikiewicz, A., Labuz, S., Malota, M., 1995, Plasma Temperature in Electro Discharge Machining, Proc. ISEM XI, pp. 143-152.

[14] Hashimoto H., Kunieda M., 1997, Spectroscopic Analysis of Temperature Variation of EDM Arc Plasma, J. JSEME, Vol. 31, No. 68, 32-40 (in Japanese).

[15] Natsu W., Ojima S., Kobayashi T., Kunieda M., 2004,Temperature Distribution Measurement in EDM Arc Plasma Using Spectroscopy, JSME Int. J. C, Vol.47, No. 1, pp. 384-390.

[16] Van Dijck, F., 1973, Physico-Mathematical Analysis of the Electro Discharge Machining Process, Dissertation of Katholieke Universiteit Leuven.

[17] Eckman, P.K., Williams, E.M., 1960, Plasma Dynamics in Arc Formed by Low-Voltage Sparkover of a Liquid Dielectric, Appl. Sci. Res., Section B, Vol. 8, pp. 299-320.

[18] Ikeda, M., 1972, The Movement of a Bubble in the Gap Depending on the Single Electrical Discharge (1st report): J. JSEME, Vol. 6, No. 11, pp. 12-25 (in Japanese).

[19] Miyajima J., Kunieda M., Masuzawa T., 1987, Observation of Bubbles generated in EDM Gap, Proc. ’87 Spring Meeting of JSPE, pp. 723-724 (in Japanese).

[20] Kunieda M., Adachi Y., Yoshida M., 2000, Study on Process Reaction Force Generated by Discharge in EDM, Proc. of 2nd Int. Conf. MMSS, pp. 313-324.

[21] Kunieda M., Tohi M., Ohsako Y., 2003, Reaction Forces Observed in Pulse Discharges of EDM, IJEM, No.8, pp. 51-56.

[22] Zolotykh, B. N., 1959, The Mechanism of Electrical Erosion of Metals in Liquid Dielectric Media, Soviet Physics-Technical Physics, Vol. 4, No. 12, pp. 1370-1373.

[23] Hockenberry, T.O., Williams, E.M., 1967, Dynamic Evolution of Events Accompanying the Low-Voltage Discharge Employed in EDM, IEEE Trans. on Industry and General Applications, IGA-3, Vol. 4, pp. 302-309.

[24] Yoshida, M., Kunieda, M., 1998, Study on the Distribution of Scattered Debris Generated by a Single Pulse Discharge in EDM Process, IJEM, No.3, pp. 39-47.

[25] Hinduja, S., Kunieda, M., 2013, Modelling of ECM and EDM Processes, Annals of the CIRP, Vol. 62, No. 2, pp. 775-797.

[26] Xia, H., Kunieda, M., Nishiwaki, N., Lior, N., 1994, Measurement of Energy Distribution into Electrodes in EDM Processes, Advancement of Intelligent Production, Elsevier Science B.V. JSPE, pp.601-606.

[27] Xia H., 1995, Study on Factors Affecting Electrode Wear Ratio and Improvement of Machining Characteristics in EDM Process, Dissertation of Tokyo University of Agriculture and Technology (in Japanese).

[28] Xia H., Hashimoto, H., Kunieda M., Nishiwaki N.,1996, Measurement of Energy Distribution in Continuous EDM Process, J. of JSPE, Vol. 62, No. 8, pp. 1141-1145 (in Japanese).

[29] Xia, H., Kunieda, M., and Nishiwaki, N., 1996, Removal Amount Difference between Anode and Cathode in EDM Process, IJEM, No. 1, pp. 45-52.

[30] Xia, H., Kunieda, M., and Nishiwaki, N., 1999, Simulation of Electrode Surface Temperature in Die-Sinking EDM Process, IJEM, No. 4, pp. 13-18.

[31] Hayakawa, S., Yuzawa, M., Kunieda, M., Nishiwaki, N., 2001, Time Variation and Mechanism of Determining Power Distribution in Electrodes during EDM Process, IJEM, 6, 19-26.

[32] Spur, G., Uhlmann, E., Doll, U., Daus, N., 1999, WEDM of Microstructured Component Parts – Heat Conduction Model, IJEM, No. 4, pp. 41-46.

[33] Klocke, F., Lung, D., Noethe, T., 2001, Micro Contouring by EDM with Fine Wires, Proc. ISEM, Vol. 13, pp. 767-779.

[34] Kawakami, T., Kunieda, M., 2005, Study on Factors Determining Limits of Minimum Machinable Size in Micro EDM, Annals of the CIRP, Vol. 54, No. 1, pp. 167-170.

[35] Kruth J.P., Bleys P., 2000, Measuring Residual Stress Caused by Wire EDM of Tool Steel, IJEM, Vol. 5, pp. 23-28.

[36] DiBitonto, D.D., Eubank, P.T., Patel, M.R., Barrufet, M.A., 1989, Theoretical Models of the Electrical Discharge Machining Process I. A Simple Cathode Erosion Model, J. Appl. Phys., Vol. 66, No. 9, 1, pp. 4095-4103.

[37] Patel, M.R., Barrufet, M.A., Eubank, P.T., DiBitonto, D.D., 1989, Theoretical Models of the Electrical Discharge Machining Process II. The Anode Erosion Model, J. Appl. Phys., Vol. 66, No.9, 1, pp. 4104-4111.

[38] Koenig, W., Wertheim, R., Zvirin, Y., Toren, M., 1975, Material Removal and Energy Distribution in Electrical Discharge Machining, Annals of the CIRP, Vol. 24, No. 1, pp. 95-100.

[39] Zingerman, A. S., 1956, Propagation of a Discharge Column, Soviet Physics-Technical Physics, Vol. 1, No. 1, 5, pp. 992-996.

[40] Kunieda M., Xia H., Nishiwaki N., 1992, Observation of Arc Column Movement during Monopulse Discharge in EDM, Annals of the CIRP, Vol. 41, No. 1, pp. 227-230.

[41] Hayakawa S., Kunieda M., 1996, Numerical Analysis of Arc Plasma Temperature in EDM Process Based on Magnetohydrodynamics, Trans. JSME (B), 62, 600, 263-269 (in Japanese).

[42] Hayakawa S., Xia H., Kunieda M., Nishiwaki N., 1996, Analysis of Time Required to Deionize an EDM Gap during Pulse Interval, Proc. of Symposium on Molecular and Microscale Heat Transfer in Materials Processing and Other Applications, 368-377.

[43] Kojima, A., Natsu, M., Kunieda, M., 2008, Spectroscopic Measurement of Arc Plasma Diameter in EDM, Annals of the CIRP, Vol. 57, pp. 203-207.

[44] Snoeys, R., Van Dijck, F., 1971, Investigations of EDM Operations by Means of Thermomathematical Models, Annals of the CIRP, Vol. 20, pp. 35-36.

[45] Snoeys, R., Van Dijck, F., 1972, Plasma Channel Diameter Growth Affects Stock Removal in EDM, Annals of the CIRP, Vol. 21, pp. 39-40.

[46] Tamura, T., Sakurai, J., 1994, Behaviour of Crack generation in EDM using Thermal Stress Analysis, J. JSEME, Vol. 30, No. 64, pp. 18-25. (In Japanese)

[47] Yang, Y., Mukoyama, Y., 1996, Three-dimensional analysis of residual stress in EDM process, IJEM, No. 1, pp. 27–33.

[48] Yadav, V., Jain, V. K., Dixit, P. M., 2002, Thermal stress due to electrical discharge machining, Int. J. of Machine Tools & Manufacture, Vol. 42, No. 8, pp. 877-888.

[49] Das, S., Klotz, M., Klocke, F., 2003, EDM simulation: finite element-based calculation of deformation, microstructure and residual stresses, J. of Materials Processing Technology, Vol. 142, No. 2, pp. 434-451.

[50] Ekmekci, B., Tekkaya, A. E., Erden, A., 2006, A semi-empirical approach for residual stresses in electrical discharge machining (EDM), Int. J. of Machine Tools & Manufacture, Vol. 46, No. 7-8, pp. 858-868.

[51] Ekmekci, B., 2007, Residual stress and white layer in electrical discharge machining (EDM), Applied Surface Science, Vol. 253, pp. 9234-9240.

[52] Kumar, P.D., 2008, Study of thermal stresses induced surface damage under growing plasma channel in electro-discharge machining, J. of Materials Processing Technology, Vol. 202, No. 1-3, pp. 86-95.

[53] Maradia, U., Boccadoro, M., Stirnimann, J., Beltrami, I., Kuster, F., Wegener, K., 2012, Die-sink EDM in meso-micro machining, Procedia CIRP, No. 1, pp. 166-171.

[54] Kaminski, P.C., Capuano, M.N., 2003, Micro hole machining by conventional penetration electrical discharge machine, Int. J. of Machine Tools & Manufacture, Vol. 43, No. 11, pp. 1143-1149.

[55] Muttamara, A., Fukuzawa, Y., Mohri, N., Tani, T., 2003, Probability of precision micro-machining of insulating Si3N4 ceramics by EDM, J. of Materials Processing Technology, Vol. 140, No. 1-3, pp. 243-247.

[56] Han, F., Yamada, Y., Kawakami, T., Kunieda, M., 2006, Experimental attempts of sub-micrometer order size machining using micro-EDM, J. of Precision Engineering, No. 30, pp. 123-131.

[57] Gurule, N. B., Pansare, S. A., Potentials of Micro-EDM, IOSR J. of Mechanical and Civil Engineering (IOSR-JMCE), pp.50-55.

[58] Uhlmann, E., Piltz, S., Doll, U., 2005, Machining of micro/miniature dies and moulds by electrical discharge machining—Recent development, J. of Materials Processing Technology Vol. 167, No. 2-3, pp. 488-493.

[59] Masaki, T., 1989, Micro electro-discharge machining, in: Proceedings of the Ninth International Symposium for Electromachining—ISEM IX, Nagoya, Japan.

[60] Wong, Y.S., Rahman, M., Lim, H.S., Han, H., Ravi, N., 2003, Investigation of micro-EDM material removal characteristics using single RC-pulse discharges, J. of Materials Processing Technology, No. 140, Issues 1-3, pp. 303-307.

[61] Rasheed, M.S., 2013, Comparison of Micro-Holes Produced By Micro-EDM with Laser Machining, Int. J. of Science and Modern Engineering Vol. 1, No.3, pp. 14-18.

[62] Valentinčič, J., Duhovnik, L., Kušer, D., Junkar, M., 2007, Comparison of material removal in micro and conventional EDM, Proceedings of the 9th Int. Conf. on Management of Innovative Technologies, Piran, Slovenia, pp. 225-228.

[63] Murray, J.W., Fay, M.W., Kunieda, M., Clare, A.T., 2013, TEM study on the electrical discharge machined surface of single-crystal silicon, J. of Materials Processing Technology, Vol. 213, No. 5, pp. 801-809.

[64] Motoki, M., Lee, C., Tanimura, T., 1967, Research on electrode Erosion Caused by Transient Arc Discharge in Dielectric Liquid, J. IEEJ, Vol. 87, No. 943, pp. 93-801 (in Japanese).

[65] Ikai, T., Hashiguchi, K., 1988, On the Tool Electrode Material with Low Erosion in the Electric Discharge Machining, T. IEEJ. D, Vol. 108, No. 3, pp. 338-343 (in Japanese).

[66] Kunieda, M., Kobayashi T., 2004, Clarifying Mechanism of Determining Tool Electrode Wear Ratio in EDM Using Spectroscopic Measurement of Vapor Density, J. of Materials Processing Technology, Vol. 149, No. 1-3, pp. 284-288.

[67] Natsu, W., Kunieda M., Nishiwaki N., 2004, Study on Influence of Inter-electrode Atmosphere on Carbon Adhesion and Removal Amount, IJEM, No. 9, pp. 43-50.

[68] Mohri, N., Suzuki, M., Furuya, M., Saito N., 1995, Electrode Wear Process in Electrical Discharge Machining, Annals of the CIRP, Vol. 44, No.1, pp. 165-168.

[69] Hayakawa, S., Kunieda, M., Nishiwaki, N., 1996, Influence of Electrode Material on Energy Distribution in EDM, Proc. Of Annual Meeting of JSEME, pp. 21-24.

[70] Xia, H., 1995, Study on Factors Affecting Electrode Wear Ratio and Improvement of Machining Characteristics in EDM Process, Dissertation of Tokyo University of Agriculture and Technology (in Japanese).

[71] Araie, I., Sano, S., Kunieda, M., 2005, Study of Craters on Micro Electrical Discharge Machining, spring meeting of JSPE, pp. 1315-1316. (In Japanese)

[72] Alexander, G., Thomas, E.W. and Harry, J.H., 1961, Handbook of Thermophysical Properties of Solid Materials, Vol. 1 – Elements, Pergamon Press.

[73] Grosse, A.V., 1969, Comparison of experimental electrical resistivities vs. densities of liquid copper up to its critical region (8500 K) with previous estimates, INORG, NUCL, CHEM, LETTERS, Vol. 5, pp. 963-968.

[74] Gathers, G.R., 1986, Dynamic methods for investigating thermophysical properties of matter at very high temperatures and pressures, Rep. Prog. Phys, Vol. 49,pp. 341-396.

[75] White, G.K. and Minges, M.L., 1997, Thermophysical Properties of Some Key Solids: An Update, Int. J. of Thermophysics, pp.1269-1327.

[76] 新編熱物性ハンドブック(Thermophysical Properties Handbook), 日本熱物性学会編,p.23, pp.103-104.

APPENDIX A

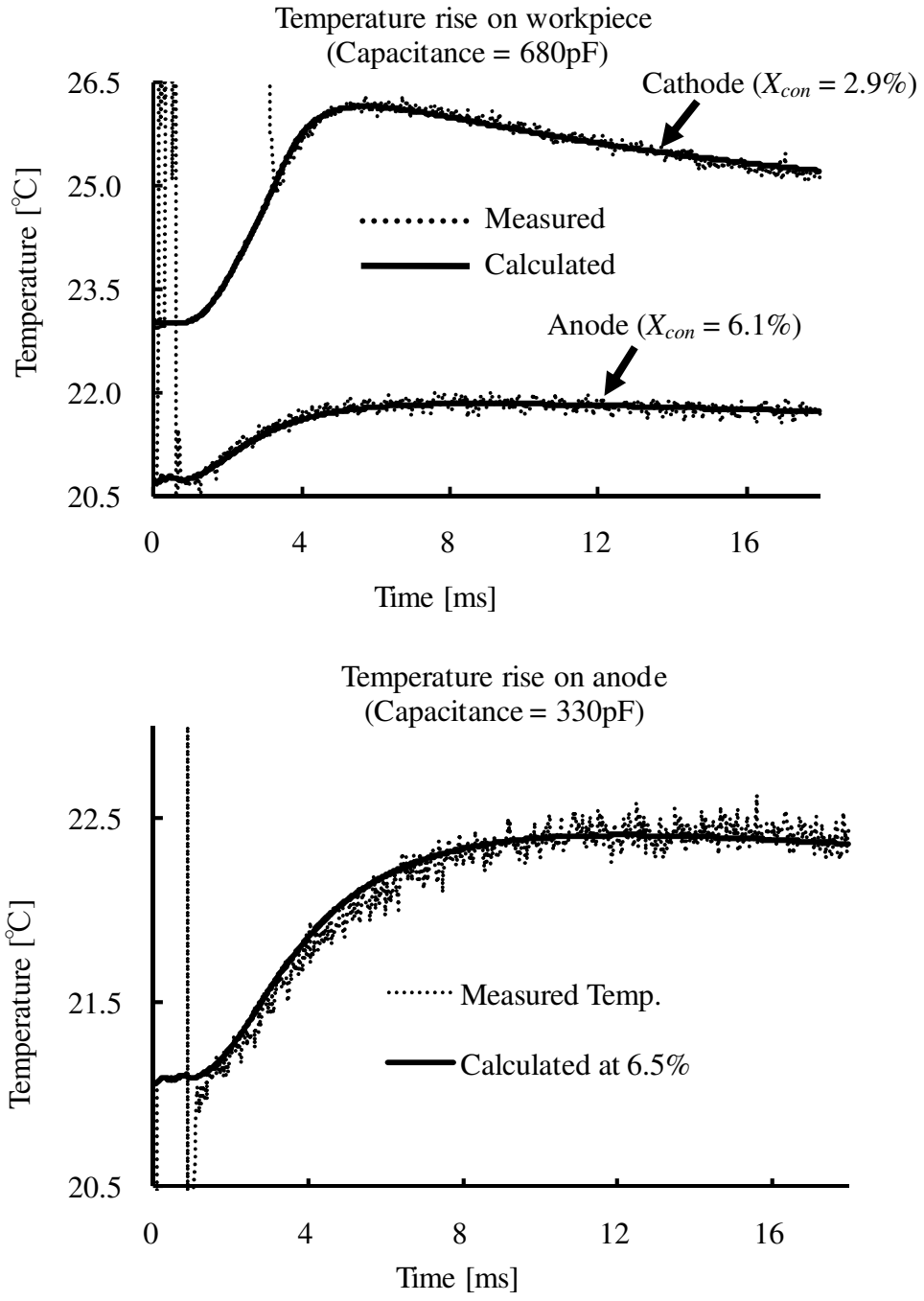

Comparison of measured and calculated temperature rise on workpiece with 680 pF and 330 pF capacitor

APPENDIX B

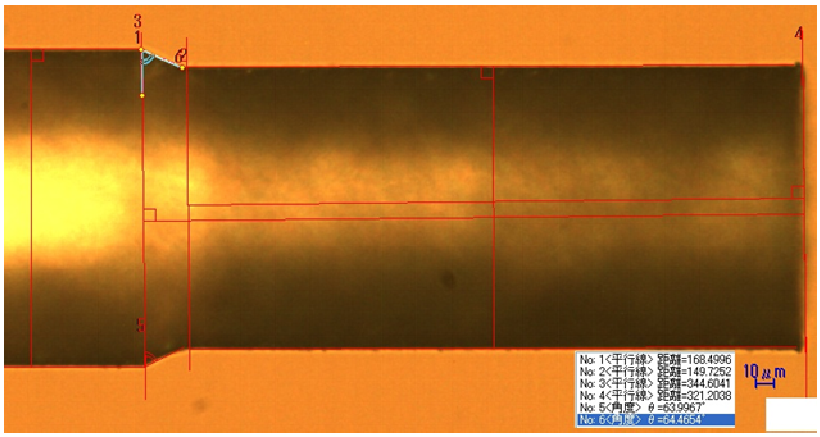

Pulses number to accomplish the machining = 916813

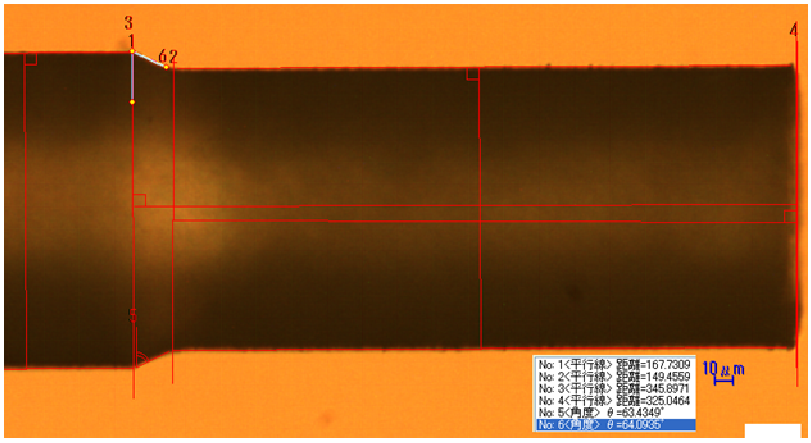

Pulses number to accomplish the machining = 869358

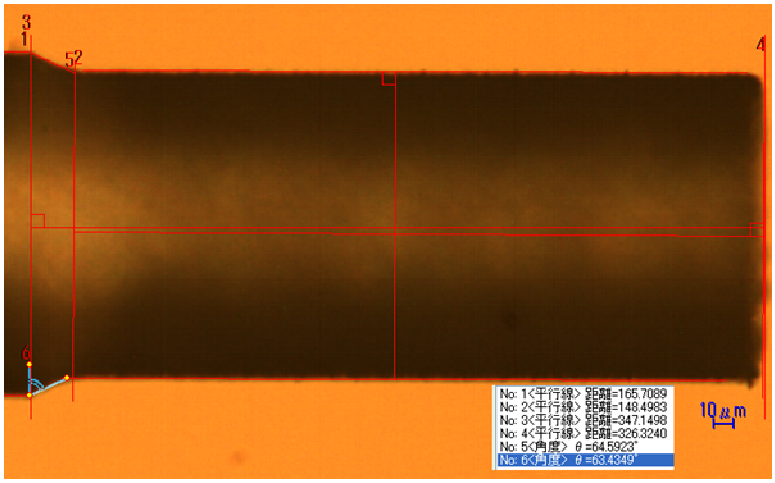

Pulses number to accomplish the machining = 814102

Cu rod machined by WEDG to determine total removal volume per pulse

APPENDIX C

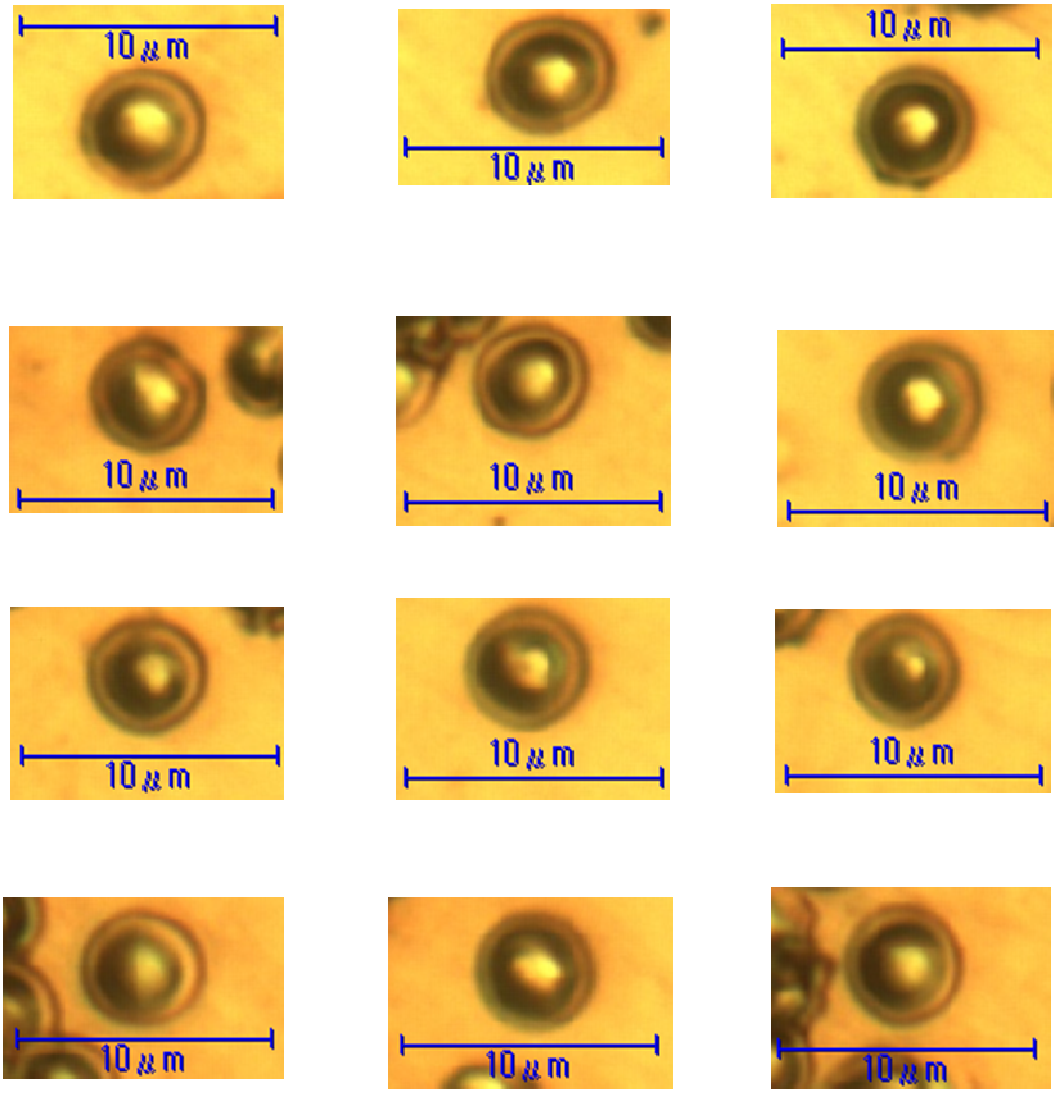

Examples of crater due to single discharge under machining setting; open circuit voltage = 100 V and capacitance = 1000 pF

APPENDIX D

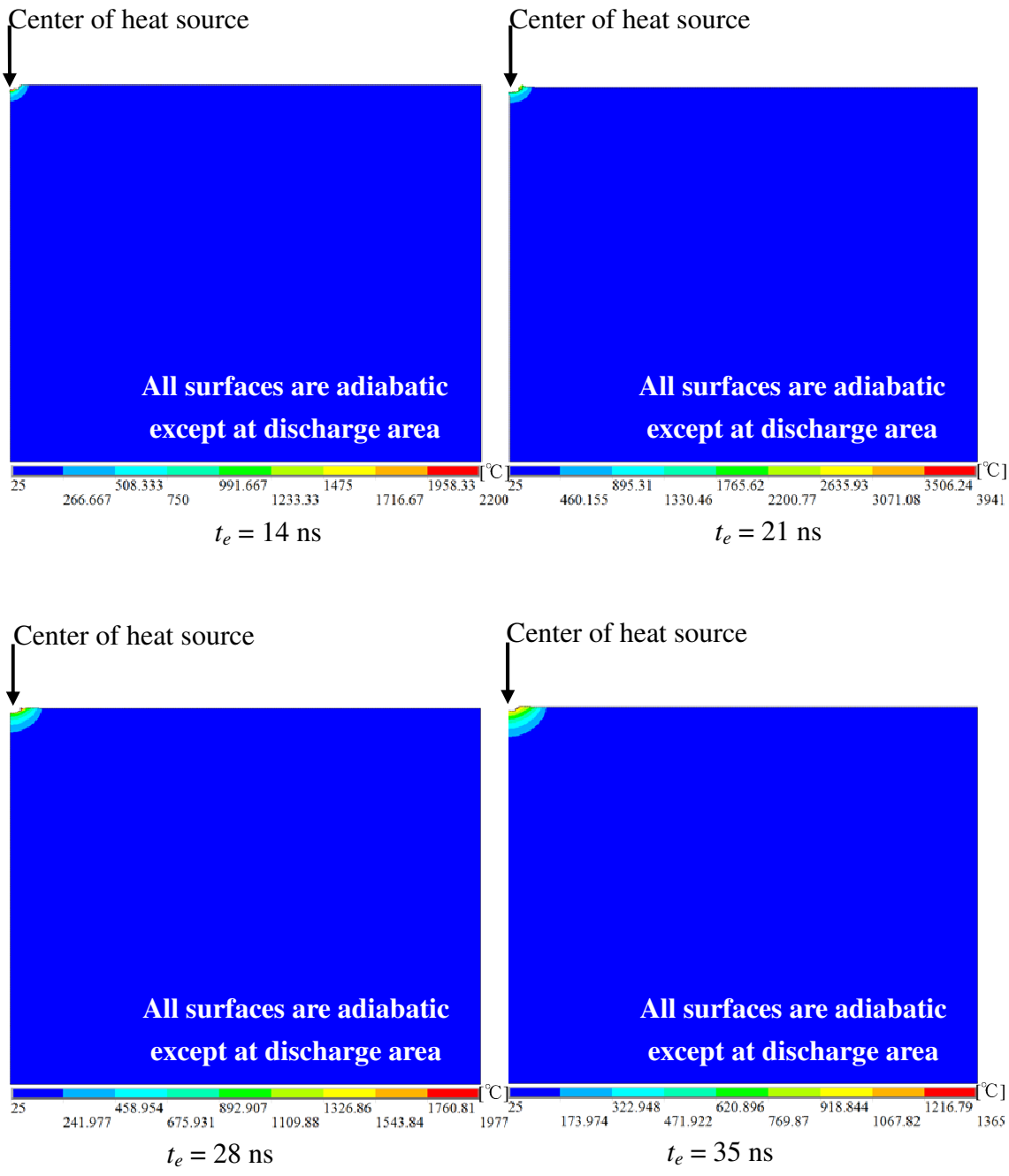

Calculated temperature distribution with respect to time during discharge duration

APPENDIX D (continue)

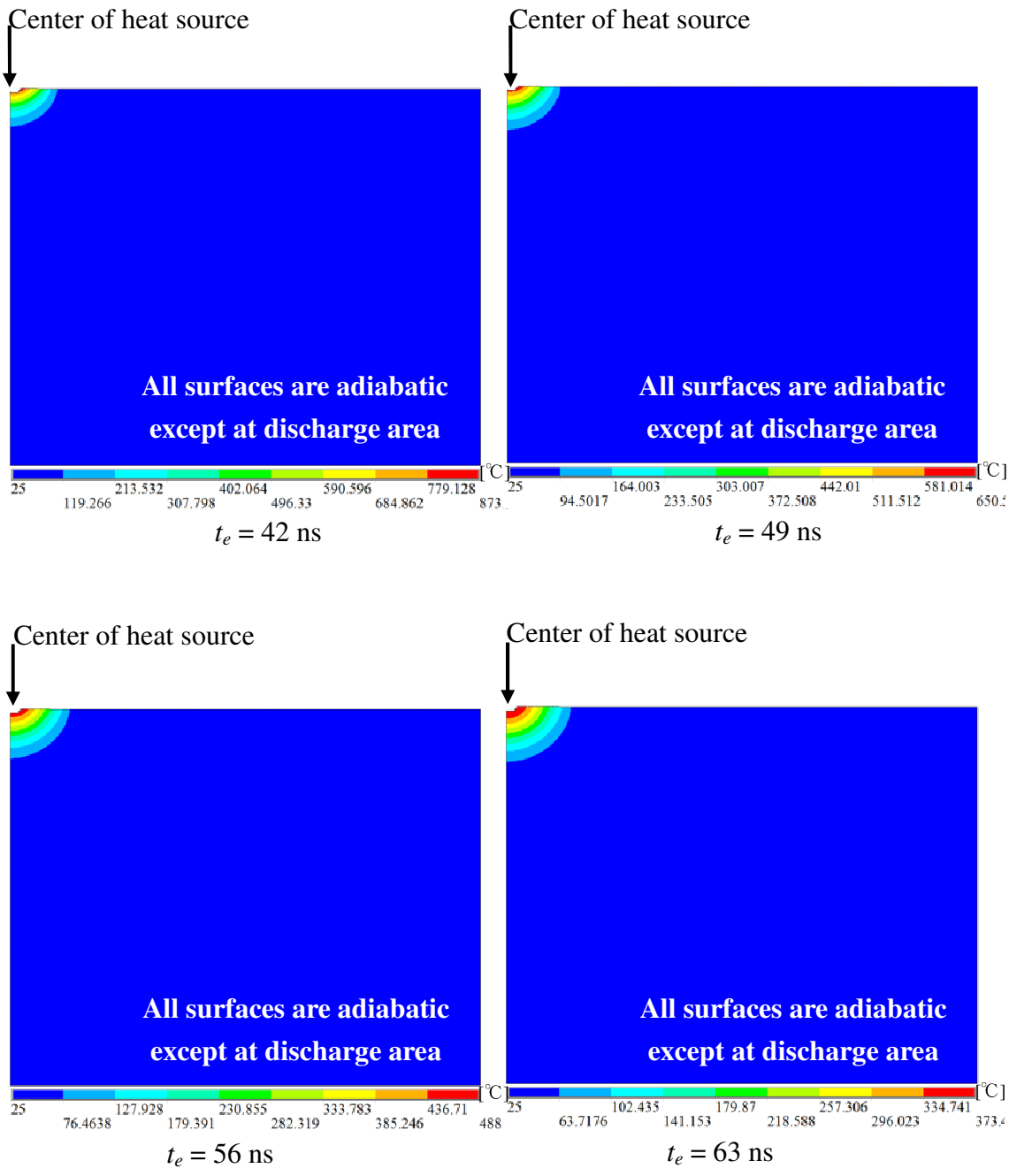

Calculated temperature distribution with respect to time during discharge duration

APPENDIX E

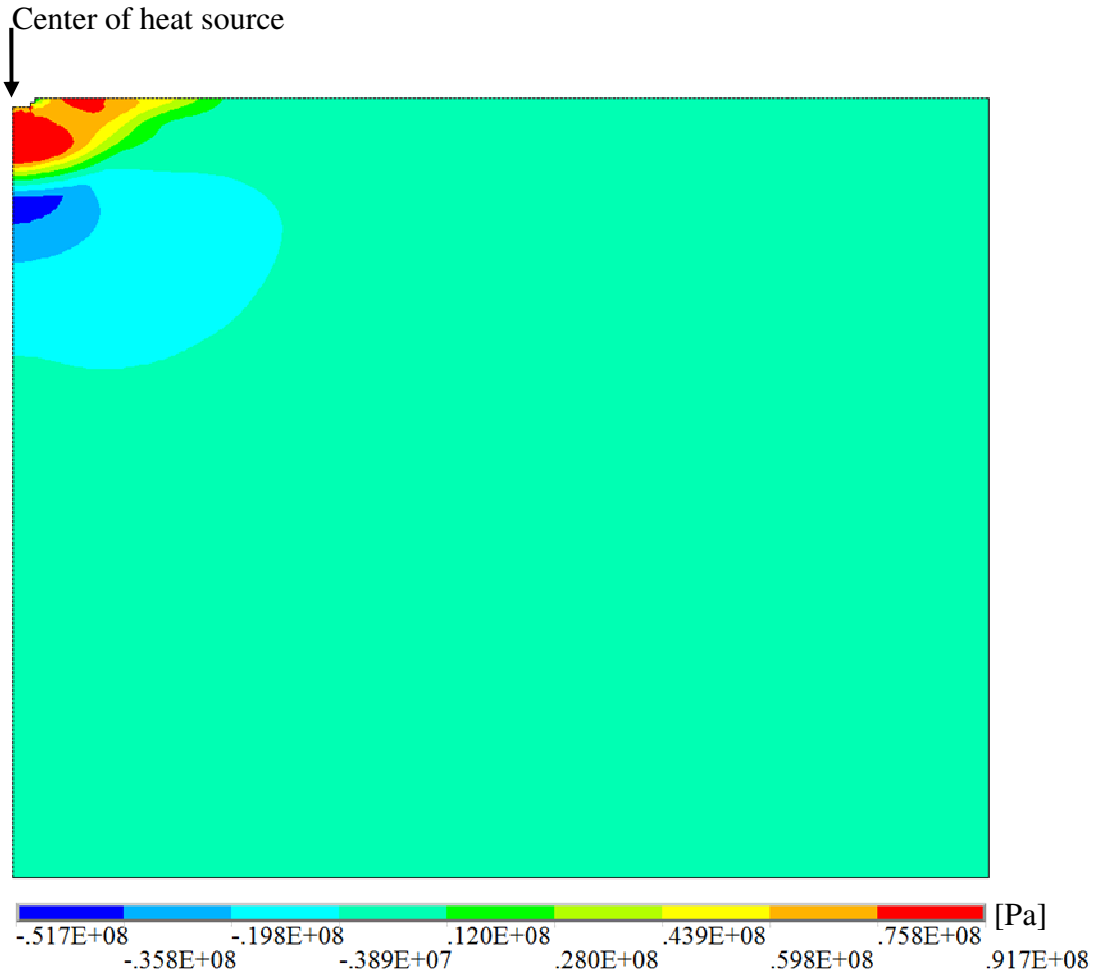

Residual stress distribution at the end of cooling time (t = 370 ns) considering material removal

Acknowledgements

First and foremost, I would like to express my sincere gratitude to my supervisor Professor Masanori Kunieda for the continuous support of my study and research during the Doctor Course, for his patience, motivation, enthusiasm, and immense knowledge. His guidance helped me in all the time of research and writing of this doctoral dissertation. I could not have imagined having a better supervisor and mentor for my study.

I also would like to express my special gratitude to all referees; Professor Higuchi, Professor Kajihara, Professor Sugita and Professor Mimura. Their precious comments and suggestions help to enhance the quality of this dissertation.

Besides my supervisor, I would like to express my gratitude towards members of KUNIEDA lab since 2008 for their kind co-operation and encouragement which help me in completion of this work.

And I would like to thank my family; Parents, wife and kids for supporting me spiritually throughout these years……

List of publications related to this research

Journals

(1) Mohd ZAHIRUDDIN and Masanori KUNIEDA, 2010, Energy distribution ratio into micro EDM electrodes, Journal of Advanced Mechanical Design, Systems, and Manufacturing Vol.4, No.6, pp. 1095-1106.
(2) Mohd ZAHIRUDDIN and Masanori KUNIEDA, 2012, Comparison of energy and removal efficiencies between micro and macro EDM, CIRP Annals – Manufacturing Technology Vol. 61,No. 1, pp. 187-190

International conferences

(1) Mohd ZAHIRUDDIN and Masanori KUNIEDA, 2009, Energy Distribution into Micro EDM Electrodes, The 5th International Conference on LEM21, Osaka Japan, pp. 835-840
(2) Mohd ZAHIRUDDIN and Masanori KUNIEDA, 2010, Thermal Effects on Electrodes in Micro EDM, ISEM-XVI, Shanghai China, pp. 561-564
(3) Mohd ZAHIRUDDIN and Masanori KUNIEDA, 2010, Determination of Removal Efficiency in Micro EDM Process, The 4th CIRP International Conference on HPC, Gifu Japan, pp. 337-342

Local conferences

(1) Mohd ZAHIRUDDIN and Masanori KUNIEDA, 2009, Energy Distribution into Electrodes in Wet and Dry Micro EDM, Fall meeting of JSPE, Kobe Japan.
(2) Mohd ZAHIRUDDIN and Masanori KUNIEDA, 2010, Determination of removal mechanism in micro EDM, Fall meeting of JSPE, Nagoya Japan.
(3) Mohd ZAHIRUDDIN and Masanori KUNIEDA, 2010, Comparison of removal characteristics between micro and macro EDM, Annual meeting of JSEME, Shizuoka Japan.